

Electronic Structure Analyses and Activation Studies of a Dinitrogen-derived Terminal Nitride of Molybdenum

by

Emma Louise Sceats
M.Sc. in Chemistry with Industrial Experience
University of Bristol
2002

Submitted to the Department of Chemistry
in Partial Fulfillment of the Requirements for the Degree of

MASTER OF SCIENCE
at the
MASSACHUSETTS INSTITUTE OF TECHNOLOGY
May 2004

© Massachusetts Institute of Technology, 2004.

Signature of Author _____

Department of Chemistry
May 25th 2004

Certified by _____

Christopher C. Cummins
Thesis Supervisor

Accepted by _____

Robert W. Field
Chairman, Departmental Committee on Graduate Students

Electronic Structure Analyses and Activation Studies of a Dinitrogen-derived Terminal Nitride of Molybdenum

Emma Louise Sceats

*Submitted to the Department of Chemistry, May 2004
Massachusetts Institute of Technology
in Partial Fulfillment of the Requirements for the Degree of Master of Science in
Chemistry*

Thesis Supervisor: Christopher C. Cummins

Title: Professor of Chemistry

Abstracts

Chapter 1: Complexes obtained by electrophilic attack on a dinitrogen-derived terminal molybdenum nitride: Electronic structure analysis by solid state CP/MAS ^{15}N NMR in combination with DFT calculations

^{15}N Solid state CP/MAS NMR spectroscopy has been used to study a dinitrogen-derived terminal nitride of molybdenum, $^{15}\text{NMo}(\text{N}[\text{tBu}]\text{Ar})_3$ ($\text{Ar} = 3,5\text{-C}_6\text{H}_3(\text{CH}_3)_2$). A number of Lewis acid adducts, including $\text{X}_3\text{E-NMo}(\text{N}[\text{tBu}]\text{Ar})_3$ ($\text{X} = \text{F}, \text{E} = \text{B}; \text{X} = \text{Cl}, \text{E} = \text{B}, \text{Al}, \text{Ga}, \text{In}; \text{X} = \text{Br}, \text{E} = \text{Al}; \text{X} = \text{I}, \text{E} = \text{Al}$) and $\text{Cl}_2\text{E-NMo}(\text{N}[\text{tBu}]\text{Ar})_3$ ($\text{E} = \text{Ge}, \text{Sn}$), were prepared by the combination of $^{15}\text{NMo}(\text{N}[\text{tBu}]\text{Ar})_3$ with 1 equiv. of Lewis acid. A series of cationic imido complexes, $[\text{RNMo}(\text{N}[\text{tBu}]\text{Ar})_3]\text{X}$ was prepared by the reaction of electrophiles, RX [$\text{R} = \text{CH}_3, \text{X} = \text{I}; \text{R} = \text{PhC}(\text{O})$ or $\text{Me}_3\text{Si}, \text{X} = \text{OTf}$ ($\text{OTf} = \text{SO}_3\text{CF}_3$)], with $\text{NMo}(\text{N}[\text{tBu}]\text{Ar})_3$. Deprotonation of $[\text{CH}_3\text{NMo}(\text{N}[\text{tBu}]\text{Ar})_3]\text{I}$ by $\text{LiN}(\text{SiMe}_3)_2$ afforded the ketimide complex $\text{H}_2\text{CNMo}(\text{N}[\text{tBu}]\text{Ar})_3$, which has been shown to undergo a reaction with neat CH_3I to form $[\text{CH}_3\text{CH}_2\text{NMo}(\text{N}[\text{tBu}]\text{Ar})_3]\text{I}$. ^{15}N solid state CP/MAS NMR spectroscopy was employed in the characterization of each complex. Complementary density functional theory (DFT) studies of $^{15}\text{NMo}(\text{N}[\text{tBu}]\text{Ar})_3$ and derivatives enabled a detailed examination of the experimental solid state NMR parameters in terms of electronic structure at the labeled N-atom. Computational analysis demonstrated that significant paramagnetic contributions to the perpendicular components of the chemical shielding tensor (δ_{11} and δ_{22}) were responsible for the huge span of the tensor measured for $^{15}\text{NMo}(\text{N}[\text{tBu}]\text{Ar})_3$ ($\Omega = 1186$ ppm). Perturbation of the electronic structure in $^{15}\text{NMo}(\text{N}[\text{tBu}]\text{Ar})_3$ upon coordination of a Lewis acid or formation of a cationic imido complex was attributed to stabilization of a σ -symmetric orbital. An upfield shift in the perpendicular components of the chemical shift tensor results from the reduced paramagnetic contribution to these tensor components upon increasing the energy gap between the magnetically-coupled occupied and virtual orbitals ($e_{\text{occ}} - e_{\text{vir}}$).

Chapter 2. Carbene chemistry in the activation of a dinitrogen-derived terminal nitride of molybdenum

The potential for metal-nitride bond activation by the addition of an electrophilic carbene to a dinitrogen-derived terminal nitride of molybdenum $\text{NMo}(\text{N}^t\text{BuAr})_3$ has been investigated. Two methods for the generation of dihalocarbenes (CCl_2 and CFCl) have been studied. The reaction of $\text{NMo}(\text{N}^t\text{BuAr})_3$ with $\text{TiCl}_4 \cdot \text{THF}_2$, LiAlH_4 and haloform (CCl_4 or CFCl_3) resulted in the 74-76% conversion of $\text{NMo}(\text{N}^t\text{BuAr})_3$ to products (measured by ^1H NMR spectroscopy versus an internal standard). Two new molybdenum-containing products (one paramagnetic and one diamagnetic) were present in solution. The paramagnetic product, formed in 24-26% yield, was identified as $\text{Cl-Mo}(\text{N}^t\text{BuAr})_3$. The identity of the diamagnetic product (**A**) has not been established. The titanium-mediated reduction of halocarbons CRX_3 ($\text{X} = \text{Cl}$, $\text{R} = \text{CH}_3$, Ph) in the generation of alkyl (or aryl) substituted halocarbenes CRX was also investigated. The reaction of $\text{NMo}(\text{N}^t\text{BuAr})_3$ with $\text{TiCl}_4 \cdot \text{THF}_2$, LiAlH_4 and CRCl_3 ($\text{R} = \text{Ph}$, CH_3) resulted in the formation and isolation of $\text{Cl-Mo}(\text{N}^t\text{BuAr})_3$ in 23-24% yield. The organic nitrogen-containing products could not be isolated. The *in situ* reduction of PhCN to PhCH_2NH_2 (or CH_3CN to $\text{CH}_3\text{CH}_2\text{NH}_2$) is expected to be at least one of the decomposition routes of the N_2 -derived organic product. The second method of dichlorocarbene generation involves the thermal extrusion of CCl_2 from the Seyferth reagent $\text{PhHgCCl}_2\text{Br}$. The thermolysis of $\text{PhHgCCl}_2\text{Br}$ in the presence of $\text{NMo}(\text{N}^t\text{BuAr})_3$ was monitored by ^1H NMR spectroscopy. This reaction is also thought to generate $\text{Cl-Mo}(\text{N}^t\text{BuAr})_3$, which in the presence of $\text{PhHgCCl}_2\text{Br}$ undergoes a rapid reaction to form a number of unidentified diamagnetic products. The fate of the N_2 -derived organic product was not determined. Finally, conditions for the one-electron reduction of $\text{Cl-Mo}(\text{N}^t\text{BuAr})_3$ have been optimized in order to enable the regeneration of $\text{Mo}(\text{N}^t\text{BuAr})_3$.

Chapter 3. Nitrogen atom transfer from dinitrogen into an organic nitrile *via* the anionic ketimide complex $(\text{THF})_2\text{Mg}[\text{O}(\text{Ph})\text{C}^{15}\text{NMo}(\text{N}^t\text{BuAr})_3]_2$

Nitrogen atom transfer from a dinitrogen-derived terminal nitride of molybdenum $^{15}\text{NMo}(\text{N}^t\text{BuAr})_3$ (**1**) into an organic nitrile has been demonstrated. Synthesis of the benzoylimido complex $[\text{PhC}(\text{O})^{15}\text{NMo}(\text{N}^t\text{BuAr})_3]\text{OTf}$ [**2**]OTf is achieved *via* reaction of complex **1** with benzoyl triflate. Subsequent two-electron reduction of [**2**]OTf, provides the anionic ketimide complex $(\text{THF})_2\text{Mg}[\text{O}(\text{Ph})\text{C}^{15}\text{NMo}(\text{N}^t\text{BuAr})_3]_2$ [**3**]₂Mg(THF)₂ in high yield. Reactions of [**3**]₂Mg(THF)₂ with $\text{RMe}_2\text{Si-OTf}$ enabled isolation of the molybdenum(IV) ketimide complexes $\text{RMe}_2\text{SiO}(\text{Ph})\text{CNMo}(\text{N}^t\text{BuAr})_3$ (**4a** $\text{R} = \text{Me}$; **4b** $\text{R} = ^t\text{Bu}$). Reactions of [**3**]₂Mg(THF)₂ with benzoyl triflate or trifluoroacetic anhydride resulted in the syntheses of molybdenum(IV) complexes $\text{RO-Mo}(\text{N}^t\text{BuAr})_3$ (**6a** $\text{R} = \text{PhCO}$; **6b** $\text{R} = \text{CF}_3\text{CO}$) together with the concomitant formation of one equivalent PhCN^{15} . Selective ^{15}N -labeling of benzonitrile was demonstrated unequivocally by the combined use of ^{15}N solution NMR studies and GC-MS measurements.

Table of Contents

Title page	
Abstracts	
Table of Contents	
List of Tables and Figures	
List of Abbreviations	
Chapter 1: Complexes obtained by electrophilic attack on a dinitrogen-derived terminal molybdenum nitride: Electronic structure analysis by solid state CP/MAS ^{15}N NMR in combination with DFT calculations	
Section 1.1: Introduction	12
Section 1.2: Results and Discussion	13
1.2.1: Synthesis and Characterization	13
1.2.2: ^{15}N Solid state CP/MAS NMR Spectroscopy of $^{15}\text{NMo}(\text{N}[\text{tBu}]\text{Ar})_3$ (1)	22
1.2.3: ^{15}N Solid state CP/MAS NMR Spectroscopy of the Lewis acid adducts of 1 (1-LA)	24
1.2.4: ^{15}N Solid state CP/MAS NMR Spectroscopy of the imido complexes [2a]I, [2b]OTf, [2c]OTf and [2d]I	26
1.2.5: ^{15}N NMR Spectroscopy of $\text{H}_2\text{CNMo}(\text{N}[\text{tBu}]\text{Ar})_3$ (3)	28
Section 1.3: Chemical shielding: Experimental measurement and computational analysis	28
1.3.1: Theoretical studies on $^{15}\text{NMo}(\text{N}[\text{tBu}]\text{Ar})_3$ (1)	30
1.3.2: Theoretical studies on the Lewis acids adducts of 1 (1-LA)	31
1.3.3: Theoretical studies on the imido cations [2a-m], [2b-m], [2c-m] and [2d-m]	32
1.3.4: Theoretical studies on $\text{H}_2\text{CNMo}(\text{N}[\text{tBu}]\text{Ar})_3$ (3)	33
Section 1.4: Concluding Remarks	36
Section 1.5: Experimental Section	37
1.5.1: General Information	37
1.5.2: X-ray Crystal Structure Determinations	38
1.5.3: NMR Measurements	39
1.5.4: Simulation and Calculation of Solid State NMR Spectra	40
1.5.5: Computational Details	40
1.5.6.1: Synthesis of $^{15}\text{NMo}(\text{N}[\text{tBu}]\text{Ar})_3$ (1)	41
1.5.6.2: Synthesis of Lewis Acid Adducts (1-LA)	41
1.5.6.3: Synthesis of $[\text{CH}_3\text{NMo}(\text{N}[\text{tBu}]\text{Ar})_3]\text{I}$ [2a]I	44
1.5.6.4: Synthesis of $[(\text{CH}_3)_3\text{Si-NMo}(\text{N}[\text{tBu}]\text{Ar})_3][\text{SO}_3\text{CF}_3]$ [2b]OTf	44
1.5.6.5: Synthesis of $[\text{PhC}(\text{O})\text{NMo}(\text{N}[\text{tBu}]\text{Ar})_3]\text{SO}_3\text{CF}_3$ [2c]OTf	45
1.5.6.6: Synthesis of $\text{H}_2\text{CNMo}(\text{N}[\text{tBu}]\text{Ar})_3$ (3)	47
1.5.6.7: Synthesis of $[\text{CH}_3\text{CH}_2\text{NMo}(\text{N}[\text{tBu}]\text{Ar})_3]\text{I}$ [2d]I	47
References	48

Chapter 2: Carbene chemistry in the activation of a dinitrogen-derived terminal nitride of molybdenum

Section 2.1: Introduction	54
Section 2.2: Results and Discussion	58
2.2.1: A brief introduction to the chemistries of dichlorocarbene (CCl ₂) and fluorochlorocarbene (CFCl)	58
2.2.2: Generation of dihalocarbenes (CX ₂) <i>via</i> the titanium-mediated reduction of haloforms and the reactions of CX ₂ with NMo(N[^t Bu]Ar) ₃ (2)	59
2.2.3: Generation of alkyl (or aryl) halocarbenes (CRX) <i>via</i> the titanium-mediated reduction of halocarbons (CRX ₃) and reactions of CRX with NMo(N[^t Bu]Ar) ₃ (2)	61
2.2.4: Generation of dichlorocarbene (CCl ₂) <i>via</i> thermal extrusion from a Seyferth reagent (PhHgCCl ₂ Br) and reactions of CCl ₂ with NMo(N[^t Bu]Ar) ₃ (2)	63
2.2.5: Independent synthesis of Cl–Mo(N[^t Bu]Ar) ₃ (1–Cl) and Br–Mo(N[^t Bu]Ar) ₃ (1–Br)	66
2.2.6: One-electron reduction reactions of Cl–Mo(N[^t Bu]Ar) ₃ (1–Cl)	67
2.2.7: Concluding remarks and future work	68
Section 2.3: Experimental Section	69
2.3.1: General Information	69
2.3.2: Synthesis of Cl–Mo(N[^t Bu]Ar) ₃ (1–Cl) from NMo(N[^t Bu]Ar) ₃ (2)	69
2.3.3: Control reaction of NMo(N[^t Bu]Ar) ₃ (2) in the presence of LiAlH ₄ and TiCl ₄ ·THF ₂	70
2.3.4: NMR quantification of NMo(N[^t Bu]Ar) ₃ (2) conversion to Cl–Mo(N[^t Bu]Ar) ₃ (1–Cl)	71
2.3.5: Analysis of volatile components produced in the reaction of ¹⁵ NMo(N[^t Bu]Ar) ₃ (2-¹⁵N) with TiCl ₄ ·THF ₂ , LiAlH ₄ and CFCl ₃	71
2.3.6: Analysis of volatile components produced in the reaction of NMo(N[^t Bu]Ar) ₃ (2) with TiCl ₄ ·THF ₂ , LiAlH ₄ and CH ₃ CCl ₃	72
2.3.7: Reaction of PhHgCCl ₂ Br with NMo(N[^t Bu]Ar) ₃ (2)	72
2.3.8: Reaction of PhHgBr with Cl–Mo(N[^t Bu]Ar) ₃ (1–Cl)	73
2.3.9: Reaction of PhHgBr with NMo(N[^t Bu]Ar) ₃ (2)	73
2.3.10: Reaction of PhHgCCl ₂ Br with Cl–Mo(N[^t Bu]Ar) ₃ (1–Cl)	73
2.3.11: Reaction of PhHgCCl ₂ Br with Mo(N[^t Bu]Ar) ₃ (1)	73
2.3.12: Reaction of PhHgCCl ₂ Br with Br–Mo(N[^t Bu]Ar) ₃ (1–Br)	74
2.3.13: Syntheses of X–Mo(N[^t Bu]Ar) ₃ (1–Cl , 1–Br) from Mo(N[^t Bu]Ar) ₃ (2)	74
2.3.14: Thermal stability of 1–Cl	75
2.3.15: One-electron reduction of Cl–Mo(N[^t Bu]Ar) ₃ (1–Cl) with magnesium	75
2.3.16: Alternate method for the one-electron reduction of Cl–Mo(N[^t Bu]Ar) ₃ (1–Cl)	76
2.3.17: Attempted one-electron reduction of 1–Cl employing Na/Hg under argon	76
2.3.18: Attempted synthesis of NMo(N[^t Bu]Ar) ₃ (2) from Cl–Mo(N[^t Bu]Ar) ₃ (1–Cl)	77

References	77
Chapter 3. Nitrogen atom transfer from dinitrogen into an organic nitrile <i>via</i> the anionic ketimide complex $(\text{THF})_2\text{Mg}[\text{O}(\text{Ph})\text{C}^{15}\text{NMo}(\text{N}[\text{tBu}]\text{Ar})_3]_2$	
Section 3.1: Introduction	82
Section 3.2: Results and discussion	83
3.2.1: One and two-electron reduction chemistry of $[\text{PhC}(\text{O})^{15}\text{NMo}(\text{N}[\text{tBu}]\text{Ar})_3]\text{SO}_3\text{CF}_3$ [2] OTf	83
3.2.2: ^{15}N Solid state CP/MAS NMR spectroscopy of $(\text{THF})_2\text{Mg}[\text{O}(\text{Ph})\text{C}^{15}\text{NMo}(\text{N}[\text{tBu}]\text{Ar})_3]_2$ [3] Mg(THF) ₂	87
3.2.3: Reactions of $(\text{THF})_2\text{Mg}[\text{O}(\text{Ph})\text{C}^{15}\text{NMo}(\text{N}[\text{tBu}]\text{Ar})_3]_2$ [3] ₂ Mg(THF) ₂ with electrophiles	89
3.2.3.1: Syntheses of ketimide complexes $\text{RO}(\text{Ph})\text{C}^{15}\text{NMo}(\text{N}[\text{tBu}]\text{Ar})_3$ (4)	90
3.2.3.2 Syntheses of ketimide complexes $\text{RC}(\text{O})\text{O}(\text{Ph})\text{C}^{15}\text{NMo}(\text{N}[\text{tBu}]\text{Ar})_3$ (5a and 5b)	92
Section 3.3: Concluding remarks	94
Section 3.4: Experimental Section	95
3.4.1: One-electron reduction of $[\text{PhC}(\text{O})\text{NMo}(\text{N}[\text{tBu}]\text{Ar})_3]\text{SO}_3\text{CF}_3$ [2] OTf with cobatocene.	96
3.4.2: Thermal Stability of $[\text{PhC}(\text{O})\text{NMo}(\text{N}[\text{tBu}]\text{Ar})_3]\text{SO}_3\text{CF}_3$ [2] OTf	96
3.4.3: Synthesis of $(\text{THF})_2\text{Mg}[\text{O}(\text{Ph})\text{C}^{15}\text{NMo}(\text{N}[\text{tBu}]\text{Ar})_3]_2$ [3] ₂ Mg(THF) ₂	97
3.4.4: Synthesis of $\text{Me}_3\text{SiO}(\text{Ph})\text{CNMo}(\text{N}[\text{tBu}]\text{Ar})_3$ (4a) and $\text{MeO}(\text{Ph})\text{CNMo}(\text{N}[\text{tBu}]\text{Ar})_3$ (4b)	98
3.4.5: Reaction of $(\text{THF})_2\text{Mg}[\text{O}(\text{Ph})\text{C}^{15}\text{NMo}(\text{N}[\text{tBu}]\text{Ar})_3]_2$ [3] ₂ Mg(THF) ₂ with $\text{PhC}(\text{O})\text{OTf}$	99
3.4.6: Reaction of $(\text{THF})_2\text{Mg}[\text{O}(\text{Ph})\text{C}^{15}\text{NMo}(\text{N}[\text{tBu}]\text{Ar})_3]_2$ [3] ₂ Mg(THF) ₂ with $(\text{CF}_3\text{CO})_2\text{O}$	100
3.4.7: Synthesis of $\text{CF}_3\text{C}(\text{O})\text{OMo}(\text{N}[\text{tBu}]\text{Ar})_3]_2$ (6b)	100
References	101
Appendix 1: Tables of selected bond lengths and angles	103
Appendix 2(a): Representative ^{15}N solid state NMR spectra for Lewis acid complexes (1-LA)	116
Appendix 2(b): Representative ^{15}N solid state NMR spectra for imido complexes (2)	121
Appendix 3: Density Functional Theory Calculations	124
Appendix 4: GC-MS data	139
Appendix 5: Synthesis of H_2TTP , $(\text{TTP})\text{Li}_2(\text{OEt}_2)_2$ and $(\text{TTP})\text{TiCl}$	141
Curriculum Vitae	143
Acknowledgements	145

List of Tables and Figures

Chapter 1: Complexes obtained by electrophilic attack on a dinitrogen-derived terminal molybdenum nitride: Electronic structure analysis by solid state CP/MAS ^{15}N NMR in combination with DFT calculations

- Figure 1. Formation of complex **1** *via* the base-catalyzed cleavage of dinitrogen.
- Figure 2. Syntheses of **1**-LA and the cationic imido complexes [**2a**]I, [**2b**]OTf and [**2c**]OTf.
- Figure 3. ORTEP representation of **1**-BF₃ with thermal ellipsoids at the 35% probability level.
- Figure 4. 35% thermal ellipsoid (ORTEP) representations of **1**-GeCl₂ (left) and **1**-SnCl₂ (right).
- Figure 5. 50% thermal ellipsoid (ORTEP) representations of cation [**2b**].
- Figure 6. 50% thermal ellipsoid (ORTEP) representations of cation [**2c**].
- Figure 7. Dehydrohalogenation of [**2a**]I in the formation of **3** and subsequent reaction with CH₃I to form [**2d**]I.
- Figure 8. 50% thermal ellipsoid (ORTEP) representation of **3**. Ketimide hydrogens, H41a and H41b, were located and refined anisotropically.
- Figure 9. 50% thermal ellipsoid (ORTEP) representation of cation [**2d**].
- Table 1. Experimental and calculated ^{15}N chemical shielding tensors for **1** and derivatives thereof. δ_{iso} is the isotropic shift, Ω is the span defined as $\delta_{11} - \delta_{33}$; κ is the skew of the shielding tensor defined as $[3(\delta_{22} - \delta_{\text{iso}})/(\delta_{11} - \delta_{33})]$; $\chi^2 = \Sigma ((\text{obs-calc})^2)/\text{calc}$.
- Figure 10. Experimental (—) and simulated (—) ^{15}N solid state CP/MAS NMR spectra for complex **1** and DFT calculated (—) NMR spectrum for complex **1m**.
- Figure 11. Experimental ^{15}N solid state CP/MAS NMR spectrum of **1**-BCl₃. The expanded portion of the spectrum shows the multiplicity of one of the spinning sidebands.
- Figure 12. Experimental ^{15}N solid state CP/MAS NMR spectrum of [**2a**]I. The expanded portion of the spectrum shows the multiplicity of one of the spinning sidebands.
- Figure 13. Optimized geometries for the model complexes **3m**-C₃ (top) and **3m**-C_s (bottom) and solid state ^{15}N spectra for complex **3**: experimental (top), calculated **3m**-C₃ (middle) and calculated **3m**-C_s (bottom).
- Figure 14. Calculated HOMO (left) and LUMO (right) of **3m**-C₃.
- Table 2. Crystallographic data.

Chapter 2: Carbene chemistry in the activation of a dinitrogen-derived terminal nitride of molybdenum

Scheme 1. Proposed catalytic pathway for N-atom incorporation from **2** into organic nitriles (RCN).

Figure 1. Singlet versus triplet states in fluoromethylene (CHF), fluorochlorocarbene (CFCl) and difluorocarbene (CF₂)

Figure 2. Synthesis of complexes **1**-X (X = Cl, Br)

Figure 3. The one-electron reduction of **1**-Cl by magnesium.

Chapter 3. Nitrogen atom transfer from dinitrogen into an organic nitrile *via* the anionic ketimide complex $(\text{THF})_2\text{Mg}[\text{O}(\text{Ph})\text{C}^{15}\text{NMo}(\text{N}[\text{tBu}]\text{Ar})_3]_2$

Scheme 1. One and two-electron reduction routes to the anionic ketimide complex $[\text{O}(\text{Ph})\text{C}^{15}\text{NMo}(\text{N}[\text{tBu}]\text{Ar})_3]^-$ [**3**].

Scheme 2. Synthesis of the anionic ketimide complex $[\text{3}]_2\text{Mg}(\text{THF})_2$ and functionalization to form neutral ketimide complexes **4** and **5**.

Figure 1. Experimental (—) and simulated (---) ^{15}N solid state CP/MAS NMR spectra for complex $[\text{3}]_2\text{Mg}(\text{THF})_2$.

Table 1. Experimental principal components of the ^{15}N chemical shift tensor for complex $[\text{3}]_2\text{Mg}(\text{THF})_2$.

Figure 2. UV-visible spectrum of $\text{Me}_3\text{SiO}(\text{Ph})\text{C}^{15}\text{NMo}(\text{N}[\text{tBu}]\text{Ar})_3$ (**4a**) (toluene, 25 °C).

Figure 3. ^{15}N Solution NMR spectrum of the reaction between complex $[\text{3}]_2\text{Mg}(\text{THF})_2$ and benzoyl triflate.

Figure 4. UV-visible spectrum of $(\text{THF})_2\text{Mg}[\text{O}(\text{Ph})\text{C}^{15}\text{NMo}(\text{N}[\text{tBu}]\text{Ar})_3]_2$ $[\text{3}]_2\text{Mg}(\text{THF})_2$ (toluene, 25 °C).

Abbreviations Used in the Text

Å	Angstrom (10^{-10} m)
Anal.	Analysis (Elemental)
anth	anthracene ($C_{14}H_{10}$)
Ar	3,5-dimethylphenyl
atm	Atmosphere
BDE	Bond Dissociation Energy
br	broad
Bu	Butyl
^t Bu	<i>tert</i> -butyl group
Calcd.	Calculated
cm^{-1}	wavenumber
CP	Cross Polarization
δ	chemical shift
d	doublet (NMR) or days
DFT	Density Functional Theory
°	degrees
e-	electron
equiv	equivalents
Et	Ethyl
Et ₂ O	diethyl ether
G	Gauss
g	grams
GC-MS	Gas Chromatography-Mass Spectroscopy
h	hours
¹ H	Proton
HOMO	Highest Occupied Molecular Orbital
Hz	Hertz
ⁱ Pr	<i>iso</i> -Propyl
IR	Infrared

J	coupling constant (in Hertz)
K	degrees Kelvin
LA	Lewis Acid
LUMO	Lowest Unoccupied Molecular Orbital
m	multiplet
MAS	Magic Angle Spinning
Me	Methyl
min	minutes
MO	Molecular Orbital
NMR	Nuclear Magnetic Resonance
ORTEP	Oak Ridge Thermal Ellipsoid Plot
OTf	SO ₃ CF ₃ , triflate, trifluoromethanesulfonate
Ph	Phenyl (C ₆ H ₅)
ppm	parts per million
Pr	Propyl
q	quartet
s	singlet
SIMPSON	<u>S</u> imulation program for <u>s</u> olid state <u>N</u> M <u>R</u> spectroscopy
t	triplet
THF	Tetrahydrofuran
TFAA	Trifluoroacetic anhydride
TMS	Trimethylsilyl (-Si(CH ₃) ₃)
Tosyl	Toluenesulphonyl
TPPM	Two Phase Pulse Modulation
UV-vis	Ultra Violet-Visible
X	Anionic One-electron donor ligand
v _{1/2}	peak width at half height
v	stretching frequency
λ _{max}	wavelength of maximum optical absorbance

Chapter 1

Complexes obtained by electrophilic attack on a dinitrogen-derived terminal molybdenum nitride: Electronic structure analysis by solid state CP/MAS ^{15}N NMR in combination with DFT calculations

Complexes obtained by electrophilic attack on a dinitrogen-derived terminal molybdenum nitride: Electronic structure analysis by solid state CP/MAS ^{15}N NMR in combination with DFT calculations

1.1 Introduction

The use of isotopic labeling of compounds with ^{15}N to probe their structure and bonding by means of solid state NMR spectroscopy is most commonly seen in biological systems and organic molecules.

¹⁻⁹ In contrast, solid state NMR spectroscopy of spin-active nuclei in transition metal complexes has been underutilized.¹⁰⁻¹⁶ The isotropic chemical shift value determined in solution NMR measurements is the most reported spectroscopic parameter, but a wealth of additional information may be gained through the acquisition of solid state NMR spectra.^{17,18} The use of ^{31}P solid state NMR spectroscopy to probe the structure and bonding in a terminal molybdenum phosphide, $\text{PMo}(\text{N}[\text{tBu}]\text{Ar})_3$ ($\text{Ar} = 3,5\text{-C}_6\text{H}_3(\text{CH}_3)_2$) was reported previously.¹⁹ The significant anisotropy of the ^{31}P chemical shift tensor and the enormous paramagnetic deshielding of the ^{31}P nucleus when the applied field is oriented perpendicular to the Mo-P triple bond were explained in terms of the magnetic coupling of filled and vacant molecular orbitals.

Herein we extend our study of structure and bonding through the use of solid state NMR spectroscopy to the analogous terminal nitride of molybdenum, $\text{NMo}(\text{N}[\text{tBu}]\text{Ar})_3$ (**1**).²⁰ The splitting of dinitrogen by a three-coordinate molybdenum(III) complex $\text{Mo}(\text{N}[\text{tBu}]\text{Ar})_3$ ($\text{Ar} = 3,5\text{-C}_6\text{H}_3(\text{CH}_3)_2$) was first reported in 1995.²¹ The ^{15}N -labeled form of **1**, $^{15}\text{NMo}(\text{N}[\text{tBu}]\text{Ar})_3$ is readily prepared through the use of ^{15}N -isotopically-enriched dinitrogen gas, thereby making this complex amenable to study by ^{15}N NMR spectroscopy.²² The potential of **1** to serve as a platform in N-atom transfer chemistry is currently under investigation in our laboratories. It is of interest to determine what insight solid state NMR spectroscopy can provide into the electronic structure for a molybdenum complex which is activated toward productive removal of the dinitrogen-

derived N-atom into an organic product. The synthesis of several derivatives of **1** and subsequent measurement of their ^{15}N solid state CP/MAS NMR spectra are described.

Complementary density functional theory analyses of **1** and its derivatives were completed utilizing a simplified ligand framework (NH_2 ligands replacing N^tBuAr). DFT permits a detailed analysis of experimental solid state NMR parameters (δ_{11} , δ_{22} and δ_{33}) *via* calculation of the absolute shielding tensors^{23–27} together with correlation to calculated molecular orbitals. The validity of our analyses of electronic structure may be assessed by comparison of the experimental tensor values with those determined computationally.

1.2 Results and Discussion

1.2.1 Synthesis and Characterization

The first reported synthesis of $\text{NMo}(\text{N}^t\text{BuAr})_3$ (**1**) from $\text{Mo}(\text{N}^t\text{BuAr})_3$ required a 3 d incubation period at $-35\text{ }^\circ\text{C}$ during which time N_2 uptake takes place.²⁰ Subsequent work focusing on the redox-catalyzed binding and splitting of dinitrogen by $\text{Mo}(\text{N}^t\text{BuAr})_3$ has led to the development of a more efficient route to the terminal nitride **1**.²⁸ Most recently, Lewis bases were found to accelerate the uptake of N_2 by $\text{Mo}(\text{N}^t\text{BuAr})_3$ enabling its quantitative conversion to **1** within 24 h. Potassium hydride (10 equiv. in THF) was found to be the most efficient base for effecting this conversion (Figure 1).²⁹

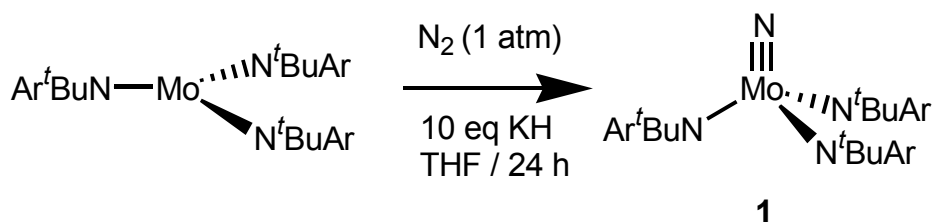


Figure 1. Formation of complex **1** *via* the base-catalyzed cleavage of dinitrogen.

Furthermore, the ease of separation of KH from the pentane soluble product (**1**) by filtration makes this route particularly attractive. Complete characterization for complex **1** was reported previously. We will however make note of the ^{15}N solution NMR shift of **1** (840 ppm) for comparison with values reported in the following discussions. While complex **1** has eluded characterization by single crystal X-ray diffraction, the structure of a related compound, $\text{NMo}(\text{N}^t\text{BuPh})_3$,²⁰ is pseudo tetrahedral with the $\text{Mo}\equiv\text{N}$ bond aligned with a crystallographic C_3 axis.

A number of neutral Lewis acid adducts of formula $\text{X}_3\text{E}-\text{NMo}(\text{N}^t\text{BuAr})_3$ ($\text{X} = \text{F}$, $\text{E} = \text{B}$; $\text{X} = \text{Cl}$, $\text{E} = \text{B}$, Al , Ga , In ; $\text{X} = \text{Br}$, $\text{E} = \text{Al}$; $\text{X} = \text{I}$, $\text{E} = \text{Al}$) and $\text{Cl}_2\text{E}-\text{NMo}(\text{N}^t\text{BuAr})_3$ ($\text{E} = \text{Ge}$, Sn), were prepared by simple combination of **1** with 1 equiv. of Lewis acid (Figure 2). Yields were generally quite high and in the range of 59 to 91%. These adducts were typically bright yellow, or sometimes pale orange, exhibiting limited solubility in pentane, benzene and Et_2O . The decomposition of these adducts to starting materials was observed in 0.5-3 h in THF solution at 25 °C.

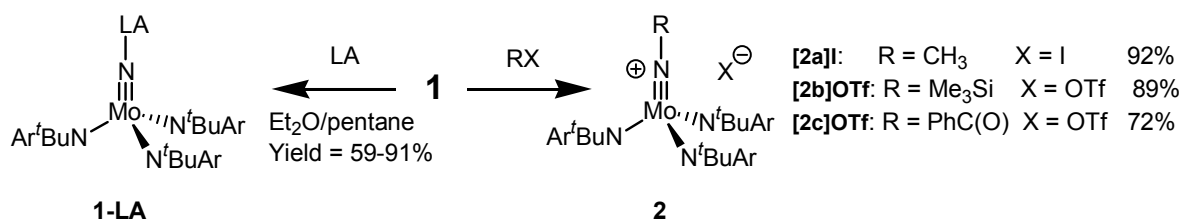


Figure 2. Syntheses of **1-LA** and the cationic imido complexes **[2a]I**, **[2b]OTf** and **[2c]OTf**.

Infrared spectroscopy yielded little information with regard to the strength of the $\text{Mo}-\text{N}$ or $\text{N}-\text{LA}$ ($\text{LA} = \text{Lewis acid}$) interactions as a result of strong absorptions (attributed to the amide ligands) in the relevant regions of the spectrum.

A feature observed in the ^1H NMR spectrum of all complexes **1-LA** was significant broadening of the ~ 5.6 ppm resonance assigned to the six ortho protons of the

N[^tBu]Ar ligands. This broadening is attributed to hindered rotation about the Mo–N_{amide} bond due to increased steric congestion at the metal center.

As expected, the ¹¹B isotropic chemical shift for **1**-BF₃ (–2.8 ppm) and **1**-BCl₃ (3.9 ppm) showed an upfield shift of each resonance with respect to the uncoordinated Lewis acid (BF₃ = 10.0 ppm, BCl₃ = 46.5 ppm).³⁰ A similar upfield shift of the ²⁷Al resonance, with respect to the uncoordinated Lewis acid, was observed for the complexes **1**-AlCl₃, **1**-AlBr₃ and **1**-AlI₃.³¹

The ¹¹⁹Sn NMR spectrum of **1**-SnCl₂ displayed a broad singlet at 333 ppm, which is shifted downfield of the resonance for SnCl₂ in THF solution (236 ppm).³² This phenomenon might be explained based on molecular orbital considerations. Magnetic coupling of the tin molecular orbital, which contains the non-bonding lone pair of electrons and the unoccupied $\sigma^*(\text{N-Sn})$ molecular orbital supplements the paramagnetic contribution to the chemical shift tensor of tin. The paramagnetic contribution to the chemical shift of tin is increased in **1**-SnCl₂ compared to the solvated Lewis acid (**1**-SnCl₂·THF) due to a reduced energy gap between the magnetically-coupled virtual and occupied orbitals. The ¹¹⁹Sn resonance for **1**-SnCl₂ compares with other SnCl₂·N-donor complexes such as SnCl₂·pyridine in which the ¹¹⁹Sn resonance occurs at 295 ppm.³³

In the ²⁷Al, ¹¹B and ¹¹⁹Sn NMR spectra of ¹⁵N-**1**-BX₃, ¹⁵N-**1**-AlX₃ and ¹⁵N-**1**-SnCl₂, coupling of the two spin active nuclei (e.g. ¹⁵N–²⁷Al) could not be resolved. In each case the resonance for the spin-active Lewis acid center was broadened upon coordination to ¹⁵N-**1** (e.g. ¹¹B NMR: ¹⁴N-**1**-BCl₃ $\nu_{1/2}$ = 16.5 Hz; ¹⁵N-**1**-BCl₃ $\nu_{1/2}$ = 36.6 Hz). Likewise, the ¹⁵N solution NMR spectrum measured for ¹⁵N-**1**-BF₃ displayed only a broad singlet at 592 ppm. This value is shifted upfield quite considerably (248 ppm) with respect to ¹⁵N-**1**.

Crystallographic characterization of **1**-BF₃ confirmed the formation of a σ -bond through donation of the terminal nitride N-lone pair into the vacant *p*-orbital on the Lewis acidic boron center (Figure 3).³⁴ The N–B bond distance of 1.609(7) Å is similar to those

reported in the literature for other Lewis acid adducts of nitridometal complexes.^{35–37} Complex **1**-BF₃ crystallized in the space group *P*-1 with the B–F bonds of the Lewis acid staggered with respect to the Mo–N_{amide} bonds. The Mo≡N bond length (1.678(4) Å) in **1**-BF₃ was identical (to within 3σ) to the Mo≡N bond in NMo(N[^tBu]Ph)₃ and, as expected, the Mo–N–B bond angle was nearly linear (177.6(4)°).

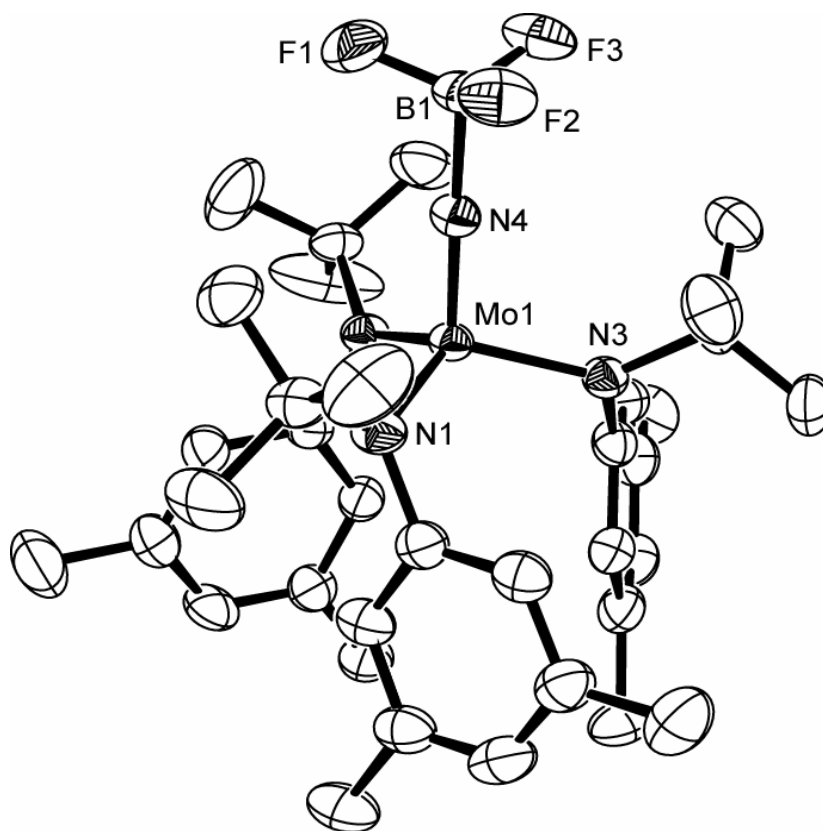


Figure 3. ORTEP representation of **1**-BF₃ with thermal ellipsoids at the 35% probability level. A single CH₂Cl₂ solvent molecule of crystallization has been omitted for clarity.

Complexes **1**-GeCl₂ and **1**-SnCl₂ were found (by X-ray crystallography) to be isomorphous (Figure 4). To the best of our knowledge, complexes **1**-GeCl₂ and **1**-SnCl₂ represent the first examples of coordination at the terminally bound nitrogen in a nitridometal complex by a divalent germanium or tin halide^{38,39}. Upon addition of GeCl₂·dioxane or SnCl₂ to **1**, simple Lewis acid adducts analogous to those of the Group 13 **1**-LA complexes were formed. Complexes **1**-GeCl₂ and **1**-SnCl₂ were characterized

by Mo≡N bond lengths of *ca.* 1.70 Å and N–Ge (or N–Sn) bond lengths typical of single bonds.

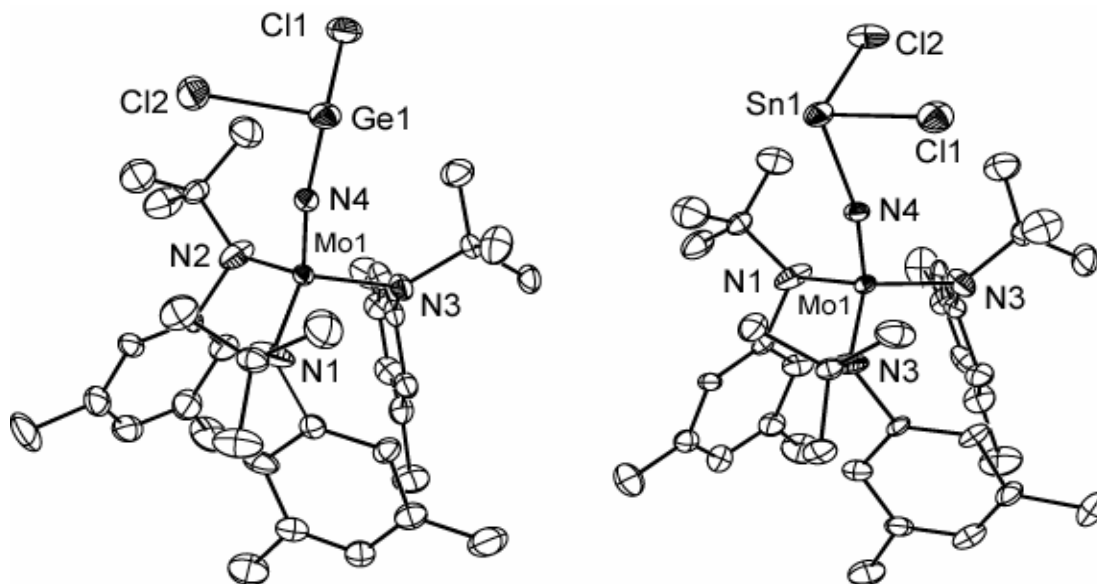


Figure 4. 35% thermal ellipsoid (ORTEP) representations of **1**-GeCl₂ (left) and **1**-SnCl₂ (right).

Transition-metal imido complexes containing an Mo≡NR bonding motif are well documented in the literature.^{40,41} Reaction of **1** with electrophiles, RX (R = CH₃, X = I and R = Me₃Si, X = SO₃CF₃ = OTf), afforded the imido salts [**2a**]I⁴² and [**2b**]OTf as bright yellow, pentane insoluble powders in high yield (92% and 89% respectively, Figure 2). In the ¹H NMR spectrum of ¹⁵N-[**2a**]I a two-bond coupling (²J_{N-H}) of 3.3 Hz was resolved for the methyl protons (¹⁵N–CH₃). Solution ¹⁵N{⁻¹H} NMR spectra for [**2a**]I and [**2b**]OTf displayed resonances at 463 and 537 ppm respectively.

The imido complex [**2b**]OTf crystallized in the cubic space group *P*2₁3 (Figure 5). The Mo–N–Si bond angle is linear as mandated by its alignment with the crystallographic *C*₃ axis. The Mo≡N bond distance of 1.715(6) Å was lengthened 0.057 Å with respect to the Mo≡N bond distance in **1** while the N–Si bond distance of 1.795(6) Å was slightly longer (~0.08 Å) than might be expected for a single N–Si bond.⁴³ While complex [**2a**]I has not been structurally characterized, the cation [CH₃NMo(N[^tBu]Ar)₃]⁺

[**2a**] is presumably a 4-coordinate monomer related to the trimethylsilylimido cation $[(\text{CH}_3)_3\text{Si}-\text{NMo}(\text{N}[\text{tBu}]\text{Ar})_3]^+$ [**2b**].

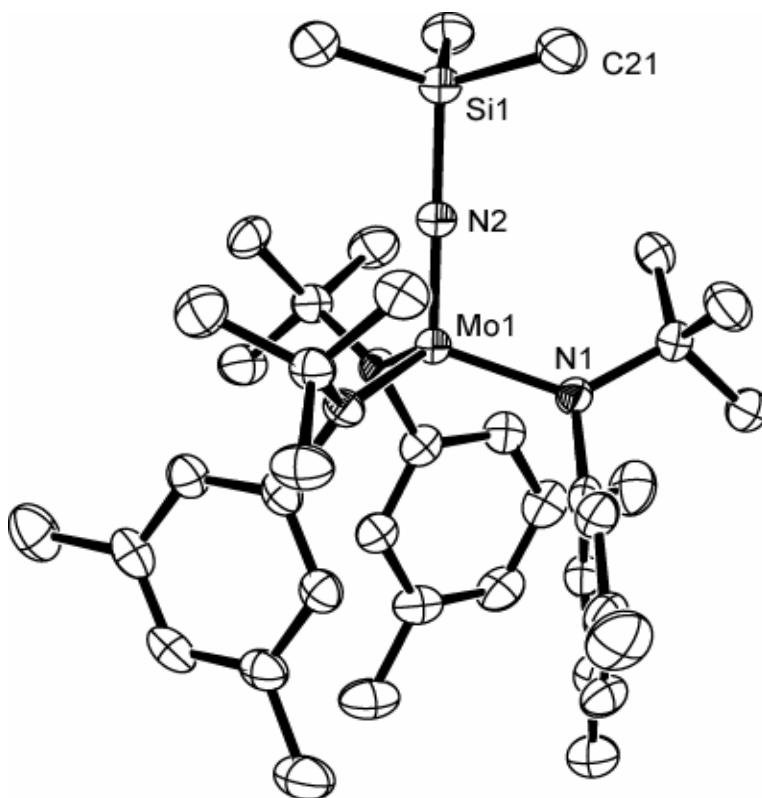


Figure 5. 50% thermal ellipsoid (ORTEP) representations of cation [**2b**].

Reaction of benzoyl triflate, $\text{PhC}(\text{O})\text{OTf}$ with **1** in CH_2Cl_2 enabled isolation of the red-orange benzoylimido complex $[\text{PhC}(\text{O})\text{NMo}(\text{N}[\text{tBu}]\text{Ar})_3]\text{OTf}$ [**2c**] OTf in 72% yield. There have been very few reports of the use of benzoyl triflate in synthetic inorganic chemistry despite this reagent's obvious utility as a potent electrophile.^{44,45,46} There are similarly few reports of transition metal complexes containing a benzoylimido moiety i.e. $\text{PhC}(\text{O})\text{N}\equiv\text{M}$.⁴⁷⁻⁵⁰ X-ray crystallographic characterization of [**2c**] OTf showed that the $\text{Mo}\equiv\text{N}$ bond is lengthened slightly with respect to the $\text{Mo}\equiv\text{N}$ bond in complex **1** (Figure 6). The $\text{N4}-\text{C41}$ bond of 1.422(5) Å is in the range typical for an N–C single bond suggesting that resonance forms involving N–C multiple bond character do not provide added stabilization in this complex.

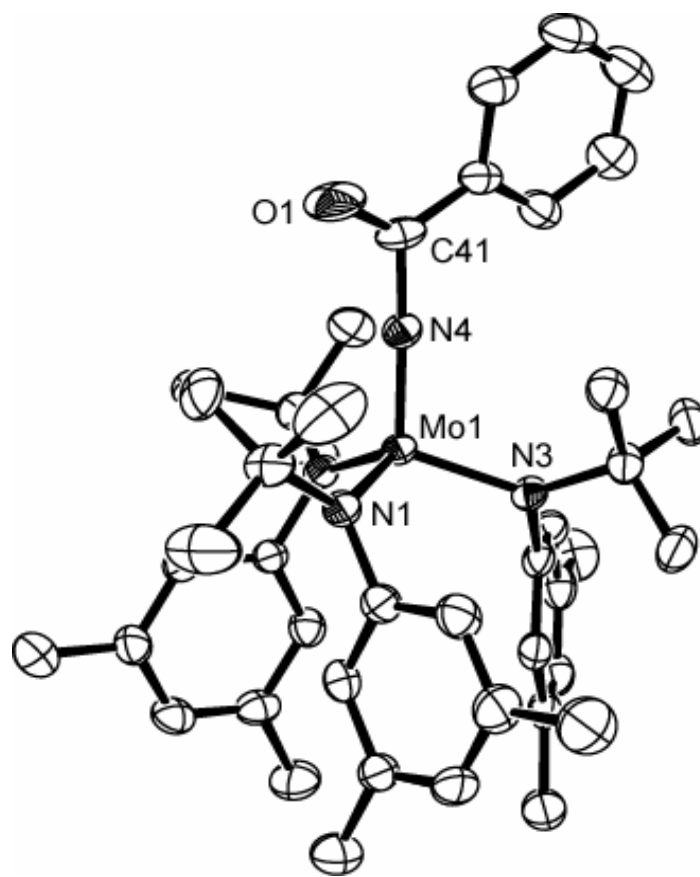


Figure 6. 50% thermal ellipsoid (ORTEP) representations of cation [2c]. A single THF solvent molecule of crystallization has been omitted for clarity.

Dehydrohalogenation of [2a]I was achieved using lithium hexamethyldisilazide in pentane (Figure 7) and resulted in isolation of the purple ketimide complex $\text{H}_2\text{CNMo}(\text{N}[\text{tBu}]\text{Ar})_3$ (**3**). Complex **3** provides a rare example of terminal $-\text{NCH}_2$ complexation,^{51–54} and represents the first example of such ligation to be structurally characterized (Figure 8). The ketimide N–C bond distance of 1.300(7) Å is consistent with the presence of an N–C double bond. The Mo–N bond distance of 1.777(4) Å is in the range between that of a Mo–N double bond and that of a Mo–N single bond. This multiple bond character is the result of π -donation from a filled Mo *d*-orbital into the ketimide $\pi^*(\text{N}-\text{C})$ molecular orbital and in the perpendicular plane, π -donation from the nitrogen lone pair of electrons into a vacant Mo *d*-orbital. Complex **3** has a distorted tetrahedral geometry (average N–Mo–N_{amide} bond angle 101.7°) with pseudo- C_3 point

symmetry courtesy of the nearly linear ($178.0(4)^\circ$) Mo–N–C bond axis of the ketimide moiety (which lies along the pseudo- C_3 axis).

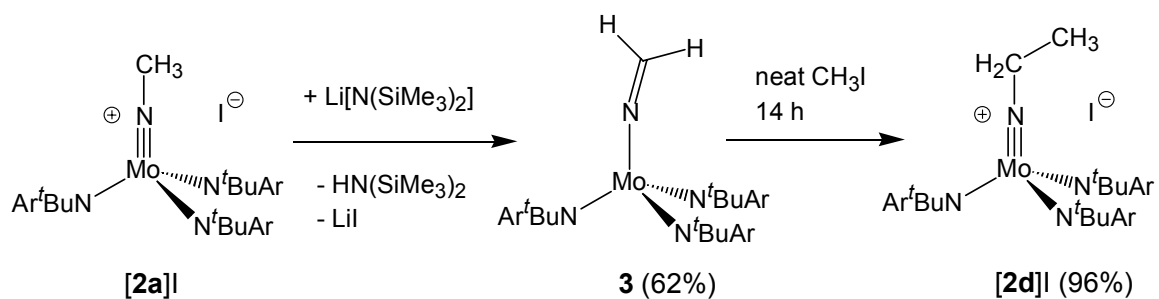


Figure 7. Dehydrohalogenation of [2a]I in the formation of **3** and subsequent reaction with CH₃I to form [2d]I.

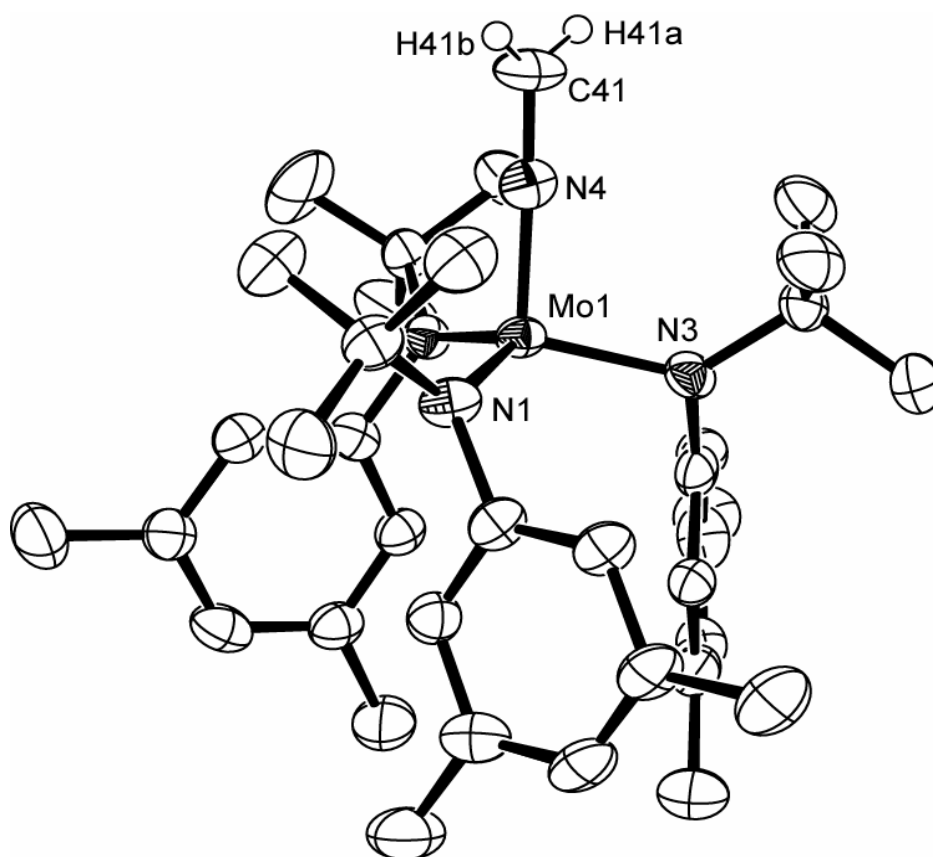


Figure 8. 50% thermal ellipsoid (ORTEP) representation of **3**. Ketimide hydrogens, H41a and H41b, were located and refined anisotropically.

The overall sequence leading to complex **3** can be viewed as formal carbene (CH_2) addition to **1**. Addition of the Group 14 halides GeCl_2 and SnCl_2 to **1** did not give products analogous to **3** (i.e. oxidation $\text{Ge/Sn}^{\text{II}} \rightarrow \text{Ge/Sn}^{\text{IV}}$ with concomitant formation of a molybdenum(IV) complex $\text{Cl}_2\text{Ge}=\text{NMo}(\text{N}[\text{tBu}]\text{Ar})_3$). This observation is consistent with the increased stability of divalent Group 14 species as the group is descended.⁵⁵

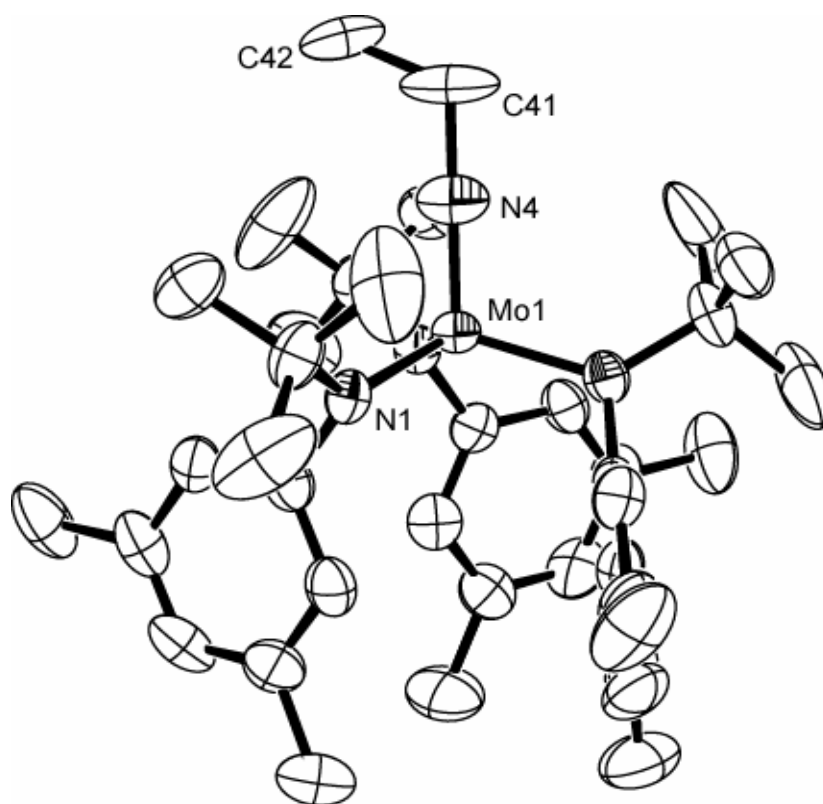


Figure 9. 50% thermal ellipsoid (ORTEP) representation of cation [**2d**]. A single CH_2Cl_2 solvent molecule of crystallization has been omitted for clarity.

Synthesis of the ethylimido complex $[\text{CH}_3\text{CH}_2\text{NMo}(\text{N}[\text{tBu}]\text{Ar})_3]\text{I}$ [**2d**]I, was achieved by reaction of **3** with CH_3I (Figure 7). This reaction demonstrates the nucleophilicity of the ketimide carbon in **3** and is in direct contrast with organic ketimines ($\text{RN}=\text{CH}_2$) which are electrophilic at carbon.⁵⁶ Interestingly, we were unable to generate [**2d**] *via* the reaction of **1** with a suitable source of $[\text{CH}_3\text{CH}_2]^+$ (e.g. EtI , EtOTf , $[\text{Et}_3\text{O}]\text{BF}_4$). The inability to generate [**2d**] in this way is consistent with the

dramatic decrease in rate observed for other nucleophilic substitution reactions (S_N2) upon increasing the steric bulk at the α -carbon of the alkyl electrophile (methyl>>ethyl>propyl).⁵⁷ Crystallographic characterization of [**2d**]I showed that an N–C single bond (1.457(11) Å) and an Mo–N triple bond (1.708(9) Å) are formed upon the reaction of complex **3** with CH₃I (Figure 9).

1.2.2 ¹⁵N Solid state CP/MAS NMR Spectroscopy of ¹⁵NMo(N[^tBu]Ar)₃ (**1**)

Measurement of the ¹⁵N solid state CP/MAS NMR spectrum of ¹⁵NMo(N[^tBu]Ar)₃ (**1**) was carried out, in order to probe experimentally the electronic structure at nitrogen. The principal components of the chemical shift tensor can be extracted from the experimental data by simulation of the experimental spectrum or by the analysis of the relative intensities of the spinning sidebands.^{58,59} The experimentally measured values of the shift tensor components for **1** and each of its derivatives are presented in Table 1.

The experimental, simulated and DFT calculated ¹⁵N solid state CP/MAS NMR spectra of **1** (calculated spectrum of complex **1m**) are presented in Figure 10. In the absence of unusual averaging effects, the shift parameter measured in solution for a given complex is equal to the isotropic chemical shift, which is calculated as the average of the principal components of the chemical shift tensor [$\delta_{\text{iso}} = \frac{1}{3}(\delta_{11} + \delta_{22} + \delta_{33})$].⁶⁰ Indeed, the isotropic shift (δ_{iso}) of 833 ppm determined for complex **1** from the solid state NMR spectrum is in close agreement with the ¹⁵N solution NMR shift of 840 ppm. The axial symmetry of complex **1** constrains the orientation of the principal components of the ¹⁵N chemical shift tensor such that the unique axis is aligned along the Mo≡N bond. Our experimental results confirm the axial nature of the chemical shift tensor ($\delta_{11} = \delta_{22} = 1229$ ppm).

Table 1. Experimental and calculated ^{15}N chemical shielding tensors for **1** and derivatives thereof. δ_{iso} is the isotropic shift, Ω is the span defined as $\delta_{11} - \delta_{33}$; κ is the skew of the shielding tensor defined as $[3(\delta_{22} - \delta_{\text{iso}})/(\delta_{11} - \delta_{33})]$; $\chi^2 = \Sigma ((\text{obs-calc})^2)/\text{calc}$.

Cplx	Model	Principal Components of Shielding Tensor (ppm)						Principal Components of Shielding Tensor (ppm)						χ^2
		Experimental						Calculated						
		δ_{iso}	δ_{11}	δ_{22}	δ_{33}	Ω	κ	δ_{iso}	δ_{11}	δ_{22}	δ_{33}	Ω	κ	
1	1m	833	1229	1229	42	1186	1	795	1137	1136	113	1024	1	61
1-BF₃	1m-BF₃	593	836	836	107	729	1	630	878	875	137	741	0.99	12
1-BCl₃	1m-BCl₃	558	765	755	152	613	0.97	562	792	791	102	690	1	27
		555	765	747	154	611	0.94							
1-AlCl₃	1m-AlCl₃	602	849	839	119	730	0.97	624	873	872	128	745	1	3
1-AlBr₃		599	835	835	126	709	1							
1-AlI₃		598	828	828	139	689	1							
		595	810	810	165	646	1							
		591	809	809	156	653	1							
1-GaCl₃	1m-GaCl₃	590	834	826	110	725	0.98	635	886	885	133	753	1	14
1-InCl₃	1m-InCl₃	608	877	876	72	805	1	645	902	902	131	771	1	30
		603	846	846	117	728	1							
1-GeCl₂	1mGeCl₂	643	918	918	93	826	1	660	930	928	123	807	1	8
1-SnCl₂	1m-SnCl₂	666	955	955	89	866	1	669	944	938	125	819	0.99	11
[2a]I	2a-m	457	614	614	143	471	1	465	610	610	174	436	1	6
		453	611	611	136	475	1							
		441	594	594	137	457	1							
		436	576	576	156	420	1							
[2b]OTf	2b-m	541	736	724	163	573	0.93	556	758	758	153	605	1	3
[2c]OTf	2c-m	467	598	597	207	391	1	507	695	642	183	513	0.79	23
[2d]I	2d-m	460	614	612	154	460	0.99	486	653	637	168	485	0.93	6
3	3m-C₃	446	591	591	154	437	1	458	600	563	212	388	0.81	18
	3m-C_s							448	570	457	318	252	0.11	125

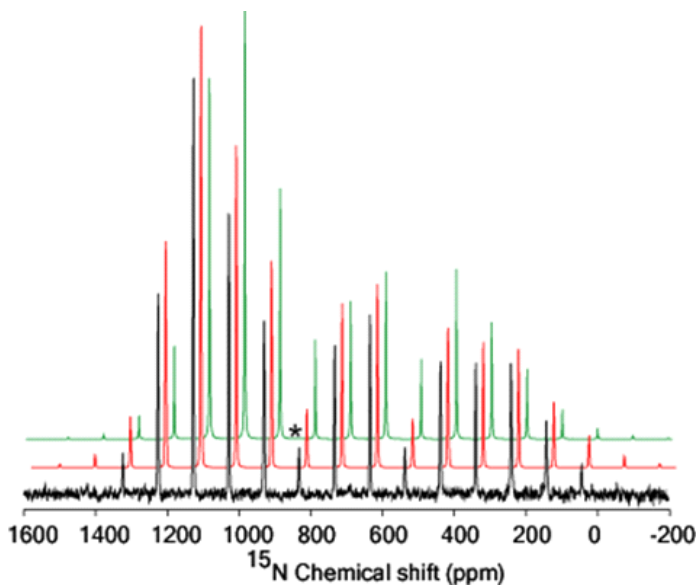


Figure 10. Experimental (—) and simulated (—) ^{15}N solid state CP/MAS NMR spectra for complex **1** and DFT calculated (—) NMR spectrum for complex **1m**. The simulated and calculated spectra are offset with respect to the experimental spectrum for clarity. The isotropic peak (δ_{iso}) is indicated by an asterisk.

A feature of the spectrum that is immediately obvious is the enormous span ($\Omega = \delta_{11} - \delta_{33}$) of the chemical shift anisotropy (CSA) tensor ($\Omega = 1186$ ppm). This effect is largely due to a significant paramagnetic shift at nitrogen when the external magnetic field is oriented perpendicular to the $\text{Mo}\equiv\text{N}$ bond. An understanding of the origin of this paramagnetic contribution was ascertained by analysis of density functional calculations (see section 3.1) performed on the model complex $\text{NMo}(\text{NH}_2)_3$ (**1m**).

1.2.3 ^{15}N Solid state CP/MAS NMR Spectroscopy of the Lewis acid adducts of **1** (**1-LA**)⁶¹

The isotropic shift of **1-BF₃** ($\delta_{\text{iso}} = 593$ ppm) determined from the experimental ^{15}N solid state NMR spectrum is in excellent agreement with δ_{iso} (591 ppm) measured in solution. The axial symmetry of **1-BF₃** was confirmed by solid state NMR measurements

($\delta_{11} = \delta_{22} = 836$ ppm). All other Lewis acid adducts of **1** (**1-LA**) exhibited similarly axially symmetric chemical shift tensors. The isotropic shift for the Lewis acid adducts (**1-LA**) studied was shifted upfield by 174 ppm (**1-SnCl₂**) to 285 ppm (**1-BCl₃**) with respect to the terminal nitride (**1**). This upfield shift in the magnitude of δ_{iso} can be explained by a reduction in the energy gap between occupied frontier molecular orbitals and low-lying virtual molecular orbitals upon coordination of a Lewis acid to the terminally bound N-atom. This information can be extracted from density functional calculations performed on model complexes (**1m-LA**) and is discussed in section 3.2.

The span (Ω) of the ^{15}N chemical shift tensor was reduced upon coordination of a Lewis acid, from 1186 ppm in **1** to between 866 ppm (**1-SnCl₂**) and 611 ppm (**1-BCl₃**). While the magnitude of the most shielded component δ_{33} varied over *ca.* 90 ppm for **1-LA**, the perpendicular components of the shift tensor, δ_{11} and δ_{22} (referred to as δ_{\perp}), varied over *ca.* 200 ppm. Thus, the variation in the span may be attributed primarily to changes in the perpendicular component of the ^{15}N chemical shielding tensor (δ_{\perp}). Again, this observation can be explained by analysis of the density functional calculations (section 3.2).

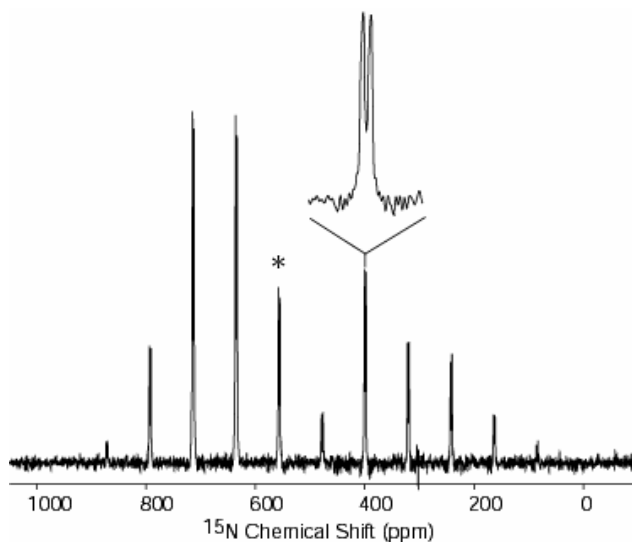


Figure 11. Experimental ^{15}N solid state CP/MAS NMR spectrum of **1-BCl₃**. The expanded portion of the spectrum shows the multiplicity of one of the spinning sidebands. The isotropic peak is marked with an asterisk.

The ^{15}N solid state NMR spectrum of **1**- BCl_3 displayed multiplicity in the isotropic peak and each of the associated spinning sidebands (Figure 11). Two unique sets of data, which differed in the magnitude of the isotropic shift (558 and 555 ppm) and the span of the chemical shift tensor (613 and 611 ppm), were obtained on simulation of the experimental spectrum. Similar multiplicity was observed in the spectra acquired for **1**- AlCl_3 and **1**- InCl_3 . This feature could be attributed either to coupling of ^{15}N with the adjacent spin-active nucleus or structural polymorphism.⁶²⁻⁶⁴

1.2.4 ^{15}N Solid state CP/MAS NMR Spectroscopy of the imido complexes **[2a]**I, **[2b]**OTf, **[2c]**OTf and **[2d]**I.⁶⁵

The cations **[2a]** and **[2b]** are three-fold symmetric and bear close resemblance to the Lewis acid adducts **1**- EX_3 . The axial symmetry of **[2a]** was apparent from the tensor components determined by simulation of the ^{15}N solid state NMR spectrum ($\delta_{11} = \delta_{22}$). The spectrum acquired for the ethylimido complex **[2d]**I was very similar to that of the methylimido complex **[2a]**I in terms of the isotropic shift, span and skew of the chemical shift tensor.

Complex **[2b]**OTf showed unexpected asymmetry in the values of the chemical shift tensor (i.e. $\delta_{11} \neq \delta_{22}$). Interestingly, the spectrum of **[2b]**OTf was more reminiscent of those acquired for the Lewis acid adducts (**1**-LA) in terms of the chemical shift tensors (δ_{nn}) and the span of the spectrum than either of the imido complexes **[2a]**I or **[2d]**I.

The acylimido complex **[2c]**OTf is unique in the series of imido complexes that are presented in this study for two reasons: (i) significant asymmetry is present in **[2c]**OTf due to the coordination of the $[\text{PhC}(\text{O})]^+$ electrophile to the terminal nitrogen; (ii) the presence of a carbonyl functional group on the fragment coordinated to N provides an opportunity for resonance stabilization of this imido complex. The lack of an axis of symmetry in **[2c]**OTf would be expected to give a rhombic chemical shift tensor ($\delta_{11} \neq \delta_{22} \neq \delta_{33}$). Rather unexpectedly, this asymmetry was not reflected in the experimental values of the chemical shift tensor for which $\delta_{11} = 598$ ppm, $\delta_{22} = 597$ ppm

and $\delta_{33} = 207$ ppm. These chemical shift tensors indicate that the Mo \equiv N moiety is not significantly perturbed by the coordination of a [PhC(O)]⁺ electrophile.

The span (Ω) of the ¹⁵N chemical shift tensors for the four imido complexes was in the range of 391 to 573 ppm, which is smaller than for both **1** ($\Omega = 1186$ ppm) and the LA adducts (**1**-LA $\Omega = 866$ – 611 ppm). This reduction in the span could be attributed (in all four complexes) to the reduced magnitude of the most deshielded component of the chemical shift tensor, δ_{11} . Again, analysis of density functional calculations performed on model complexes enabled a rationalization of this effect in terms of perturbation of the electronic structure of **1** upon coordination of an electrophile (section 3.3).

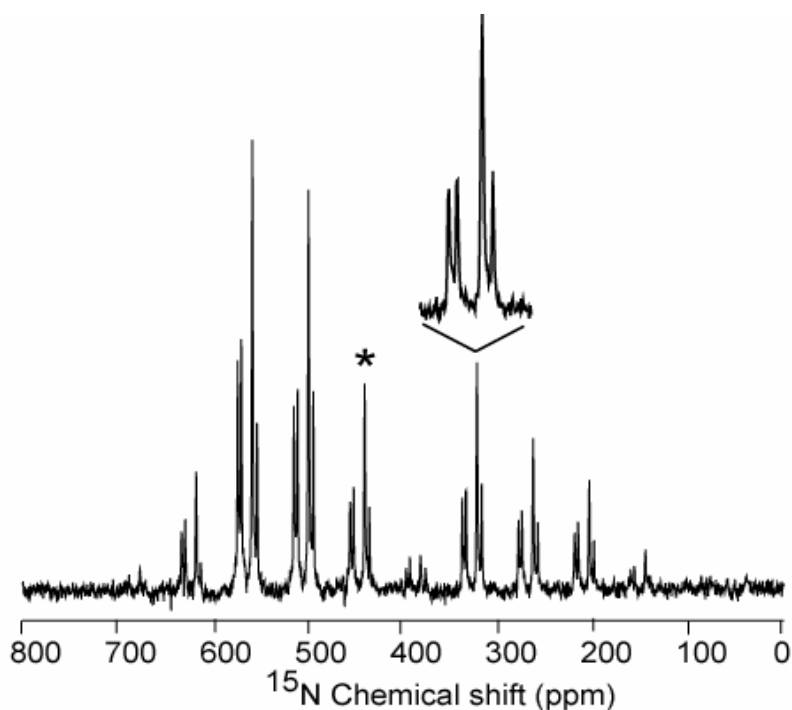


Figure 12. Experimental ¹⁵N solid state CP/MAS NMR spectrum of [**2a**]I. The expanded portion of the spectrum shows the multiplicity of one of the spinning sidebands. The isotropic peak is marked with an asterisk.

Multiplicity in the isotropic peak and the associated spinning sidebands was observed in the ¹⁵N solid state NMR spectrum of [**2a**]I (Figure 12). Four isotropic peaks

were identified and the span of the chemical shift tensor varied between 420 and 475 ppm. Unlike the Lewis acid adducts (**1-LA**) for which this multiplicity might be attributed to the adjacent spin-active nucleus, complex [**2a**]I is thought to display this multiplicity due to structural polymorphism.⁶²⁻⁶⁴

1.2.5 ¹⁵N NMR Spectroscopy of H₂CNMo(N[^tBu]Ar)₃ (**3**)

The experimental ¹⁵N solid state NMR spectrum of **3** displays a number of noteworthy features. First, the principal components of the chemical shift tensor suggest that complex **3** is axially symmetric ($\delta_{11} = \delta_{22} = 591$ ppm). This symmetry is expected due to the Mo–N multiple bonding in **3** which is attributed to the π -donor/acceptor character of the ketimide (NCH₂) ligand. The isotropic peak in the ¹⁵N solid state NMR spectrum was in close agreement with that obtained in solution. Complex **3** has the most shielded value of δ_{11} with respect to all other complexes measured in this study and a narrow span of the shift tensor ($\Omega = 437$ ppm).

1.3 Chemical shielding: Experimental measurement and computational analysis⁶⁰

The measurement of solid state NMR spectra allows for the experimental determination of the principal components (δ_{11} , δ_{22} and δ_{33}) of the chemical shift tensors. To complement our experimental measurements and enable a more complete analysis of these compounds at the electronic level, DFT calculations were performed on model complexes in which the bulky amido ligands N[^tBu]Ar were replaced by three NH₂ ligands (for computational expediency). In most cases, the calculated tensors compared favorably with the experimental data⁶⁶ thus discussion of the electronic structure based on DFT calculations can be assumed to be valid. A summary of the analysis of the chemical shielding tensors, together with equations relevant to this analysis, are presented here in brief.

The absolute shielding tensor σ (calculated using DFT), is related to the chemical shift tensor δ (Equation 2):

$$\delta = \sigma_{\text{ref}} - \sigma \quad (2)$$

where σ_{ref} is the calculated absolute shielding tensor of the reference compound. NMR calculations based on the density functional method have been used to identify the individual contributions to the total shielding tensor made by the diamagnetic (σ_{dia}), paramagnetic (σ_{para}) and spin orbit (σ_{so}) components (Equation 3):

$$\sigma_{\text{total}} = \sigma_{\text{dia}} + \sigma_{\text{para}} + \sigma_{\text{so}} \quad (3)$$

For complexes presented in this study, spin orbit contributions to the total shielding tensor were included^{67,68} but in most cases this contribution was found to be negligible.⁶⁹ The diamagnetic contribution is dependent upon the core electron density and acts to reduce the applied magnetic field at the nucleus under observation. In the presence of an applied field σ_{dia} will generally show insignificant variation in its contribution to the total shielding tensor. The paramagnetic contribution reinforces the applied field and is determined primarily by magnetic perturbation of the frontier molecular orbitals. Overall, σ_{para} shows the most significant variation in its contribution to the total shielding tensor due to the sensitivity of this term to changes in the electronic environment.^{70,71} The paramagnetic contribution to the shielding tensor (σ_{para}) is proportional to the magnetic coupling of high-lying occupied molecular orbitals with low-lying virtual molecular orbitals (M_k) and inversely proportional to the energy difference between these orbitals ($e_{\text{occ}} - e_{\text{vir}}$). The Gauge Including Atomic Orbitals (GIAO) formalism makes it possible to analyze the contributions to the shielding in terms of orbital contributions.⁷²⁻⁷⁷ A molecular orbital analysis of these contributions is contained within the NMR output file of a density functional calculation.⁷⁸ This analysis provides a list of the leading contributions to the k^{th} component ($k = 1, 2, 3$) of the magnetic field and includes information about the individual pairs of molecular orbitals (which mix in the applied field), the energy difference between these orbitals ($e_{\text{occ}} - e_{\text{vir}}$) and the magnitude of the coupling (M_k). Occasionally, one pair of magnetically-coupled molecular orbitals is

found to provide the major contribution to the paramagnetic deshielding for each component of the magnetic field (k_1 , k_2 and k_3).

1.3.1 Theoretical studies on $^{15}\text{NMo}(\text{N}[\text{tBu}]\text{Ar})_3$ (**1**)

The NMR shift calculation for **1m** predicted an axially symmetric chemical shift tensor in which $\delta_{11(\text{calc})} = \delta_{22(\text{calc})} = 1137$ ppm. The primary contributions to $\delta_{11(\text{calc})}$ and $\delta_{22(\text{calc})}$ resulted from rotational mixing in the presence of an applied field of HOMO-3, $\sigma(\text{N } p_z - \text{Mo } d_z^2)$ with LUMO, $\pi^*(\text{N } p_y - \text{Mo } d_{yz})$ and LUMO+1, $\pi^*(\text{N } p_y - \text{Mo } d_{yz})$. There is a relatively small energy gap ($e_{\text{occ}} - e_{\text{vir}}$) between the filled N p_z orbital (of A symmetry in the point group C_3), which contains the nitrogen lone pair, and the empty $\pi^*(\text{Mo}-\text{N})$ orbitals (a degenerate E set in C_3). Since the paramagnetic contribution to the chemical shielding tensor is proportional to the coupling between these virtual and occupied orbitals and inversely proportional to the energy gap between them, it follows that the components of the shift tensor (δ_{11} and δ_{22}) that are aligned perpendicular to the $\text{Mo}\equiv\text{N}$ bond will exhibit extreme paramagnetic shifts.

The large paramagnetic contribution to the perpendicular components of the chemical shift tensor (δ_{\perp}) is reminiscent of that observed for related terminal phosphide and carbide complexes.^{19,79} In all three examples, the principal contributions to δ_{\perp} are the result of mixing in the applied field of a high-lying orbital of σ -symmetry with a relatively low-lying doubly degenerate E set of π -symmetry.

For **1** and the derivatives presented in this article, there is a much less significant variation in the magnitude of the most shielded component (δ_{33}) compared to either δ_{11} or δ_{22} . Where as $\delta_{11(\text{expt})}$ varies over 653 ppm (1229 ppm to 576 ppm), $\delta_{33(\text{expt})}$ varies over a much smaller range of 165 ppm (from 207 to 42 ppm). This can be understood if one considers the chemical shift for a linear molecule. The shift in C_{∞} symmetric molecules is dominated by the diamagnetic contribution; the paramagnetic contribution disappears completely along the molecular axis. In **1**, a paramagnetic component to the shift tensor is introduced when the C_{∞} symmetry of the $\text{Mo}\equiv\text{N}$ axis is broken by the addition of

ligands to the metal. This paramagnetic component of δ_{33} is fairly constant for all of the complexes presented herein.

1.3.2 Theoretical studies on the Lewis acids adducts of **1** (1-LA)

DFT calculations performed on the model complexes **1m**-LA predicted the Lewis acid adducts to be axially symmetric, as evidenced by the calculated skew of the tensor ($\kappa = 1$ or 0.99 in all cases). The optimized geometry of **1m**-BF₃ predicted similar Mo–N and N–B bond lengths to those measured for **1**-BF₃, however, in the model complex the B–F bonds of the Lewis acid were eclipsed with respect to the Mo–N_{amide} bonds. Calculations were performed on model complexes in which either the eclipsed or staggered geometries were enforced in order to gauge the effect of rotation about the N–LA bond on the ¹⁵N chemical shift. In general, calculations for the eclipsed and staggered geometries predicted very similar values of the principal components of the ¹⁵N chemical shift tensor.

In each of the model Lewis acid adducts (**1m**-LA) the principal contributions to δ_{\perp} resulted from rotational mixing in the applied field of an occupied σ -orbital with a vacant $\pi^*(\text{Mo–N})$ orbital. The occupied orbital is characterized by significant N p_z character, involved in donation of the N-lone pair into the vacant orbital on the Lewis acid's central atom. For example, analysis of the DFT calculation performed on **1m**-GaCl₃ shows that the principal contributions to δ_{11} and δ_{22} are provided by mixing in the applied field of HOMO–6, $\sigma(\text{N } p_z \text{ –LA } sp)$ with LUMO, $\pi^*(\text{N } p_y \text{ –Mo } d_{yz})$ and LUMO+1, $\pi^*(\text{N } p_x \text{ –Mo } d_{xz})$ respectively.

The energy gap ($e_{\text{occ}} - e_{\text{vir}}$) between the occupied $\sigma(\text{N–LA})$ bonding orbital and the vacant $\pi^*(\text{Mo–N})$ orbitals was found to depend principally on the extent to which Lewis acid coordination to the terminal N-atom lowers the energy of the $\sigma(\text{N } p_z \text{ –LA } sp)$ orbital. In **1**, the occupied (N p_z) orbital contains a non-bonding lone pair of electrons and is at a relatively high energy. Formation of a σ -bond to the Lewis acid lowers the energy of this orbital thereby increasing the energy gap between the magnetically-coupled virtual and

occupied orbitals ($e_{\text{occ}}-e_{\text{vir}}$). This in turn reduces the paramagnetic contribution to the perpendicular component of the chemical shift tensor resulting in more upfield shifted values of δ_{11} and δ_{22} .

Complex **1m**-BCl₃ has a smaller energy gap ($e_{\text{occ}}-e_{\text{vir}} = 3.65$ eV) compared to **1m**-BF₃ ($e_{\text{occ}}-e_{\text{vir}} = 5.06$ eV) but also a reduced paramagnetic contribution to the chemical shift, as evidenced by the more upfield shift of $\delta_{11(\text{calc})}$. This apparently anomalous result can be explained if one accounts for the proportional relationship between the paramagnetic contribution to the chemical shift and the magnitude of the coupling (M_k) of occupied and virtual molecular orbitals in the presence of an applied magnetic field. Analysis of the DFT calculations for these two complexes shows that M_k in **1m**-BF₃ (0.438) is more than twice that calculated for **1m**-BCl₃ (0.206). This suggests that a much larger contribution to the paramagnetic term is made by N-based orbitals in **1m**-BF₃ compared to **1m**-BCl₃.

1.3.3 Theoretical studies on the imido cations [2a-m], [2b-m], [2c-m] and [2d-m]

Calculations performed on the model cations [2a-m] and [2b-m] predicted axially symmetric spectra ($\delta_{11(\text{calc})} = \delta_{22(\text{calc})}$), which were in close agreement with the data obtained experimentally for complexes [2a]I and [2b]OTf. Upon formation of an N-E (E = C or Si) single bond in these imido complexes there is a more significant lowering in energy of the $\sigma(\text{N-E})$ molecular orbital compared to that observed for the Lewis acid adducts (**1**-LA) discussed previously. This can be attributed to the build up of positive charge on the complex and the increased bond strength of the $\sigma(\text{N-E})$ bond compared to the $\sigma(\text{N-LA})$ bond. All four of the imido complexes exhibit a significant energy gap ($e_{\text{occ}}-e_{\text{vir}}$) between the filled $\sigma(\text{N-E})$ orbital to the lowest lying unoccupied orbitals of π -symmetry. The stabilization of this $\sigma(\text{N-E})$ bonding orbital prohibits its participation in mixing interactions that supplement the paramagnetic contribution to the chemical shift tensor. For the model cations [2a-m], [2b-m] and [2d-m] the principal contributions to δ_{\perp} result from rotational mixing in the applied field of two occupied orbitals of π -symmetry (a doubly degenerate E set) with a vacant orbital of σ symmetry (A symmetry

in C_3). Analysis of the DFT calculation performed on [**2b-m**] shows that the principal contributions to δ_{11} and δ_{22} ($\delta_{11(\text{calc})} = \delta_{22(\text{calc})} = 758$ ppm) are provided by mixing in the applied field of HOMO-1, $\pi(\text{Mo } d_{xz} - \text{N } p_x)$ and HOMO-2, $\pi(\text{Mo } d_{yz} - \text{N } p_y)$ with LUMO+2, $\sigma^*(\text{N } p_z - \text{Si } sp)$.

The lack of an axis of symmetry in the optimized geometry for model cation [**2c-m**] is immediately apparent from the calculated values of the chemical shift tensor for [**2c-m**] ($\delta_{11(\text{calc})} = 695$, $\delta_{22(\text{calc})} = 642$ and $\delta_{33(\text{calc})} = 183$ ppm). Our experimental results for complex [**2c**]OTf displayed smaller asymmetry ($\kappa = 1$) compared to the calculated spectrum ($\kappa = 0.79$). The experimental values of δ_{11} and δ_{22} are more deshielded in [**2c**]OTf compared to both complexes [**2a**]I and [**2d**]I. Analysis of the NMR calculation carried out on [**2c-m**] provides the explanation for this phenomenon. The principal contribution to $\delta_{11(\text{calc})}$ is provided by mixing in the applied field of HOMO-3, $\sigma(\text{N } p_z - \text{C } sp)$ with LUMO+1, $\pi^*(\text{Mo } d_{xz} - \text{N } p_x)$. The principal contribution to $\delta_{22(\text{calc})}$ is provided by mixing in the applied field of HOMO-9, $\pi(\text{Mo } d_{xz} - \text{N } p_x)$ with LUMO+2, $\sigma^*(\text{N } p_z - \text{C } sp)$. For [**2c-m**] the $\sigma(\text{N } p_z - \text{C } sp)$ orbital is much higher in energy than the σ -orbital comprising the N-C bond in [**2a-m**] and [**2d-m**]. Indeed, the energy ordering of the frontier orbitals in [**2c-m**] is more reminiscent of that seen in the Lewis acid adducts (**1-LA**) than the other imido complexes. This implies that a weaker bonding interaction exists between the terminal N-atom and the electrophilic C-atom of the benzoyl fragment (compared to the interaction in other imido complexes) suggesting that resonance forms do not provide significant stabilization in complex [**2c**]OTf. These facts are consistent with the crystal structure of [**2c**]OTf in which the N-C single bond does not appear to be shortened through additional π -interactions.

1.3.4 Theoretical studies on $\text{H}_2\text{CNMo}(\text{N}[\text{tBu}]\text{Ar})_3$ (**3**)

The overall sequence leading to ketimide **3** embodies formal carbene (CH_2) addition to complex **1**, a process that encompasses C=N bond formation along with the reduction of molybdenum from the +6 to the +4 oxidation state.⁸⁰ Carbene addition to **1** is recognized as a potentially valuable means for the activation of complex **1** in the

context of nitrogen atom transfer from N_2 into organic molecules.⁸¹ It was therefore of interest to determine what insight solid state NMR spectroscopy could provide, in conjunction with DFT analysis of the experimental shift tensors into the electronic structure at this N-atom which is activated toward productive removal from the molybdenum complex into an organic product.

Interestingly, attempts to use DFT to reproduce the observed ^{15}N solid state CP/MAS NMR spectrum of **3** using $H_2CNMo(NH_2)_3$, (the structure of which converged to near C_s symmetry) as the computational model were not entirely satisfactory. We probed further and found that the larger model $H_2CNMo(N[CH_3]Ph)_3$ (**3m**) converged either to a pseudo- C_s (**3m- C_s**) or to a pseudo- C_3 (**3m- C_3**) conformation depending upon the initial geometry employed. The ^{15}N spectrum calculated for **3m- C_3** was a good match to the observed spectrum of **3** ($\chi^2 = 18$), while that calculated for **3m- C_s** deviated noticeably ($\chi^2 = 125$) (Figure 13). The two local minima for **3m** differ with respect to rotation about the Mo- N_{amide} bonds, leading to differing Mo- N_{amide} $d\pi - p\pi$ overlap, to which the ketimide nitrogen electronic environment is clearly sensitive. Analyses of the NMR calculation performed on **3m- C_3** reveals that the principal contributions to the most deshielded components of the tensor, δ_{11} and δ_{22} (600 and 563 ppm respectively), result from mixing in the applied field of HOMO, $\pi(N-C)$ with LUMO, $\pi^*(Mo d_{yz} - N p_y)$ and LUMO+1, $\pi^*(Mo d_{xz} - N p_x)$. The same orbitals are responsible for the paramagnetic contributions to δ_{11} and δ_{22} in **3m- C_s** ($\delta_{11} = 570$ ppm, $\delta_{22} = 457$ ppm) however, the energy gap ($e_{occ} - e_{vir}$) between the HOMO and LUMO orbitals in **3m- C_3** is appreciably smaller than in **3m- C_s** (1.498 eV versus 1.696 eV). This increased energetic separation of the orbitals in **3m- C_s** reduces the degree of magnetic coupling and results in a more shielded value of δ_{11} .

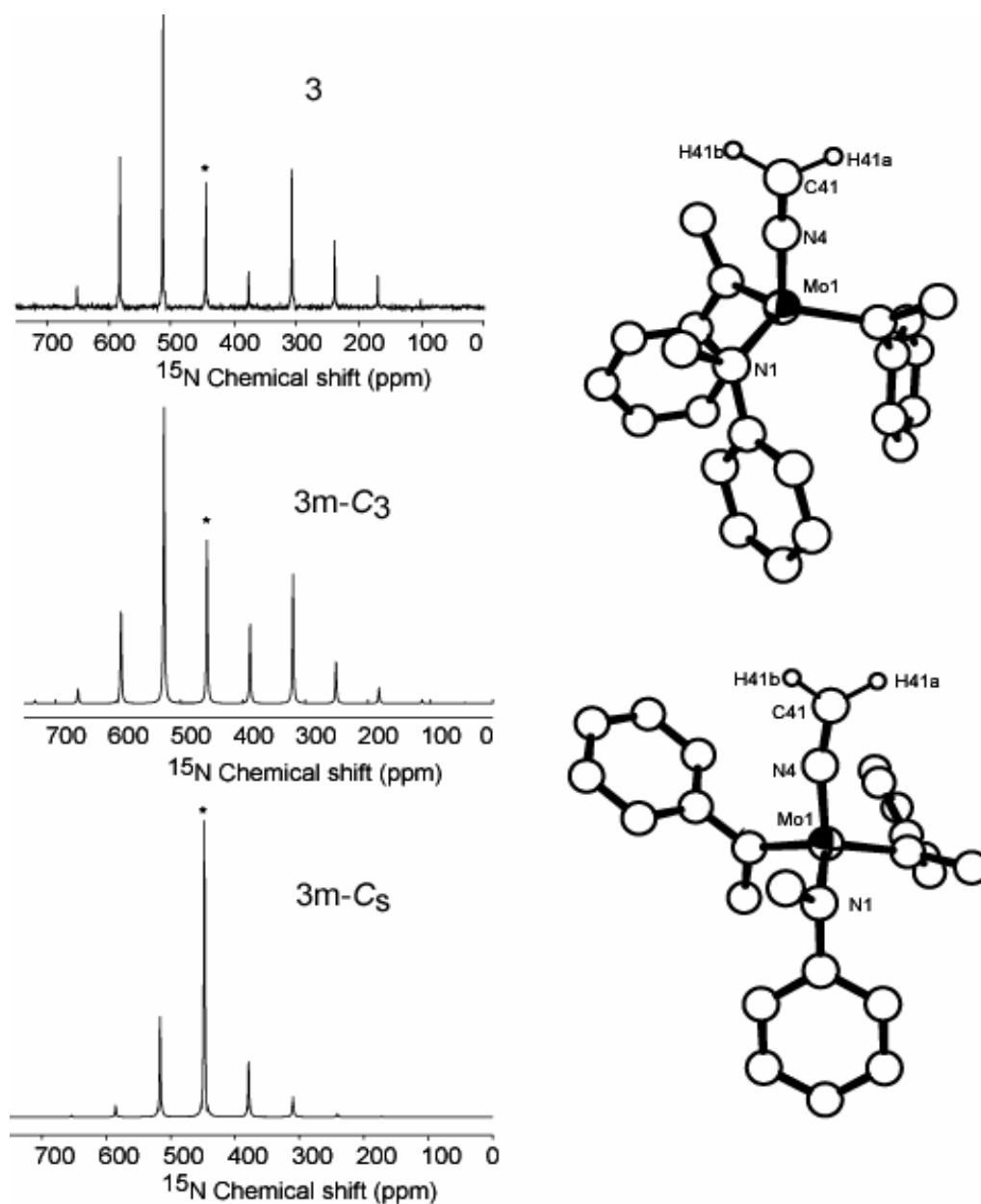


Figure 13. Optimized geometries for the model complexes **3m-C₃** (top) and **3m-C₅** (bottom) and solid state ^{15}N spectra for complex **3**: experimental (top), calculated **3m-C₃** (middle) and calculated **3m-C₅** (bottom). The isotropic peak is indicated by an asterisk.

In addition, the calculated molecular orbitals for **3m-C₃** show significant *p* orbital contribution from the ketimide carbon to the HOMO (Figure 14). This indicates that the ketimide carbon has been rendered nucleophilic upon dehydrohalogenation of the

methylimido complex [2a]I. Experimental evidence for this is demonstrated by the reaction of **3** with CH₃I to generate the ethylimido complex [2d]I.

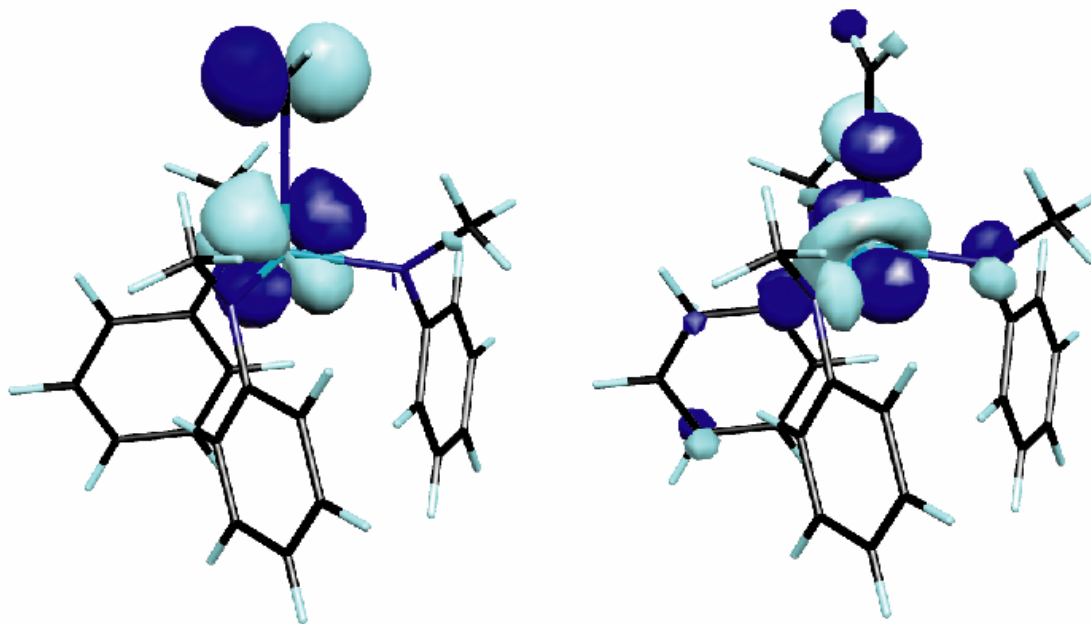


Figure 14. Calculated HOMO (left) and LUMO (right) of **3m-C₃**.

1.4. Concluding Remarks

The electronic structure of a dinitrogen-derived terminal molybdenum nitride complex $\text{NMo}(\text{N}[\text{tBu}]\text{Ar})_3$ (**1**) has been studied by the combined use of ¹⁵N solid state CP/MAS NMR spectroscopy and DFT calculations. Parallels may be drawn between the bonding observed in this terminal nitride complex and the analogous terminal phosphide and carbide complexes. Perturbation of the electronic structure in the terminal molybdenum nitride complex (**1**) upon coordination of a Lewis acid can be attributed to stabilization of a σ -symmetric orbital as a result of N–LA bond formation. Upon formation of a Lewis acid adduct of **1**, the increased energy gap ($\epsilon_{\text{occ}} - \epsilon_{\text{vir}}$) between magnetically-coupled occupied and virtual orbitals, is seen to correlate with a reduction in the magnitude of the perpendicular components of the chemical shift tensor (δ_{11} and δ_{22}).

The reaction of **1** with electrophiles RX, results in further stabilization of the σ -symmetric orbital containing the N-lone pair of electrons. The paramagnetic contribution to the chemical shift tensor in this series of cationic imido complexes results from rotational mixing in the applied field of high-lying $\pi(\text{Mo-N})$ orbitals with a low-lying $\sigma^*(\text{N-E})$ (E = C, Si) orbital.

Finally, the strength of this combined approach to studying the electronic structure of spin-active nuclei in transition metal complexes is highlighted by our investigations into a ketimide complex, $\text{H}_2\text{CNMo}(\text{N}[\text{tBu}]\text{Ar})_3$ (**3**). Computational studies performed on the model complex $\text{H}_2\text{CNMo}(\text{N}[\text{CH}_3]\text{Ph})_3$ (**3m**) identified two geometries to which this complex could converge. The variation in Mo-N $d\pi-p\pi$ overlap in the two structures is reflected in the calculated chemical shift tensors. A quantitative comparison of the experimental spectrum with the calculated spectra indicates that a closer match is provided by the pseudo- C_3 symmetric model, the optimized geometry of which is in good agreement with X-ray crystallographic data for complex **3**.

1.5. Experimental Section

1.5.1 General Information

Unless stated otherwise, all operations were performed in a Vacuum Atmospheres drybox under an atmosphere of purified nitrogen. Diethyl ether, pentane and dichloromethane were dried and deoxygenated using the method of Grubbs.⁸² THF was distilled from purple Na/benzophenone ketyl and collected under nitrogen. C_6D_6 and CDCl_3 were degassed and dried over 4 Å molecular sieves. $^{15}\text{N}_2$ was purchased from Cambridge Isotope Laboratories (CIL) in 0.1 mL break-seal glass vessels. CH_3I was, freeze-pump-thaw degassed and stored over 4 Å sieves prior to use. $\text{Mo}(\text{N}[\text{tBu}]\text{Ar})_3$ ²⁰ and benzoyl triflate⁴⁴ were prepared according to literature procedures. Other chemicals were purified and dried by standard procedures⁸³ or were used as received. Celite,

alumina and 4 Å molecular sieves were dried *in vacuo* for 36 h at ~250 °C. Infrared spectra were recorded on a Bio-Rad 135 Series FT-IR spectrometer.

1.5.2 X-ray Crystal Structure Determinations³⁴

The X-ray data collections were carried out on a Siemens Platform three-circle diffractometer mounted with a CCD or APEX CCD detector and outfitted with a low-temperature, nitrogen-stream aperture. The structures were solved by direct methods, with the exception of **1-BF₃**, which was solved using the Patterson Method, in conjunction with standard difference Fourier techniques and refined by full-matrix least-squares procedures. A summary of crystallographic data is given in Table 2. The systematic absences in the diffraction data were uniquely consistent with the assigned space groups of *P*2₁ for **3** and *P*2₁3 for both [**2b**]OTf and [**2d**]I (Flack parameters are 0.01(4), -0.01(4) and 0.00(3), respectively). No symmetry higher than triclinic was indicated in the diffraction data for **1-BF₃**. These choices led to chemically sensible and computationally stable refinements. All hydrogen atoms were placed in calculated positions, with the exception of the ketimide protons of **3**, which were located in the electron density map and refined isotropically. The Mo1-N2-C21 unit of [**2d**]I was found to be coincident with a three-fold axis of the *P*2₁3 space group, thus imposing three-site positional disorder in the corresponding methyl group (C22). This disorder was modeled and no hydrogen atoms were generated for methylene carbon C21. Complex [**2c**]OTf crystallized in the centrosymmetric space group *P*2₁/*n* with two-site positional disorder found for the triflate counter ion. This disorder was modeled to 70:30 occupancy over the two sites as indicated by the refinement statistics and resulted in chemically sensible geometries.

Isomorphous **1-GeCl₂** and **1-SnCl₂** were found to crystallize in the centrosymmetric space group *P*2₁/*c* and both contained two-site positional disorder of the aryl-ring and ECl₂ residues. Both possible chiral, three-blade propeller orientations of the aryl rings were present and were modeled each with 50 % occupancy as indicated by the refinement statistics. Additionally, each aryl-ring orientation corresponded to distinct

ECl_2 orientation and was similarly modeled. Only one orientation of **1-GeCl₂** and **1-SnCl₂** is presented in the text. No hydrogen atoms were generated for the aryl rings of **1-GeCl₂** and **1-SnCl₂** due to the disorder. All software for diffraction data processing and crystal-structure solution and refinement are contained in the SHELXTL (v6.14) program suite (G. Sheldrick, Bruker XRD, Madison, WI).

1.5.3 NMR Measurements

Solution state ^1H , ^{13}C and ^{19}F NMR spectra were recorded on a Varian Mercury-300 spectrometer operating at 300 MHz for ^1H . Solution state ^{27}Al , ^{11}B and ^{119}Sn NMR spectra were recorded on a Varian INOVA-500 spectrometer operating at 500 MHz for ^1H . ^{15}N Solution state NMR spectra were acquired on a Bruker DRX600 spectrometer operating at 600 MHz for ^1H (60 MHz for ^{15}N) and equipped with a triple resonance ($^1\text{H}/^{13}\text{C}/^{15}\text{N}$) probe. All solution NMR chemical shifts are reported in parts per million (ppm) and coupling constants (J) in Hertz (Hz). ^1H and ^{13}C chemical shifts are reported with respect to the internal solvent (C_6D_6 , 7.16 and 128.39; THF-d_8 , 3.58 and 1.73, 67.57 and 25.37; CDCl_3 , 7.27 and 77.0). ^{15}N chemical shifts are referenced to external neat CH_3NO_2 ($\delta = 380.2$ ppm with respect to neat liquid NH_3 (0.0 ppm)).²² Other nuclei were referenced using an external standard, as follows: ^{19}F spectra were referenced with respect to CFCl_3 (0.0 ppm); ^{27}Al spectra were referenced to $\text{Al}(\text{D}_2\text{O})_6^{3+}$ (1.0 M AlCl_3 in D_2O ; 0.0 ppm); ^{11}B spectra were referenced to neat $\text{BF}_3\cdot\text{OEt}_2$ (0.0 ppm); ^{119}Sn spectra were referenced to 0.5 M $\text{Sn}(\text{CH}_3)_4$ in CH_2Cl_2 (0.0 ppm). Solid state ^{15}N NMR spectra were acquired using a custom-designed spectrometer operating at 501 MHz for ^1H (50.8 MHz for ^{15}N). All spectra were acquired using a triple-resonance ($^1\text{H}/^{13}\text{C}/^{15}\text{N}$) magic-angle spinning (MAS) probe from Chemagnetics (Fort Collins, CO) configured for 4.0 mm zirconium rotors. Spinning frequencies of 3-6.5 kHz were used. The identity of the isotropic peak (δ_{iso}) was confirmed by measurement of the spectra at several different spinning speeds. Proton-nitrogen cross-polarization (CP) under the Hartmann-Hahn match was used to enhance the sensitivity of all ^{15}N NMR spectra.⁸⁴ Samples were referenced indirectly to the ^{13}C CP/MAS spectrum of adamantane or directly to the ^{15}N CP/MAS spectrum of NH_4Cl (acquired prior to each sample acquisition).

1.5.4 Simulation and Calculation of Solid State NMR Spectra

The principal components of the chemical shift tensors were determined experimentally by fitting simulated spectra to the experimental data^{58,59} using Simpson⁸⁵ (a general simulation program for NMR spectroscopy). The residuals between the simulated spectrum and the experimental spectrum could, in most cases, be reduced to <5%. The Simpson program was also used to calculate spectra based on values of the chemical shift tensor (in ppm) that were calculated using ADF.

1.5.5 Computational Details

Theoretical calculations were carried out using the Amsterdam Density Functional package (version *ADF2002.02*).⁸⁶⁻⁸⁹ The Slater-type orbital (STO) basis sets were of triple- ζ quality augmented with two polarization functions (ADF basis TZ2P). Full electronic configuration was used for all atoms. Relativistic effects were included by virtue of the zero order regular approximation (ZORA).⁹⁰⁻⁹² The local density approximation (LDA) by Vosko, Wilk and Nusair (VWN)⁹³ was used together with the exchange correlation corrections of Becke⁹⁴ and Perdew⁹⁵ (BP-86).

The ¹⁵N NMR chemical shielding calculations were performed using a multi-step procedure. First, the geometry of the compound of interest was optimized using X-ray parameters as a starting point. The optimized geometry was then subjected to a single-point calculation incorporating spin-orbit effects. The output of this calculation was used as the input for the ADF NMR utility.⁹⁶

Values of the absolute shielding tensor, calculated using density functional methods, were converted to referenced chemical shifts (δ ppm) using Equation 1:⁹⁷

$$\delta(\text{S, calc}) = \sigma(\text{N}_2, \text{calc}) - \sigma(\text{S, calc}) + \delta(\text{N}_2, \text{ref}) \quad (1)$$

where $\delta(\text{S, calc})$ is the calculated chemical shift (ppm) of the compound of interest (S), $\sigma(\text{N}_2, \text{calc})$ is the calculated absolute shielding tensor for the reference compound (N₂ gas; $\sigma(\text{N}_2, \text{calc}) = -80.012$ ppm), $\sigma(\text{S, calc})$ is the calculated absolute shielding tensor of S and

$\delta(\text{N}_2, \text{ref})$ is the experimental chemical shift (ppm) of the reference compound (N_2 gas). The NMR shielding (σ) of N_2 (with reference to neat nitromethane) = +74.2 ppm, therefore $\delta(\text{N}_2, \text{ref}) = 380.2 - 74.2 = 306$ ppm (referenced to liquid NH_3 at 0 ppm).^{98,99}

1.5.6.1 Synthesis of $^{15}\text{NMo}(\text{N}[\text{tBu}]\text{Ar})_3$ (1)

A 300 mL 3-neck flask fitted with a 0.1 L break-seal flask containing $^{15}\text{N}_2$ was charged with KH (3.52 g, 88 mmol). THF (50 mL) was added and the slurry was stirred while sparging with argon for 15 minutes. Stirring was paused and the headspace of the flask was evacuated. Under a static vacuum the break-seal was opened and the slurry was stirred vigorously as the headspace filled with $^{15}\text{N}_2$. In a second flask, $\text{Mo}(\text{N}[\text{tBu}]\text{Ar})_3$ (5.5 g, 8.8 mmol) was dissolved in THF (35 mL) and the solution was stirred while sparging with argon for 10 minutes. Addition of the $\text{Mo}(\text{N}[\text{tBu}]\text{Ar})_3$ solution *via* syringe to the KH/THF slurry afforded a dark orange mixture. Stirring was continued for 24 h after which time the solution was filtered through Celite. Solvent removal *in vacuo* gave an orange powder, which upon dissolution in pentane and storage at -35 °C gave amber crystals of the desired terminal nitride complex, $^{15}\text{NMo}(\text{N}[\text{tBu}]\text{Ar})_3$ (4.72g, 7.40 mmol, 84%). This procedure is a modification of previously reported syntheses for complex **1**.^{20,29}

1.5.6.2 Synthesis of Lewis Acid Adducts (1-LA)

A solution of $\text{NMo}(\text{N}[\text{tBu}]\text{Ar})_3$ in pentane (5 mL) was prepared in a 20 mL scintillation vial and chilled to -35 °C. In a second vial a solution of the Lewis acid (1 equiv. in 2 mL pentane) was prepared and chilled to -35 °C. The Lewis acid solution was added to the $\text{NMo}(\text{N}[\text{tBu}]\text{Ar})_3$ solution and stirred at room temperature for 1 h. Upon addition of the Lewis acid a yellow solid precipitated from solution. Filtration of the suspension, washing with pentane and subsequent drying under a dynamic vacuum afforded the desired product. Recrystallization from a concentrated CH_2Cl_2 solution layered with pentane at -35 °C afforded yellow crystals of $\text{X}_3\text{E}-\text{NMo}(\text{N}[\text{tBu}]\text{Ar})_3$.

Isolated yield of yellow **1**-BF₃·CH₂Cl₂ (from 0.115 g of **1**): 0.092 g, 0.130 mmol, 72%. Anal. Calcd. for C₃₆H₅₄N₄MoBF₃: C 61.19, H 7.70, N 7.93. Anal. Found: C 60.94, H 7.76, N 7.86. ¹H NMR (300 MHz, CD₂Cl₂, 20 °C) δ: 6.92 (s, 3 H, para), 5.71 (br s, 6 H, ortho), 2.15 (s, 18 H, ArCH₃), 1.31 (s, 27 H, NC(CH₃)₃). ¹³C NMR (75.0 MHz, CD₂Cl₂, 20 °C) δ: 147.8 (ipso), 138.4 (meta), 129.9 (ortho), 129.1 (para), 65.95 (NC(CH₃)₃), 32.14 (NC(CH₃)₃), 21.60 (ArCH₃). ¹⁹F NMR (282 MHz, CD₂Cl₂, 20 °C) δ: 143.7 (m, BF₃). ¹¹B NMR (160 MHz, CD₂Cl₂, 20 °C) δ: -2.83 (m, BF₃). ¹⁵N-**1**-BF₃: ¹¹B NMR (160 MHz, CDCl₃, 20 °C) δ: -1.72 (br s, *v*_{1/2} = 49 Hz). ¹⁵N NMR (60 MHz, CDCl₃, 20 °C) δ: 591.9 (s).

Isolated yield of yellow **1**-BCl₃ (from 0.110 g of **1**): 0.104 g, 0.138 mmol, 80%. Anal. Calcd. for C₃₆H₅₄N₄MoBCl₃: C 57.20, H 7.20, N 7.41. Anal. Found: C 57.11, H 7.14, N 7.45. ¹H NMR (300 MHz, CD₂Cl₂, 20 °C) δ: 6.98 (s, 3 H, para), 5.7 (br s, 6 H, ortho), 2.19 (s, 18 H, ArCH₃), 1.35 (s, 27 H, NC(CH₃)₃). ¹³C NMR (75.0 MHz, CD₂Cl₂, 20 °C) δ: 148.0 (ipso), 138.2 (meta), 130.8 (ortho), 128.6 (para), 67.56 (NC(CH₃)₃), 31.74 (NC(CH₃)₃), 21.65 (ArCH₃). ¹¹B NMR (160 MHz, CD₂Cl₂, 20 °C) δ: 3.91 (s, *v*_{1/2} = 16.5 Hz). ¹⁵N-**1**-BCl₃: ¹¹B NMR (160 MHz, CD₂Cl₂, 20 °C) δ: 4.02 (br s, *v*_{1/2} = 36.6 Hz).

Isolated yield of yellow **1**-AlCl₃ (from 0.075 g **1**): 0.081 g, 0.104 mmol, 89%. Anal. Calcd. for C₃₆H₅₄N₄MoAlCl₃: C 55.69, H 7.01, N 7.73. Anal. Found: C 55.84, H 7.11, N 7.22. ¹H NMR (300 MHz, CD₂Cl₂, 20 °C) δ: 6.95 (s, 3 H, para), ~5.6 (br s, 6 H, ortho), 2.16 (s, 18 H, ArCH₃), 1.34 (s, 27 H, NC(CH₃)₃). ¹³C NMR (75.0 MHz, CD₂Cl₂, 20 °C) δ: 148.2 (ipso), 138.4 (meta), 130.1 (ortho), 128.9 (para), 66.38 (NC(CH₃)₃), 32.40 (NC(CH₃)₃), 21.61 (ArCH₃). ²⁷Al NMR (130.1 MHz, CD₂Cl₂, 20 °C) δ: 89.30 (s, *v*_{1/2} = 10 Hz). ¹⁵N-**1**-AlCl₃: ²⁷Al NMR (130.1 MHz, CD₂Cl₂, 20 °C) δ: 87.76 (m).

Isolated yield of bright yellow **1**-AlBr₃ (from 0.070 g **1**): 0.083 g, 0.092 mmol, 84%. Anal. Calcd. for C₃₆H₅₄N₄MoAlBr₃: C 47.75, H 6.01, N 6.19. Anal. Found: C 47.63, H 5.88, N 6.12. ¹H NMR (300 MHz, CD₂Cl₂, 20 °C) δ: 6.95 (s, 3 H, para), 5.70 (br s, 6 H, ortho), 2.16 (s, 18 H, ArCH₃), 1.35 (s, 27 H, NC(CH₃)₃). ¹³C NMR (75.0 MHz, CD₂Cl₂, 20 °C) δ: 148.2 (ipso), 138.3 (meta), 130.1 (ortho), 129.0 (para), 66.66

(NC(CH₃)₃), 32.50 (NC(CH₃)₃), 21.62 (ArCH₃). ²⁷Al NMR (130.1 MHz, CH₂Cl₂, 20 °C) δ: 80.17 (br s, $\nu_{1/2}$ = 85 Hz). ¹⁵N-**1**-AlBr₃: ²⁷Al NMR (130.1 MHz, CH₂Cl₂, 20 °C) δ: 80.18 (br s, $\nu_{1/2}$ = 88 Hz).

Isolated yield of yellow **1**-AlI₃ (from 0.100 g **1**): 0.111 g, 0.106 mmol, 68%. Anal. Calcd. for C₃₆H₅₄N₄MoAlI₃: C 41.16, H 5.18, N 5.71. Anal. Found: C 41.16, H 5.23, N 5.26. ¹H NMR (300 MHz, CDCl₃, 20 °C) δ: 6.46 (s, 3 H, para), 5.47 (br s, 6 H, ortho), 1.83 (s, 18 H, ArCH₃), 1.14 (s, 27 H, NC(CH₃)₃). ¹³C NMR (75.0 MHz, CDCl₃, 20 °C) δ: 136.4 (meta), 128.1 (para), 32.36 (NC(CH₃)₃), 20.70 (ArCH₃). ²⁷Al NMR (130.1 MHz, CDCl₃, 20 °C) δ: 26.03 (s, $\nu_{1/2}$ = 226 Hz). ¹⁵N-**1**-AlI₃: ²⁷Al NMR (130.1 MHz, THF, 20 °C) δ: 24.34 (br s, $\nu_{1/2}$ = 357 Hz).

Isolated yield of bright yellow **1**-GaCl₃ (from 0.150 g **1**): 0.174 g, 0.214 mmol, 91%. Anal. Calcd. for C₃₆H₅₄N₄MoGaCl₃: C 53.06, H 6.68, N 6.88. Anal. Found: C 53.20, H 6.62, N 6.95. ¹H NMR (300 MHz, CD₂Cl₂, 20 °C) δ: 6.95 (s, 3 H, para), 5.62 (br s, 6 H, ortho), 2.16 (br s, 18 H, ArCH₃), 1.33 (s, 27 H, NC(CH₃)₃). ¹³C NMR (75.0 MHz, CD₂Cl₂, 20 °C) δ: 148.0 (ipso), 138.4 (meta), 130.1 (ortho), 128.9 (para), 66.26 (NC(CH₃)₃), 32.42 (NC(CH₃)₃), 21.61 (ArCH₃).

Isolated yield of yellow **1**-InCl₃ (from 0.175 g **1**): 0.198 g, 0.230 mmol, 84%. Anal. Calcd. for C₃₆H₅₄N₄MoInCl₃: C 50.28, H 6.33, N 6.52. Anal. Found: C 50.41, H 6.38, N 6.67. ¹H NMR (300 MHz, CDCl₃/THF, 20 °C) δ: 6.59 (s, 3 H, para), ~5.6 (br s, 6 H, ortho), 1.95 (s, 18 H, ArCH₃), 1.26 (s, 27 H, NC(CH₃)₃). ¹³C NMR (75.0 MHz, CDCl₃/THF, 20 °C) δ: 136.7 (meta), 128.4 (ortho), 32.62 (NC(CH₃)₃), 21.05 (ArCH₃).

Isolated yield of yellow **1**-GeCl₂ (from 0.075 g **1** and 0.027 g GeCl₂.dioxane): 0.069 g, 0.079 mmol, 68%. Anal. Calcd. for C₃₆H₅₄N₄MoGeCl₂: C 54.99, H 6.92, N 7.63. Anal. Found: C 55.21, H 6.91, N 7.12. ¹H NMR (300 MHz, CDCl₃, 20 °C) δ: 6.88 (s, 3 H, para), 5.66 (br s, 6 H, ortho), 2.15 (s, 18 H, ArCH₃), 1.37 (s, 27 H, NC(CH₃)₃). ¹³C NMR (75.0 MHz, CDCl₃, 20 °C) δ: 148.4 (ipso), 137.7 (meta), 129.2 (ortho), 128.8 (para), 65.11 (NC(CH₃)₃), 32.66 (NC(CH₃)₃), 21.56 (ArCH₃).

Isolated yield of yellow **1**-SnCl₂ (from 0.165 g **1**): 0.160 g, 0.193 mmol, 75%.
 Anal. Calcd. for C₃₆H₅₄N₄MoSnCl₂: C 51.95, H 6.54, N 7.21. Anal. Found: C 52.28, H 6.53, N 6.69. ¹H NMR (300 MHz, CD₂Cl₂, 20 °C) δ: 6.89 (s, 3 H, para), 5.68 (br s, 6 H, ortho), 2.14 (s, 18 H, ArCH₃), 1.35 (s, 27 H, NC(CH₃)₃). ¹³C NMR (75.0 MHz, CD₂Cl₂, 20 °C) δ: 144.6 (ipso), 138.1 (meta), 129.4 (ortho), 129.1 (para), 64.60 (NC(CH₃)₃), 32.93 (NC(CH₃)₃), 21.59 (ArCH₃). ¹¹⁹Sn NMR (186 MHz, THF, 20 °C) δ: 333 (s, ν_{1/2} = 31 Hz). ¹⁵N-**1**-SnCl₂: ¹¹⁹Sn NMR (186 MHz, THF, 20 °C) δ: 333 (s, ν_{1/2} = 57 Hz).

1.5.6.3 Synthesis of [CH₃NMo(N^tBu)Ar]₃I [**2a**]

Crystalline **1** (0.120 g, 0.188 mmol) was dissolved in neat CH₃I (0.8 mL, 12.8 mmol) in a 20 mL vial. The solution was stirred at 25 °C for 20 h after which time removal of excess CH₃I *in vacuo* and a pentane wash afforded a bright yellow powder in 92% yield (0.137 g, 0.173 mmol). ¹H NMR (300 MHz, CDCl₃, 20 °C) δ: 6.99 (s, 3 H, para), 5.67 (br s, 6 H, ortho), 5.16 (s, 3 H, NCH₃), 2.19 (s, 18 H, ArCH₃), 1.29 (s, 27 H, NC(CH₃)₃). ¹³C NMR (75.0 MHz, CDCl₃, 20 °C) δ: 145.3 (ipso), 138.6 (meta), 130.8 (para), 128.4 (ortho), 68.50 (NC(CH₃)₃), 65.60 (NCH₃), 32.30 (NC(CH₃)₃), 21.70 (ArCH₃). NMR data for ¹⁵N-**2a**I: ¹H NMR (300 MHz, CDCl₃, 20 °C) δ: 5.11 (d, ²J_{N-H} 3.3 Hz, 3 H, ¹⁵N-CH₃). ¹⁵N NMR (60 MHz, CH₃I/CDCl₃, 20 °C) δ: 462.6. Anal. Calcd. for C₃₇H₃₉D₁₈N₄MoI:⁴² C 55.63, H 7.19, N 7.01. Anal. Found: C 56.13, H 7.64, N 6.53.

1.5.6.4 Synthesis of [(CH₃)₃Si-NMo(N^tBu)Ar]₃][SO₃CF₃] [**2b**]OTf

A 20 mL scintillation vial was charged with **1** (0.10 g, 0.157 mmol) and Et₂O (2 mL). In a second vial a solution of trimethylsilyl trifluoromethanesulfonate [CF₃SO₃Si(CH₃)₃] (0.174 g, 5 equiv, 0.783 mmol) in Et₂O (1 mL) was prepared. The contents of the two vials were combined and the solution stirred at 25 °C for 10 h. Solvent removal resulted in the isolation of a bright yellow-orange powder; yield 89% (0.120 g, 0.139 mmol). Anal. Calcd: C 55.75 H 7.32 N 6.50; Anal. Found: C 55.54 H 7.75 N 6.60. ¹H (300 MHz, CDCl₃, 20 °C) δ: 6.91 (s, 3 H, para), 5.62 (br s, 6 H, ortho), 2.17 (s, 18 H, ArCH₃), 1.34 (s, 27 H, N(CH₃)₃), 0.69 (s, 9 H, Si(CH₃)₃). ¹³C NMR (75.0

MHz, CDCl₃, 20 °C) δ : 147.7 (ipso), 137.5 (meta), 129.5 (ortho), 128.0 (para), 66.04 (NC(CH₃)₃), 32.44 (NC(CH₃)₃), 21.65 (ArCH₃), 1.94 (Si(CH₃)₃). ¹⁹F NMR (282 MHz, CDCl₃, 20 °C) δ : -78.44 (s, SO₃CF₃). ¹⁵N NMR (60 MHz, CDCl₃, 20 °C) δ : 537.

1.5.6.5 Synthesis of [PhC(O)NMo(N^tBu)Ar]₃SO₃CF₃ [2c]OTf

Crystalline **1** (0.200 g, 0.31 mmol) was dissolved in CH₂Cl₂ (2 mL) in a 20 mL scintillation vial and chilled to -35 °C. A solution of PhC(O)OTf (0.89 g, 0.37 mmol, 1.2 equiv) in CH₂Cl₂ was prepared and similarly chilled to -35 °C. The PhC(O)OTf solution was added to the stirred solution of NMo(N^tBu)Ar₃ and an immediate darkening of the solution to a brown-orange color was noted. The solution was stirred at 25 °C for 1 h before concentration of the solution (to ~0.5 mL) and addition of cold Et₂O caused precipitation of a red powder. The solution was filtered and the precipitate washed with pentane to afford a red-orange powder in 72 % yield (0.198 g, 0.225 mmol). Material suitable for elemental analysis and crystallographic characterization was prepared by recrystallization from a concentrated THF solution layered with pentane. Anal. Calcd: C 58.63, H 6.75, N 6.36; Anal. Found: C 59.04, H 6.73, N 6.20. IR (KBr plates, THF); ν_{CO} 1668 cm⁻¹. ¹H NMR (500 MHz, CDCl₃, 20 °C) δ : 8.32 (m, 2 H, meta Ph), 7.83 (m, 1 H, para Ph), 7.77 (m, 2 H, ortho Ph), 7.10 (s, 3 H, para), 5.74 (br s, 6 H, ortho), 2.26 (s, 18 H, ArCH₃), 1.34 (s, 27 H, NC(CH₃)₃). ¹³C NMR (125 MHz, CDCl₃, 20 °C) δ : 147.7 (ipso), 139.1 (meta), 136.3 (Ph), 131.5 (Ph), 131.42 (Ph), 130.0 (para), 126.8 (ortho), 72.0 (NC(CH₃)₃), 31.8 (NC(CH₃)₃), 21.7 (ArCH₃). ¹⁹F NMR (282.23 MHz, CDCl₃, 20 °C) δ : -78.3.

Table 2. Crystallographic data.

Compound	1-BF₃	1-GeCl₂	1-SnCl₂	[2b]OTf	[2c]OTf	[2d]I	3
<i>Crystal data</i>							
Empirical formula	C ₃₇ H ₅₆ N ₄ MoBCl ₂ F ₃	C ₃₆ H ₅₄ N ₄ MoGeCl ₂	C ₃₆ H ₅₄ N ₄ MoSnCl ₂	C ₄₀ H ₆₃ N ₄ MoF ₃ SO ₃ S	C ₄₈ H ₆₇ F ₃ N ₄ MoO ₅ S	C ₃₉ H ₅₇ N ₄ MoCl ₂ I	C ₃₇ H ₅₆ N ₄ Mo
Formula weight	791.51	781.54	828.36	861.03	965.06	875.63	652.80
T(K)	193(2)	193(2)	193(2)	193(2)	193(2)	193(2)	193(2)
Crystal system	Triclinic	Monoclinic	Monoclinic	Cubic	Monoclinic	Cubic	Monoclinic
Space group	<i>P</i> -1	<i>P</i> 2 ₁ / <i>c</i>	<i>P</i> 2 ₁ / <i>c</i>	<i>P</i> 2 ₁ 3	<i>P</i> 2 ₁ / <i>n</i>	<i>P</i> 2 ₁ 3	<i>P</i> 2 ₁
<i>a</i> (Å)	10.5757(6)	14.803(3)	14.803(3)	16.5578(5)	12.3168(8)	16.3118(6)	11.2145(10)
<i>b</i> (Å)	12.1291(7)	13.711(3)	13.711(3)	16.5578(5)	26.7028(17)	16.3118(6)	11.0462(10)
<i>c</i> (Å)	16.6647(10)	19.132(4)	19.132(4)	16.5578(5)	14.7598(10)	16.3118(6)	14.7723(13)
α (°)	93.3220(10)	90	90	90	90	90	90
β (°)	107.3170(10)	90.12(3)	90.12(3)	90	90.4400(10)	90	94.367(2)
γ (°)	94.7260(10)	90	90	90	90	90	90
Unit cell volume (Å ³)	2026.2(2)	3883.0(13)	3883.0(13)	4539.5(2)	4854.3(6)	4340.2(3)	1824.6(3)
<i>Z</i>	2	4	4	4	4	4	2
<i>Data Collection</i>							
λ (Mo K α) (Å)	0.71073	0.71073	0.71073	0.71073	0.71073	0.71073	0.71073
ρ_{calcd} (g cm ⁻³)	1.297	1.292	1.370	1.260	1.321	1.340	1.188
μ (mm ⁻¹)	0.499	1.261	1.131	0.412	0.373	1.166	0.388
Reflections collected	8791	16135	9171	19536	20454	18731	6978
Independent collections	5282 ($R_{\text{int}} = 0.0355$)	5070 ($R_{\text{int}} = 0.0387$)	6358 ($R_{\text{int}} = 0.0308$)	1988 ($R_{\text{int}} = 0.0601$)	6353 ($R_{\text{int}} = 0.0489$)	1907 ($R_{\text{int}} = 0.0620$)	4511 ($R_{\text{int}} = 0.0592$)
Absorption correction	Empirical	None	None	Empirical	None	None	Empirical
Maximum and minimum transmission	0.3804 and 0.3026	na	na	0.2741 and 0.2191	na	na	0.3092 and 0.2137
<i>Structure refinement</i>							
Refinement method	Full-matrix least squares on F^2 was used for all complexes						
Observed reflections [$I > 2\sigma(I)$]	5282	5070	6358	1988	6353	1907	4511
Number of parameters	433	552	552	160	572	151	387
Number of restraints	0	0	0	0	0	0	1
Goodness-of-fit on F^2	0.947	1.237	1.217	1.074	1.044	1.068	1.053
$R[I > 2\sigma(I)]$	0.0487	0.0461	0.0620	0.0269	0.0464	0.0314	0.0406
$wR2$	0.1249	0.1176	0.1602	0.0658	0.1153	0.0744	0.1063

1.5.6.6 Synthesis of $\text{H}_2\text{CNMo}(\text{N}[\text{tBu}]\text{Ar})_3$ (**3**)

To a chilled suspension of $[\text{CH}_3\text{NMo}(\text{N}[\text{tBu}]\text{Ar})_3]\text{I}$ (0.098 g, 0.126 mmol) in pentane (5 mL) was added a chilled solution of 1.1 equiv. $\text{LiN}[(\text{Si}(\text{CH}_3)_3)_2]$ (0.023 g, 0.138 mmol) in pentane (4 mL). Within a few minutes of adding base the yellow suspension turned bright red. The suspension was stirred for 12 h at 25 °C after which time the solution had turned dark purple and no suspended solids were observed. The solution was filtered through Celite and solvent removed *in vacuo* to yield a dark red-purple solid. Recrystallization from Et_2O yielded dark red crystals 0.051 g (0.077 mmol, 62%). Anal. Calcd: C 68.017, H 8.579, N 8.583; Anal. Found: C 68.22, H 8.51, N 8.68. m.p: 124 -135 °C (dec). IR (Et_2O solution, cm^{-1}): 1600 (m, ν_{NC}), 1587 (s, $\nu_{\text{Ar-CH}_3}$). ^1H NMR (300 MHz, C_6D_6 , 20 °C) δ : 6.69 (s, 3 H, para), 6.289 (s, 3 H, ortho), 6.287 (s, 3 H, ortho), 5.91 (s, 2 H, NCH_2), 2.16 (s, 18 H, ArCH_3), 1.41 (s, 27 H, $\text{NC}(\text{CH}_3)_3$). ^{13}C NMR (75.0 MHz, C_6D_6 , 20 °C); δ : 150.2 (ipso), 138.9 (NCH_2), 137.4 (meta), 129.9 (ortho), 127.7 (para), 63.1 ($\text{NC}(\text{CH}_3)_3$), 32.8 ($\text{NC}(\text{CH}_3)_3$), 22.1 (ArCH_3). **3**- ^{15}N : ^1H NMR (300 MHz, C_6D_6 , 20 °C) δ : 5.90 (d $^2J_{\text{N-H}}$ 1.37 Hz, 2 H, $^{15}\text{NCH}_2$). ^{13}C NMR (75.0 MHz, C_6D_6 , 20 °C) δ : 138.9 (d $^1J_{\text{N-C}}$ 5.78 Hz, $^{15}\text{NCH}_2$). ^{15}N NMR (60 MHz, C_6D_6 , 20 °C) δ : 454.6.

1.5.6.7 Synthesis of $[\text{CH}_3\text{CH}_2\text{NMo}(\text{N}[\text{tBu}]\text{Ar})_3]\text{I}$ [**2d**]**I**

Crystalline $\text{H}_2\text{CNMo}(\text{N}[\text{tBu}]\text{Ar})_3$ (**3**, 0.074 g, 0.113 mmol) was dissolved in neat CH_3I (0.8 mL) in a 20 mL scintillation vial. The solution was stirred at 25 °C for 14 h after which time removal of excess CH_3I *in vacuo* and a pentane wash afforded a bright yellow powder in 96% yield (0.086 g, 0.109 mmol). Recrystallization from a concentrated CH_2Cl_2 solution layered with Et_2O afforded yellow crystals of $[\text{2d}]\text{I}\cdot\text{CH}_2\text{Cl}_2$. ^1H NMR (300 MHz, CDCl_3 , 20 °C) δ : 6.98 (s, 3 H, para), 5.60 (br s, 6 H, ortho), 5.38 (q, 2 H, $^3J_{\text{HH}}$ 7.2 Hz, NCH_2CH_3), 2.17 (s, 18 H, ArCH_3), 1.95 (t $^3J_{\text{HH}}$ 7.2 Hz, 3 H, NCH_2CH_3), 1.27 (s, 27 H, $\text{NC}(\text{CH}_3)_3$). ^{13}C NMR (75.0 MHz, CDCl_3 , 20 °C) δ : 145.9 (ipso), 138.6 (meta), 130.7 (para), 128.3 (ortho), 77.6 (NCH_2CH_3), 68.1 ($\text{NC}(\text{CH}_3)_3$), 32.4 ($\text{NC}(\text{CH}_3)_3$), 21.7 (ArCH_3), 17.5 (NCH_2CH_3). Anal. Calcd: C 57.43, H 7.48, N 7.55; Anal. Found: C 57.52, H 7.44, N 7.89.

References

- [1] Laws, D. D.; Bitter, H-M. L.; Jerschow, A. *Angew. Chem. Int. Ed.* **2002**, *41*, 3096.
- [2] Griffin, R. G. *Nat. Struct. Biol.* **1998**, *5*, 508.
- [3] Opella, S. J.; Morden, K. M. *Dynamic Properties of Biomolecular Assemblies*; Harding, S. E.; Rowe, A. J. Eds.; The Royal Society of Chemistry: Cambridge, 1989, p. 196.
- [4] Chekmenev, E. Y.; Zhang, Q.; Waddell, K. W.; Mashuta, M. S.; Wittebort, R. J. *J. Am. Chem. Soc.* **2004**, *126*, 379.
- [5] Luca, S.; Heise, H.; Baldus, M. *Acc. Chem. Res.* **2003**, *36*, 858.
- [6] Shoji, A.; Ando, S.; Kuroki, S.; Ando, I.; Webb, G. A. "Structural Studies of Peptides and Polypeptides in the Solid State by Nitrogen-15 NMR" in *Annu. Rep. NMR Spec.* **1993**, *26*, 55.
- [7] Jaroniec, C. P.; Lansing, J.; Tounge, B.; Belenky, M.; Herzfeld, J.; Griffin, R. G. *J. Am. Chem. Soc.* **2001**, *123*, 12929.
- [8] McDermott, A. E.; Polenova, T.; Bockmann, A.; Zilm, K. W.; Montellione, G. T. *J. Biomol. NMR* **1999**, *16*, 209219.
- [9] Castellani, F.; van Rossum, B.; Diehl, A.; Schubert, M.; Rehbein, K.; Oschkinat, H. *Nature* **2002**, *420*, 98.
- [10] Bryce, D. L.; Wasylishen, R. E. *Phys. Chem. Chem. Phys.* **2002**, *4*, 3591.
- [11] Huang, Y.; Gilson, D. F. R.; Butler, I. S. *J. Chem. Soc. Dalton Trans.* **1992**, 2881.
- [12] Salzmann, R.; Wojdelski, M.; McMahon, M.; Havlin, R. H.; Oldfield, E. *J. Am. Chem. Soc.* **1998**, *120*, 1349.
- [13] Bernard, G. M.; Wasylishen, R. E. *Phys. Organomet. Chem.* **2002**, *3*, 165.
- [14] Salzmann, R.; Ziegler, C. J.; Godbout, N.; McMahon, M. T.; Suslick, K. S.; Oldfield, E. *J. Am. Chem. Soc.* **1998**, *120*, 11323.
- [15] Godbout, N.; Sanders, L. K.; Salzmann, R.; Havlin, R. H.; Wojdelski, M.; Oldfield, E. *J. Am. Chem. Soc.* **1999**, *121*, 3829.
- [16] Gobetto, R. *Materials Chemistry and Physics* **1991**, *29*, 221.
- [17] Mehring, M. *Principals of High Resolution NMR in Solids*, 2nd ed.; Springer-Verlag: Berlin, 1983.
- [18] *Solid-state NMR: Principals and Applications*; Duer M. J. Ed.; Blackwell Science: Oxford, 2002.
- [19] Wu, G.; Rovnyak, D.; Johnson, M. J. A.; Zanetti, N. C.; Musaev, D. G.; Morokuma, K.; Schrock, R. R.; Griffin, R. G.; Cummins, C. C. *J. Am. Chem. Soc.* **1996**, *118*, 10654.
- [20] Laplaza, C. E.; Johnson, M. J. A.; Peters, J. C.; Odom, A. L.; Kim, E.; Cummins, C. C.; George, G. N.; Pickering, I. J. *J. Am. Chem. Soc.* **1996**, *118*, 8623.
- [21] Laplaza, C. E.; Cummins, C. C.; *Science* **1995**, *268*, 861.
- [22] von Philipsborn, W.; Müller, R. *Angew. Chem. Int. Ed.* **1986**, *25*, 383.
- [23] The ADF package utilized in this study allows the calculation of NMR shielding tensors: Schreckenbach, G.; Ziegler, T. *J. Phys. Chem.* **1995**, *99*, 606.
- [24] Schreckenbach, G.; Ziegler, T. *Int. J. Quantum Chem.* **1996**, *60*, 753.
- [25] Schreckenbach, G.; Ziegler, T. *Int. J. Quantum Chem.* **1997**, *61*, 899.
- [26] Wolff, S. K.; Ziegler, T. *J. Chem. Phys.* **1998**, *109*, 895.
- [27] Schreckenbach, G.; Ziegler, T. *Theor. Chem. Acc.* **1998**, *99*, 71.

- [28] Peters, J. C.; Cherry, J-P. F.; Thomas, J. C.; Baraldo, L.; Mindiola, D. J.; Davis, W. M.; Cummins, C. C. *J. Am. Chem. Soc.* **1999**, *121*, 10053.
- [29] Tsai, Y.-C.; Cummins, C. C. *Inorg. Chim. Acta.* **2003**, *345*, 63.
- [30] NMR shifts reported in methylcyclohexane solution; referenced to $\text{BF}_3 \cdot \text{OEt}_2$ at 0.0 ppm.
- [31] Hinton, J. F.; Briggs, R. W. *NMR and the Periodic Table*; B. E. Mann, R. K. Harris, Eds.; Academic Press: London, 1978, Ch. 9. ^{27}Al NMR (reference $[\text{Al}(\text{D}_2\text{O})_6]^{3+}$, 0.0 ppm) Al_2Cl_6 (2 M, Et_2O) δ 105 ppm; Al_2Br_6 (1.5 M, Et_2O) δ 95 ppm; Al_2I_6 (1.5 M, Et_2O) δ 40 ppm.
- [32] Lauterbur, P. C.; Burke, J. J. *J. Am. Chem. Soc.* **1961**, *83*, 326.
- [33] Hsu, C. C.; Geanangel, R. A. *Inorg. Chem.* **1980** *19*, 110.
- [34] Tables of selected bond lengths and angles for all complexes characterized by X-ray crystallography are collected in Appendix 1.
- [35] Doerrer, L. H.; Graham, A. J.; Green, M. L. H. *J. Chem. Soc. Dalton Trans.* **1998**, 3941.
- [36] Dantona, R.; Schweda, E.; Strähle, J. Z. *Naturforsch. B* **1984**, *39*, 733.
- [37] Abram, U.; Schmidt-Brücken, B.; Hagenbach, A.; Hecht, M.; Kirmse, R.; Voigt, A. *Z. Anorg. Allg. Chem.* **2003**, *629*, 838.
- [38] Tin halide adducts with N-donor molecules: Donaldson, J. D.; Nicholson, D. G. *Inorg. Nuc. Chem. Lett.* **1970**, *6*, 151.
- [39] Du Mont, W. W.; Kroth, H. J. *Naturforsch.* **1980**, *35B*, 700.
- [40] Nugent, W. A.; Mayer, J. M. *Metal-Ligand Multiple Bonds*; John Wiley & Sons: New York, 1988.
- [41] Eikey, R. A.; Abu-Omar, M. M. *Coord. Chem. Rev.* **2003**, *243*, 83 and references therein.
- [42] Deuterated isotopomer synthesized by A. J. Johnson, Ph.D. Thesis, Massachusetts Institute of Technology, Cambridge, MA, 1997.
- [43] N–Si single bond distances are typically *ca.* 1.711 Å: *CRC Handbook of Chemistry and Physics*, 86th Ed.; Lide, D. R. Ed.; CRC Press: London, 2003, 9-11.
- [44] Brown, L.; Koreeda, M. *J. Org. Chem.* **1984**, *49*, 3875.
- [45] Effenberger, F.; Sohn, E.; Epple, G. *Chem. Ber.* **1983**, *116*, 1195.
- [46] Dissociation equilibrium of benzoyl triflate: Effenberger, F.; Epple, G.; Eberhard, J. K.; Buehler, U.; Sohn, E. *Chem. Ber.* **1983**, *116*, 1183.
- [47] Wigley, D. E. *Prog. Inorg. Chem.* **1994**, *42*, 239.
- [48] Nielson, A. J.; Hunt, P. A.; Rickard, C. E. F.; Schwerdtfeger, P. *J. Chem. Soc. Dalton Trans.* **1997**, 3311.
- [49] Tong, C.; Bottomley, L. A. *J. Porphyrins Phthalocyanines* **1998**, *2*, 261.
- [50] Clough, C. R.; Greco, J. B.; Figueroa, J. S.; Diaconescu, P. L.; Davis, W. M.; Cummins, C. C. *J. Am. Chem. Soc.* **2004**, In Press.
- [51] Mösch-Zanetti, N. C.; Schrock, R. R.; Davis, W. M.; Wanninger, K.; Seidel, W. S.; O'Donoghue, M. B. *J. Am. Chem. Soc.* **1997**, *119*, 11037.
- [52] Shapley, P. A.; Shusta, J. M.; Hunt, J. L. *Organometallics* **1996**, *15*, 1622.
- [53] Hills, A.; Hughes, D.L.; Macdonald, C. J.; Mohammed, M. Y.; Pickett, C. J. *J. Chem. Soc. Dalton Trans.* **1991**, 121.
- [54] Chatt, J.; Dosser, R. J.; Leigh, G. J. *Chem. Commun.* **1972**, 1243.

-
- [55] Greenwood, N. N.; Earnshaw, A. *Chemistry of the Elements*, 2nd Ed.; Butterworth-Heinemann: Oxford, MA, 1998, p. 375.
- [56] Ketimines undergo reactions with organolithium reagents (R'Li) to form R(Li)N–C(R')H₂ via addition of nucleophilic [R'][–] to the electrophilic carbon of the ketimine: Huet, J. *Bull. Soc. Chim. Fr.* **1964**, 952, 960, 967 and 973.
- [57] Smith, M. B.; March, J. *March's Advanced Organic Chemistry*, 5th Ed.; John Wiley & Sons: New York, 2001, p. 431.
- [58] Maricq, M. M.; Waugh, J. S. *J. Chem. Phys.* **1979**, 70, 3300.
- [59] Herzfeld, J.; Berger, A. E. *J. Chem. Phys.* **1980**, 73, 6021.
- [60] Conventions followed in this paper are defined in the following article: Mason, J. *Solid State Nucl. Magn. Reson.* **1993**, 2, 285.
- [61] Refer to Appendix 2(a) for representative ¹⁵N solid state NMR spectra of complexes 1-LA.
- [62] Polymorphism and characterization by solid state NMR spectroscopy: Strohmeier, M.; Orendt, A. M.; Alderman, D. W.; Grant, D. M. *J. Am. Chem. Soc.* **2001**, 123, 1713.
- [63] Zell, M. T.; Padden, B. E.; Grant, D. J.; Chapeau, M.-C.; Prakash, I.; Munson, E. J. *J. Am. Chem. Soc.* **1999**, 121, 1372.
- [64] Smith, J.; MacNamara, E.; Raferty, D.; Borchardt, T.; Byrn, S. *J. Am. Chem. Soc.* **1998**, 120, 11710.
- [65] Refer to Appendix 2(b) for representative ¹⁵N solid state NMR spectra of imido complexes.
- [66] Appendix 3: A 3.15 Plot of the Experimental ¹⁵N chemical shift tensor (δ_{11} , ppm) vs. Calculated ¹⁵N chemical shift tensor (δ_{11} , ppm).
- [67] Cui, Q.; Musaev, D. G.; Svensson, M.; Sieber, S.; Morokuma, K. *J. Am. Chem. Soc.* **1995**, 117, 12366.
- [68] Neyman, K. M.; Nasluzov, V. A.; Hahn, J.; Landis, C. R.; Rösch, N. *Organometallics* **1997**, 16, 995.
- [69] For most of the complexes studied the spin-orbit contribution to the principal components of the chemical shift tensor was <5 ppm.
- [70] Jameson, C. J.; Mason, J. *Multinuclear NMR*, J. Mason, Ed.; Plenum Press: New York, 1987, p. 51.
- [71] Schreckenbach, G. *J. Chem. Phys.* **1999**, 110, 11936.
- [72] Ruiz-Morales, Y.; Ziegler, T. *J. Phys. Chem. A* **1998**, 102, 3970.
- [73] Ruiz-Morales, Y.; Schreckenbach, G.; Ziegler, T. *J. Phys. Chem. A* **1997**, 101, 4121.
- [74] Ruiz-Morales, Y.; Schreckenbach, G.; Ziegler, T. *Organometallics* **1996**, 15, 3920.
- [75] Ruiz-Morales, Y.; Schreckenbach, G.; Ziegler, T. *J. Phys. Chem.* **1996**, 100, 3359.
- [76] Schreckenbach, G.; Ruiz-Morales, Y.; Ziegler, T. *J. Chem. Phys.* **1996**, 104, 8605.
- [77] Ehlers, A. W.; Ruiz-Morales, Y.; Baerends, E. J.; Ziegler, T. *Inorg. Chem.* **1997**, 36, 5031.
- [78] Appendix 3: Representative input and output files of an NMR calculation.
- [79] Greco, J. B.; Peters, J. C.; Baker, T. A.; Davis, W. M.; Cummins, C. C.; Wu, G. *J. Am. Chem. Soc.* **2001**, 123, 5003.
- [80] ΔH_{RXN} of CH₂ addition to NMo(NH₂)₃ is calculated to be –93 kcal mol^{–1}.
- [81] Henderickx, H.; Kwakkenbos, G.; Peters, A.; van der Spoel, J.; de Vries, K. *Chem. Commun.* **2003**, 2050.

-
- [82] Pangborn, A. B.; Giardello, M. A.; Grubbs, R. H.; Rosen, R. K.; Timmers, F. J. *Organometallics* **1996**, *15*, 1518.
- [83] Perrin, D. D.; Armarego, W. L. F. *Purification of Laboratory Chemicals*, 3rd ed.; Pergamon Press: Oxford, 1988.
- [84] Theoretical basis of the cross polarization experiment: Hartmann, S. R.; Hahn, E. L. *Phys. Rev.* **1962**, *128*, 2042.
- [85] Bak, M.; Rasmussen, J. T.; Nielsen, N. C. *J. Magn. Reson.* **2000**, *147*, 296.
- [86] Baerends, E. J.; Ellis, D. E.; Ros, P. *Chem. Phys.* **1973**, *2*, 41.
- [87] Versluis, L.; Ziegler, T. *J. Chem. Phys.* **1988**, *322*, 88.
- [88] te Velde, G.; Baerends, E. J. *J. Comput. Phys.* **1992**, *99*, 84.
- [89] Fonseca Guerra, C.; Snijders, J. G.; te Velde, G.; Baerends, E. J. *Theor. Chem. Acc.* **1998**, *99*, 391.
- [90] Snijders, J. G.; Baerends, E. J.; Ros, P. *Mol. Phys.* **1979**, *38*, 1909.
- [91] Ziegler, T.; Tschinke, V.; Baerends, E. J.; Snijders, J. G.; Ravenek, W. J. *Phys Chem.* **1989**, *93*, 3050.
- [92] van Lenthe, E.; Baerends, E. J.; Snijders, J. G. *J. Chem. Phys.* **1993**, *99*, 4597.
- [93] Vosko, S. H.; Wilk, L.; Nusair, M. *Can. J. Phys.* **1980**, *58*, 1200.
- [94] Becke, A.D. *Phys. Rev. A* **1988**, *38*, 3098.
- [95] Perdew, J. P. *Phys. Rev. B* **1986**, *33*, 8822.
- [96] Schreckenback, G.; Ziegler, T. *J. Phys. Chem.* **1995**, *99*, 606.
- [97] van Wüllen, C. *Phys. Chem. Chem. Phys.* **2000**, *2*, 2137.
- [98] Witanowski, W.; Sicinska, W.; Webb, G. A. *Spectroscopy* **1991**, *9*, 55.
- [99] Jameson, C. J.; Jameson, A. K.; Oppusunggu, D.; Wille, S.; Burrell, P. M.; Mason, J. *J. Chem. Phys.* **1981**, *74*, 81.

Chapter 2

**Carbene chemistry in the activation of a dinitrogen-derived
terminal nitride of molybdenum**

Carbene chemistry in the activation of a dinitrogen-derived terminal nitride of molybdenum

2.1 Introduction

The splitting of dinitrogen by a three-coordinate molybdenum(III) complex $\text{Mo}(\text{N}[\text{tBu}]\text{Ar})_3$ (**1**, $\text{Ar} = 3,5\text{-C}_6\text{H}_3\text{Me}_2$) was first reported in 1995,^{1,2} representing one of few existing examples of the homogeneous six-electron reduction of dinitrogen by a well-defined organometallic complex.³⁻⁸ The uptake and cleavage of dinitrogen by **1** have been studied synthetically and theoretically,² permitting a detailed description of the intermediates on the N_2 -scission pathway, which include the purple bimetallic $\mu\text{-N}_2$ species $(\mu\text{-N}_2)\{\text{Mo}(\text{N}[\text{tBu}]\text{Ar})_3\}_2$ [**1**₂- N_2]. A lengthy incubation period (76 h) is required to form **1**₂- N_2 prior to its facile, first-order decomposition to 2 equiv of the terminal nitride complex $\text{NMo}(\text{N}[\text{tBu}]\text{Ar})_3$ (**2**). Recent studies have shown that in the presence of certain Lewis bases (e.g. N-heterocyclic bases, potassium hydride) the binding of N_2 by **1** is accelerated, thus enabling a more expedient route to **2**.^{9,10} The mild conditions under which **1** has been shown to facilitate N_2 -cleavage could in principle be made catalytic if a convenient means for the regeneration of **1** from complex **2** were found.

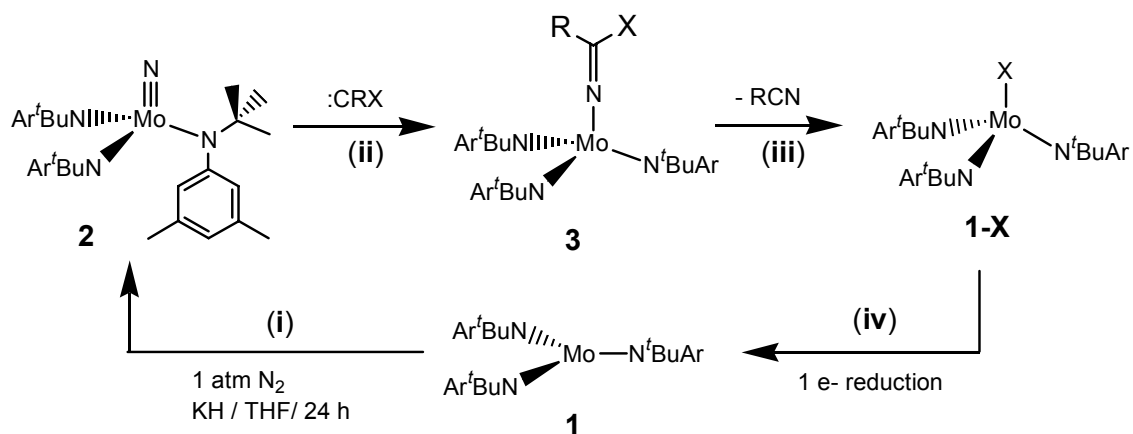
The development of nitrogen atom transfer routes from $\text{NMo}(\text{N}[\text{tBu}]\text{Ar})_3$ (**2**) has remained a paradigm in the chemistry of this complex since the first report of its isolation.¹ The favorability of N_2 -cleavage by complex **1** results from the exothermic formation of two Mo–N triple bonds (BDE *ca.* 165 kcal mol⁻¹), which compensates thermodynamically for the endothermic cleavage of one N–N single bond.^{11,12} Overcoming the inherent stability of the metal-nitride functionality represents a significant challenge that must be addressed before the successful inclusion of N_2 -cleavage into N-atom transfer reactions can be realized.¹³

Both complete and incomplete N-atom transfer reactions¹⁴⁻¹⁶ from molybdenum(VI) nitride species, mediated by low-coordinate, early transition metal

reductants, have been explored.¹⁷⁻¹⁹ In contrast, only one example of the activation of **2** in the context of N-atom transfer into organic molecules has been reported.²⁰ Henderickx and coworkers demonstrated that $\text{CF}_3\text{C}(\text{O})^{15}\text{NH}_2$ is formed in the reaction of ^{15}N -**2** with trifluoroacetic anhydride $[(\text{CF}_3\text{CO})_2\text{O}]$. An unfortunate aspect of this chemistry, with respect to the catalytic application of complex **2** in N-atom transfer from N_2 into organic nitriles, is the degradation of one amide ligand to afford the octahedral complex $[\text{N}(\text{R})\text{Ar}](\text{NAr})\text{Mo}(\eta^2\text{-CF}_3\text{CO}_2)(\text{O}_2\text{CF}_3)_2$ ($\text{R} = \text{C}(\text{CD}_3)_2\text{CH}_3$, $\text{Ar} = 3,5\text{-C}_6\text{H}_3\text{Me}_2$). With this in mind, we set out to discover N-atom transfer reactions that simultaneously produced nitrogen-containing organic products and a molybdenum complex bearing intact *tris*-amide ligands, amenable to further transformations.

The reactivity of early metal nitrides towards electrophilic or Lewis acidic substrates is well documented.²¹⁻²⁵ Indeed, the terminal nitride (**2**) has been shown to form stable Lewis acid adducts with Group 13 and 14 halides.²⁶ A preliminary investigation of the reactivity of **2** towards electrophiles resulted in the synthesis of the methylimido salt $[\text{CH}_3\text{NMo}(\text{N}[\text{tBu}]\text{Ar})_3]\text{I}$ *via* the reaction of **2** with neat CH_3I .²⁷ More recently, the treatment of $[\text{CH}_3\text{NMo}(\text{N}[\text{tBu}]\text{Ar})_3]\text{I}$ with lithium hexamethyldisilazide enabled the isolation of a ketimide complex, $\text{H}_2\text{C}=\text{NMo}(\text{N}[\text{tBu}]\text{Ar})_3$ (**3a**).²⁸

The synthesis of ketimide **3a** represents formal carbene (CH_2) addition to nitride **2**, a process that involves C–N double bond formation together with the reduction of molybdenum from the +6 to the +4 oxidation state (Scheme 1, reaction (ii)). DFT calculations carried out on the model complex $\text{NMo}(\text{NH}_2)_3$ (**2m**) predicted the enthalpy of reaction (ΔH_{rxn}) of methylene (CH_2) addition to the terminally-bound N-atom of **2m** to be $-93 \text{ kcal mol}^{-1}$. Hence, the addition of an electrophilic carbene to **2** and subsequent formation of a ketimide complex (**3**) was considered a potentially important means of activating **2** towards N-atom transfer into organic molecules. Significantly, the isolobal activation of the terminal nitride complex, $[\text{Os}^{\text{IV}}(\text{tpy})(\text{Cl})_2\text{N}]\text{BF}_4$ (tpy = 2,2':6',2''-terpyridine) was demonstrated by Meyer and coworkers *via* the transfer of an oxygen-atom to the terminally-bound N-atom in the formation of a terminal nitrosyl complex $[\text{Os}^{\text{II}}(\text{tpy})(\text{Cl})_2(\text{NO})]\text{BF}_4$.²⁹



Scheme 1. Proposed catalytic pathway for N-atom incorporation from **2** into organic nitriles (RCN). (i) Base-catalyzed cleavage of N_2 forming complex **2**. (ii) Trapping of a carbene (CRX) by **2** resulting in the formation of ketimide **3**. (iii) β -X Elimination from **3** to yield **1-X**. (iv) One-electron reduction of **1-X** to yield **1**.

Transition-metal ketimide complexes with the general formula $(\text{RR}'\text{C}=\text{N})_x\text{-ML}_n$ are well documented in the literature.^{30–34} A particularly interesting group of metal ketimides are the chalcogenobenzimidato complexes $(\text{Ph}[\text{PhE}]\text{C}=\text{N})\text{-Mo}(\text{N}^t\text{BuAr})_3$ (E = S, Se, Te) reported recently by Mendiratta *et al.*³⁵ Formation of these complexes was achieved *via* a radical pathway involving the previously characterized η^2 -benzonitrile adduct of **1**, $(\eta^2\text{-PhCN})\text{-Mo}(\text{N}^t\text{BuAr})_3$ [**1**- $\eta^2\text{PhCN}$].³⁶ The sequential treatment of **1** with 1.0 equiv of PhCN and 0.5 equiv of PhEPh (E = S, Se, or ~60 equiv PhCN and 0.5 equiv PhTePh) enabled the isolation of the corresponding molybdenum chalcogenobenzimidato complex. Upon heating, these complexes (E = Se, Te) extruded PhCN with concomitant formation of a molybdenum phenylchalcogenoate $\text{PhE-Mo}(\text{N}^t\text{BuAr})_3$ (**1-EPh**). Thermodynamic and kinetic studies confirmed that PhCN extrusion occurred *via* a unimolecular β -EPh elimination process.

Generation of an organic nitrile from ketimide complex **3** would be an important achievement if the ketimide nitrogen was derived from N_2 . An extensive search of the literature reveals that, with the exception of complex **3a**, there are no examples of metal ketimide complexes wherein the nitrogen atom of the ketimide moiety derives from N_2 .

Because of the known β -EPh elimination chemistry of chalcogenobenzimidato complexes, the addition of chalcogenoaryl-substituted carbenes [C(EPh)R] to **2** is an attractive synthetic target. While there are no reported means for the generation of chalcogenoaryl-substituted carbenes [C(EPh)Ph], a similar pathway for the regeneration of **1** from **2** could be envisaged upon the addition of any electrophilic carbene (Figure 1, reaction (i)) to form a ketimide complex in which the substituent on the ketimide carbon is unstable with respect to β -elimination. Dihalocarbenes³⁷ represent one of the most studied forms of divalent carbon³⁸ and their generation has been the subject of numerous investigations.^{39–42} Addition of dichlorocarbene to **2** was predicted to yield Cl–Mo(N[^tBu]Ar)₃ (**1-Cl**) and gaseous cyanogen chloride (Cl–CN) *via* β -Cl elimination from the intermediate ketimide complex (Cl₂C=N)–Mo(N[^tBu]Ar)₃ (**3b**). Complex **3b** was a particularly attractive target molecule for a number of reasons:

- Ease of separation of cyanogen chloride from the resulting molybdenum complex by vacuum transfer;
- Well documented reactivity of cyanogen chloride with nucleophilic alkyl and aryl reagents (e.g. RMgX),⁴³ amines, phenolates and thiolates⁴⁴ in the synthesis of organic nitriles, cyanamides, cyanates and thiocyanates;
- Precedent for the one-electron reduction of **1-Cl** to **1**.⁴⁵

The focus of this chapter is a preliminary investigation of metal-nitride bond activation by carbenes. Two methods for the generation of dichlorocarbene (or dihalocarbene) in the presence of complex **2** have been studied. Since the regeneration of **1** from **1-X** (X = Cl, EPh) (Figure 1, reaction (iv)) is important in recycling the metal center, conditions for the one-electron reduction of **1-Cl** have been optimized during the course of this investigation.

2.2 Results and Discussion

2.2.1 A brief introduction to the chemistries of dichlorocarbene (CCl_2) and fluorochlorocarbene (CFCl)

Dichlorocarbene (CCl_2) and fluorochlorocarbene (CFCl) have been the subject of numerous experimental and theoretical investigations.^{37, 39-42, 46-50} A carbene's reactivity and structure is known to depend strongly upon its spin state^{39, 51-53} and the selectivity demonstrated by a carbene correlates closely with the energy difference between the singlet and triplet states (ΔE_{ST}).^{49, 54-58}

The chemistries of dichlorocarbene and fluorochlorocarbene have received more attention compared to other mono and dihalocarbenes for two main reasons: (i) their enhanced reactivity towards a broad range of unsaturated substrates;⁵⁹⁻⁶⁷ (ii) the development of relatively straightforward and safe procedures for their generation.^{38,68,69} Both dichlorocarbene and fluorochlorocarbene exhibit singlet ground states that are stabilized (thermodynamically) relative to the triplet state by π -donation from the halogen substituents (Figure 1).⁷⁰

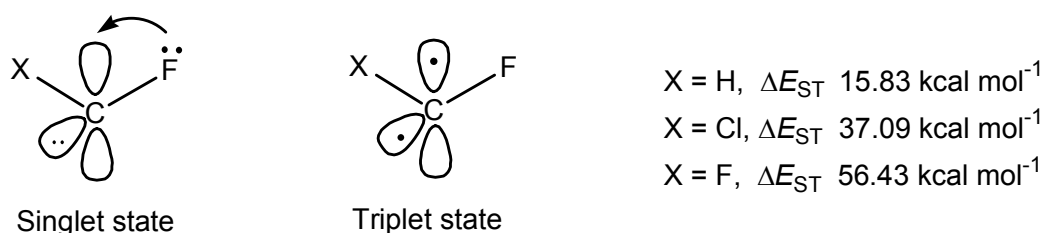


Figure 1. Singlet versus triplet states in fluoromethylene (CHF), fluorochlorocarbene (CFCl) and difluorocarbene (CF_2). All three carbenes exhibit singlet ground states (ΔE_{ST} is the energy difference between singlet and triplet states of each carbene).^{71,72}

The enhanced reactivity of dichlorocarbene and fluorochlorocarbene compared for example with difluorocarbene reflects the relative stability of the singlet ground state.⁷³

Difluorocarbene is more highly stabilized and less reactive than other halo and dihalocarbenes due to the strong π -donor capability of the two substituent fluorine atoms.⁷⁰ For this reason, difluorocarbene is often generated *via* high temperature routes. The use of dichlorocarbene and fluorochlorocarbene in this study reflects the mild conditions under which both carbenes can be generated and their singlet ground state multiplicities.[†]

2.2.2 Generation of dihalocarbenes (CX₂) *via* the titanium-mediated reduction of haloforms and the reactions of CX₂ with NMo(N[^tBu]Ar)₃ (**2**)

The convenient preparation of *gem*-dichlorocyclopropanes by the reaction of carbon tetrachloride with reduced titanium (1:1 ratio of TiCl₄ and LiAlH₄) at 0 °C in the presence of various alkenes was first reported by Onaka *et al.* in 1975.⁷⁴ This method was subsequently extended to the generation of other mono and dihalocarbenes in the work of Dolbier and Burkholder.^{75,76} Good yields of the desired *gem*-dihalocyclopropanes were achieved when the reactions were carried out using a 3:3:3:1 ratio of haloform, TiCl₄, LiAlH₄ and alkene. In their most recent study, measurement of *syn/anti* product ratios enabled the authors to conclude that the reaction involved a free carbene rather than a carbenoid species. The use of nitride complex **2** as the carbene trap in these reactions has been the subject of investigation in our laboratories.

Initially, control reactions were carried out (under conditions identical to those used in the generation of dihalocarbenes) to ensure that complex **2** did not undergo a reaction with TiCl₄·THF₂[‡] or LiAlH₄ (individually or when mixed). The robust nature of the terminal nitride complex **2** was emphasized by its lack of reactivity toward the highly reducing TiCl₄·THF₂/LiAlH₄ mixture.

[†] Complex **2** is expected to undergo reactions with singlet carbenes *via* nucleophilic attack of the N-atom lone pair on the vacant *p*-orbital of the carbene.

[‡] Replacement of TiCl₄ (a volatile liquid) by its *bis*-THF adduct, TiCl₄·THF₂ (a yellow powder), was chosen for reasons of improved ease of handling.

Reactions of complex **2** (in THF at 0 °C) with 3 equiv CFCl₃ or CCl₄ in the presence of TiCl₄·THF₂ (3 equiv) and LiAlH₄ (3 equiv) were carried out on both preparative and NMR scales. On a preparative scale, isolation of Cl–Mo(N[^tBu]Ar)₃ (**1**-Cl) was achieved in yields of 24% (CFCl₃) and 26% (CCl₄) by removal of THF solvent *in vacuo* from the product mixture followed by extraction with copious amounts of pentane and filtration through Celite to remove the insoluble titanium- and lithium-containing solids. Precipitation of **1**-Cl from a minimum amount of cold pentane enabled its separation from the unreacted pentane-soluble complex **2**. Some minor (<10%) diamagnetic impurities were observed in the ¹H NMR spectrum of **1**-Cl isolated from this reaction.

The consumption of complex **2** in this reaction was quantified by ¹H NMR (THF-d₈) versus an internal standard (Cp₂Fe). Analysis of the crude product mixture revealed partial consumption of **2** (76% consumption in the reaction with CFCl₃ and 77% consumption in the reaction with CCl₄) and the generation of two new molybdenum-containing products - one paramagnetic and one diamagnetic. The paramagnetic product, generated in 30% (CFCl₃) and 32% (CCl₄) yield, respectively, was identified as Cl–Mo(N[^tBu]Ar)₃ (**1**-Cl) by comparison of the ¹H NMR spectrum with that obtained for an independently prepared sample (section 2.2.6). The identity of the diamagnetic product (**A**) is unknown due to the inability to obtain a pure sample of this material.

Analysis of the volatile products, when CFCl₃ was employed as the haloform, was carried out using both the ¹⁴N and ¹⁵N-labeled (**2**-¹⁵N) isotopomers of complex **2** in conjunction with ¹⁹F NMR spectroscopy. The ¹⁹F NMR spectrum was identical for both isotopomers, revealing three peaks at δ 0.0 ppm (singlet, CFCl₃), –80.4 ppm (doublet, *J* 55 Hz) and –169.4 ppm (triplet, *J* 49 Hz). The –80.4 ppm resonance was also observed in control reactions carried out in the absence of complex **2**. The presence of the triplet resonance at –169.4 ppm in the ¹⁹F spectra acquired for both isotopomers indicates that the splitting is not the result of ¹⁵N–¹⁹F coupling. Assignments of the –80.4 ppm and –169.4 ppm resonances could not be determined.

The originally proposed route to the molybdenum(IV) complex $\text{Cl-Mo}(\text{N}[\text{tBu}]\text{Ar})_3$ involved dihalocarbene addition to $\text{NMo}(\text{N}[\text{tBu}]\text{Ar})_3$ to form a ketimide complex $(\text{X}_2\text{C}=\text{N})\text{-Mo}(\text{N}[\text{tBu}]\text{Ar})_3$. These ketimide complexes are presumed to undergo rapid β -X elimination to form $\text{X-Mo}(\text{N}[\text{tBu}]\text{Ar})_3$ (**1-X**) and one equivalent of cyanogen halide (X-CN). While complex **1-Cl** is formed in the reaction of complex **2** with haloforms (CFCl_3 and CCl_4) in the presence of reduced titanium, the failure of this study to determine (i) the fate of the dinitrogen-derived N-atom and (ii) the identity of the diamagnetic product (**A**) makes it impossible to provide definitive proof for this mechanism.

The conversion of complex **2** to **1-Cl** was not optimized and further studies involving this reaction were not pursued. There exist numerous limitations to the general application of this method, specifically, the use of the highly reducing mixture of $\text{TiCl}_4 \cdot \text{THF}_2$ and LiAlH_4 in the generation of the dihalocarbene. The stability of the dinitrogen-derived product of these reactions under such reducing conditions is not known but we suggest that its isolation is prohibited by reactions of this product with reagents used in the generation of the reactive carbene fragments.^{77,78}

2.2.3 Generation of alkyl (or aryl) halocarbenes (CRX) via the titanium-mediated reduction of halocarbons (CRX_3) and reactions of CRX with $\text{NMo}(\text{N}[\text{tBu}]\text{Ar})_3$ (2**)**

The scope of the reaction developed by Dolbier and Burkholder for the cyclopropanation of olefins (described in the preceding section) was investigated in their second article.⁷⁶ The authors determined that the same synthetic protocol could be applied in the generation of alkyl (or aryl) substituted halocarbenes (CRX, R = alkyl or aryl, X = Cl). Subsequently, the addition of phenylchlorocarbene ($\text{C}(\text{Ph})\text{Cl}$) and methylchlorocarbene ($\text{C}(\text{Me})\text{Cl}$) to tetra(methyl)ethylene ($\text{Me}_2\text{C}=\text{CMe}_2$) was demonstrated in yields of 58% and 15% respectively.

In the present study, the generation of phenylchlorocarbene and methylchlorocarbene in the presence of the terminal nitride complex (**2**) have been

investigated. These reactions were performed using a 3:3:3:1 ratio of haloform (either α,α,α -trichlorotoluene (PhCCl_3) or 1,1,1-trichloromethane (MeCCl_3)), $\text{TiCl}_4 \cdot \text{THF}$, LiAlH_4 and **2**. Following the removal of solvent (*in vacuo*) from the crude product mixture, the consumption of complex **2** was quantified by ^1H NMR spectroscopy (THF-d_8) versus an internal standard (Cp_2Fe). Analysis of the crude product mixture revealed a 30% (PhCCl_3) and 25% (MeCCl_3) yield of complex **1-Cl**, 60% (PhCCl_3) and 65% (MeCCl_3) unreacted complex **2**, and several unidentified diamagnetic resonances. Resonances attributed to benzonitrile (when PhCCl_3 was employed as the halocarbon) could not be assigned unambiguously in the ^1H NMR spectrum. An infrared absorption consistent with ν_{CN} of benzonitrile was not observed. The *in situ* reduction of benzonitrile (PhCN) to benzylamine (PhCH_2NH_2) is expected to be at least one of the decomposition routes of this N_2 -derived organic product.⁷⁹

^1H NMR spectroscopy was used to probe the volatile products of the reaction between complex **2** and 1,1,1-trichloromethane (MeCCl_3) in the presence of reduced titanium at 0 °C. THF and unreacted MeCCl_3 were observed in the ^1H NMR spectrum together with multiplet resonances at *ca.* δ 6.1 ppm and 5.6 ppm (integrating in a 1:2 ratio), consistent with the reported values for 1-chloroethylene ($\text{H}_2\text{C}=\text{CHCl}$).⁸⁰ Hence, the low yield of **1-Cl** (25%) when MeCCl_3 is employed as the halocarbon can be explained in part by the instability of methylchlorocarbene ($\text{C}(\text{Me})\text{Cl}$) toward 1,2-rearrangements.⁸¹

Four other resonances (δ 2.16 (s), 1.98 (m), 1.96 (m) and 0.8 (s) ppm) were observed in the ^1H NMR spectrum of the volatile products of the reaction between complex **2** and 1,1,1-trichloromethane (in the presence of reduced titanium at 0 °C). In order to determine whether one of these resonances might be assigned to acetonitrile, (the anticipated organic nitrogen-containing product) this reaction was repeated using the ^{15}N -labeled isotopomer of complex **2** (**2**- ^{15}N). This was expected to result in the observation of a doublet resonance in the ^1H NMR spectrum attributable to ^{15}N - ^1H coupling in ^{15}N -labeled acetonitrile ($\text{CH}_3\text{CN}^{15}$).⁸² The splitting of one of the four unassigned resonances in the ^1H NMR spectrum was not observed.

In summary, reactions of $\text{NMo}(\text{N}^t\text{Bu}[\text{Ar}]_3)$ (**2**) with two halocarbons; α,α,α -trichlorotoluene (PhCCl_3) and 1,1,1-trichloromethane (MeCCl_3) in the presence of reduced titanium at 0 °C have been shown to generate $\text{Cl-Mo}(\text{N}^t\text{Bu}[\text{Ar}]_3)$ (**1-Cl**) in 30% and 25% yield respectively. The low conversion of complex **2** to **1-Cl** when MeCCl_3 is employed was attributed in part to the instability of methylchlorocarbene ($\text{C}(\text{Me})\text{Cl}$) toward 1,2-rearrangements. Additionally, the low conversions achieved (**2** \rightarrow **1-Cl**) using phenylchlorocarbene and methylchlorocarbene are most likely a consequence of the reduced reactivity of these carbenes when compared with dihalocarbenes such as dichlorocarbene. The high reactivity of dichlorocarbene has been attributed to the low LUMO in this reactive fragment, as predicted by frontier molecular orbital theory.^{47,54}

2.2.4 Generation of dichlorocarbene (CCl_2) *via* thermal extrusion from a Seyferth reagent ($\text{PhHgCCl}_2\text{Br}$) and reactions of CCl_2 with $\text{NMo}(\text{N}^t\text{Bu}[\text{Ar}]_3)$ (**2**)

The transfer of dihalocarbenes from phenyl(trihalomethyl)mercury compounds (PhHgCX_3 , X = halogen) was pioneered by Seyferth and coworkers in the 1960's.⁶⁹ Research spanning more than two decades led to the development of a variety of mercuric compounds that act as efficient reagents for the transfer of alkyl (or aryl) substituted halocarbenes $\text{C}(\text{Cl})\text{R}$ (R = Ph,⁸³ CH_3 ,⁸⁴ CF_3 ,⁸⁵ CO_2Me ⁸⁶)

Seyferth reported that certain mercurial compounds were sufficiently thermally unstable (decomposition of solid and solution samples occurred on standing at 25 °C) that purification of the desired product was challenging. In other cases the thermal stability of the mercurial reagent limited its use as a divalent carbon source due to the high temperatures required to effect the thermal extrusion of a carbene from the metal compound.⁸⁷ Phenyl(bromodichloromethyl)mercury ($\text{PhHgCCl}_2\text{Br}$) is the most convenient mercuric reagent for the generation of dichlorocarbene.⁸⁸ Phenyl(bromodichloromethyl)mercury can be prepared in multi-gram quantities and isolated as an analytically pure material with relative ease.⁸⁸ Heating of $\text{PhHgCCl}_2\text{Br}$ at 65 °C in the presence of an olefin such as α -methylstyrene (1:1 ratio of reagents) results in complete consumption of the olefin and formation (>95%) of the corresponding *gem*-

dicyclopropane $\text{Ph}(\text{CH}_3)\text{C}(\text{CCl}_2)\text{CH}_2$.^{89,90} The mercurial product PhHgBr is insoluble in hydrocarbon solvents and may be separated from the organic product by filtration. Furthermore, PhHgBr is used as a starting material in the synthesis of $\text{PhHgCCl}_2\text{Br}$ so the mercurial product can be recycled.

Reaction of $\text{PhHgCCl}_2\text{Br}$ with **2** was carried out in C_6D_6 in a sealed NMR tube and monitored by ^1H NMR spectroscopy. A number of reaction conditions were surveyed in an attempt to optimize the conversion of **2** to products.

- Stoichiometric $\text{PhHgCCl}_2\text{Br}$ resulted in partial conversion of **2** to products after 24 h at 65 °C while complete consumption of **2** was effected by 5 equiv of $\text{PhHgCCl}_2\text{Br}$ within 24 h at 65 °C.
- The rate of conversion of **2** to products was slowed considerably when reactions were performed at temperatures below 60 °C (e.g. at 50 °C complete consumption of **2** occurred in ~50 h). The temperature of reaction was not increased beyond 70 °C in an effort to prevent unwanted side reactions or the thermal decomposition of products.

Monitoring the reaction of **2** with 5 equiv of $\text{PhHgCCl}_2\text{Br}$ over 24 h at 65 °C (^1H NMR) (reaction **I**), the complete consumption of **2** and the appearance of eleven new peaks in the diamagnetic region of the spectrum (0-8 ppm) were observed. No resonances attributable to **1-Cl** were seen at any time. PhHgBr was seen to precipitate from solution and, following isolation, its characterization was confirmed by a melting point analysis.⁸⁸

A number of control reactions were carried out (at a temperature of 65 °C in C_6D_6 solvent, unless noted otherwise) and monitored by ^1H NMR spectroscopy:

Reaction of 2 with PhHgBr	(II)
Reaction of 1-Cl with PhHgBr	(III)
Reaction of 1-Cl with $\text{PhHgCCl}_2\text{Br}$ (25 °C and 65 °C)	(IVa and IVb)
Thermal stability of 1-Cl in solution	(V)

Reaction of **1** with 5 equiv PhHgCCl₂Br (25 °C) (VI)

Reaction of **1-Br** with PhHgCCl₂Br (VII)

It was hoped that these control reactions might aid in the assignment of the eleven new resonances observed in the ¹H NMR spectrum for reaction (I).

PhHgBr showed no reaction with either **2** or **1-Cl** after 24 h (reactions II and III). This is presumed to be due to the very low solubility of PhHgBr in benzene solvent.

Addition of a benzene solution of PhHgCCl₂Br to **1-Cl** at 25 °C (IVa) resulted in the complete consumption of **1-Cl** within 48 h and the appearance of eleven new peaks in the diamagnetic region of the ¹H NMR spectrum. When repeated at 65 °C (IVb) the same eleven resonances were seen in the ¹H NMR spectrum (in approximately the same ratio of peak integrals) with complete consumption of **1-Cl** observed within 24 h. Reaction IV is not thought to occur *via* attack of free dichlorocarbene on **1-Cl** due to the efficiency of this reaction at 25 °C (at this temperature the rate of dichlorocarbene extrusion is reduced, as evidenced by the slow (>5 d) conversion of olefins to the corresponding *gem*-dichloropropanes).⁹¹

The thermal stability of **1-Cl** in solution (V) was tested under a number of conditions. Decomposition of **1-Cl** to a single diamagnetic product was observed upon standing in benzene solution at 25 °C. The half-life (*t*_{1/2}) of **1-Cl** varied from 15 h to 4 d depending upon the sample. The reason for this variation is possibly due to the different concentrations at which these thermal stability experiments were performed. This would indicate that decomposition of **1-Cl** occurs *via* a bimolecular (or higher) pathway. The rate of decomposition of **1-Cl** was reduced when the sample was monitored in THF or diethyl ether solvent (*t*_{1/2} = 2-4 d). Decomposition was also inhibited upon storage at low temperatures (e.g. **1-Cl** in C₆D₆ at 0-5 °C, *t*_{1/2} ~2 d). At 35 °C the decomposition of **1-Cl** to a new paramagnetic product, free amine (HN[^tBu]Ar) and several other unidentified diamagnetic products was observed. The resonances attributed to the decomposition

products of **1-Cl** are not consistent with any of the eleven diamagnetic peaks seen in reaction **I**.

Complex **1** was observed to undergo reaction with 5 equiv PhHgCCl₂Br (**VI**) upon mixing at 25 °C. A ¹H NMR spectrum obtained 10 min after combining **1** with PhHgCCl₂Br displayed resonances attributed to the formation of **1-Cl** and **1-Br**.

Reaction of **1-Br** with 1 equiv PhHgCCl₂Br (**VII**) in C₆D₆ at 25 °C was monitored by ¹H NMR spectroscopy. After 10 min, 60% **1-Br** remained and complex **1-Cl** was observed in 20% yield. Eleven new peaks in the diamagnetic region of the spectrum were consistent with those observed in the reaction of **1-Cl** with PhHgCCl₂Br (**IV**).

In summary, the chemical shift and ratio of peak integrals observed in the ¹H NMR spectra for reactions **I** and **IV** indicate that **1-Cl** is most probably formed in the reaction of PhHgCCl₂Br with **2**. The thermal decomposition products of **1-Cl** are not observed in the ¹H NMR spectrum of reaction **I** because the consumption of complex **1-Cl** by PhHgCCl₂Br occurs more rapidly. The intermediacy of complexes **1** and **1-Br** cannot be ruled out since the reaction of **1** with PhHgCCl₂Br (**V**) yields **1-Cl** and **1-Br** and the reaction of **1-Br** with PhHgCCl₂Br (**V**) yields **1-Cl** and several unidentified diamagnetic products whose ¹H NMR resonances are consistent with those observed in the reaction of **1-Cl** with PhHgCCl₂Br (**IV**).

2.2.5 Independent synthesis of Cl–Mo(N[^tBu]Ar)₃ (**1-Cl**) and Br–Mo(N[^tBu]Ar)₃ (**1-Br**)

The independent synthesis of complexes **1-X** (Figure 2, X = Cl, Br) was achieved by the reaction of complex **1** with 1,2-dichloroethane (**1-Cl**, 66% yield) or 1,2-dibromoethane (**1-Br**, 69% yield). While **1-Cl** has been reported previously,^{45,92} our attempts to synthesize **1-Cl** by reaction of **1** in CH₂Cl₂ gave only low yields of **1-Cl** together with the formation of other, unidentified products.⁹³

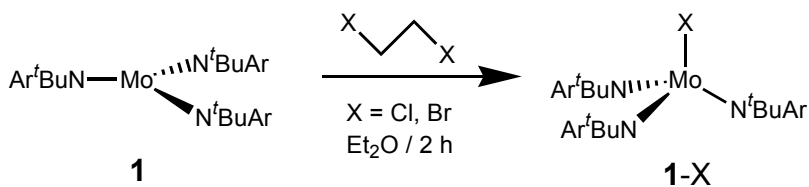


Figure 2. Synthesis of complexes **1-X** (X = Cl, Br)

Complexes **1-Cl** and **1-Br** are orange-brown paramagnetic compounds with distinctive broad resonances in their ^1H NMR spectra at *ca.* 24 ppm and 17 ppm, respectively. Both complexes were thermally stable in solution and in the solid state when stored at -35 °C. Decomposition of **1-Cl** to an unidentified diamagnetic product was observed when the sample was stored at 25 °C in C_6D_6 (*vide supra*).

2.2.6 One-electron reduction reactions of $\text{Cl}-\text{Mo}(\text{N}^t\text{BuAr})_3$ (**1-Cl**)

The one-electron reduction of $\text{Cl}-\text{Mo}(\text{N}^t\text{BuAr})_3$ (**1-Cl**) was achieved using 10 equivalents of magnesium metal in THF (Figure 3). The ease of separation of MgCl_2 and excess magnesium metal from the solution of **1** made this an attractive means for the generation of **1** from **1-Cl**.

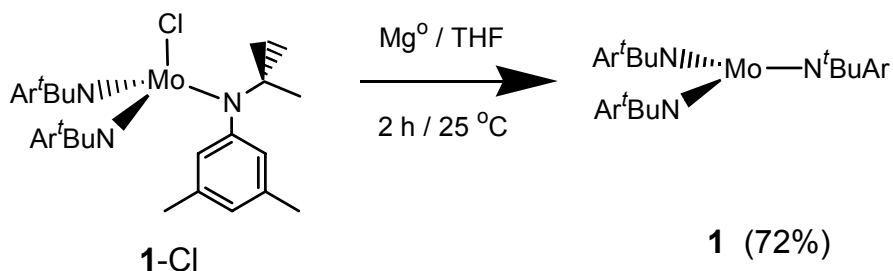


Figure 3. The one-electron reduction of **1-Cl** by magnesium.

The three-coordinate titanium(III) complex $\text{Ti}(\text{N}^t\text{BuAr})_3$ is an excellent one-electron reductant⁹⁴ and readily forms titanium(IV) complexes $\text{X}-\text{Ti}(\text{N}^t\text{BuAr})_3$ (X = Cl, Br, OTf). Addition of $\text{Ti}(\text{N}^t\text{BuAr})_3$ to **1-Cl** resulted in the clean formation of **1** and

Cl–Ti(N[^tBu]Ar)₃ after 30 min. The more difficult separation of the two products and the time-consuming synthesis of Ti(N[^tBu]Ar)₃ make this route considerably less favorable than the magnesium reduction of **1-Cl**.

Attempts to reduce **1-Cl** using sodium amalgam (Na/Hg) under an atmosphere of argon resulted in low conversion to **1** and substantial amounts of free amine HN[^tBu]Ar. The one-pot conversion of **1-Cl** to **2** using Na/Hg⁹ under an atmosphere of nitrogen effected the complete consumption of **1-Cl** within 6 h. ¹H NMR spectroscopy indicated that only low conversion to **2** (<15%) had been achieved together with the formation of free amine HN[^tBu]Ar.

2.2.7 Concluding remarks and future directions

Reactions of the terminal molybdenum nitride complex NMo(N[^tBu]Ar)₃ (**2**) with haloforms (and halocarbons) in the presence of reduced titanium represent unique examples of metal-nitride bond activation toward removal of the dinitrogen-derived N-atom by a non-metallic species in homogeneous solution. Importantly, the molybdenum *tris*-amide framework is not compromised by the conditions under which the reaction is performed, thereby rendering the molybdenum(IV) product Cl–Mo(N[^tBu]Ar)₃ (**1-Cl**) available for further transformations. The one-electron reduction chemistry of **1-Cl** has been investigated and the conditions for the generation of Mo(N[^tBu]Ar)₃ (**1**) have been optimized.

There exist significant limitations to this method of activating the metal-nitride functionality. Primarily, isolation of the nitrogen-containing organic products of these reactions (wherein the N-atom derives from molecular N₂) is prohibited by their reaction with reagents used in the generation of reactive carbene fragments.

Activation of complex **2** toward removal of the terminal N-atom, *via* reaction with the Seyferth reagent PhHgCCl₂Br resulted in the conversion of **2** to a number of unidentified diamagnetic products. These products are suggested to result from the

reaction of complex **1-Cl** with PhHgCCl₂Br. We propose that this reaction proceeds *via* dichlorocarbene addition to complex **2** followed by β -Cl elimination to yield complex **1-Cl**.

The search for electrophilic carbenes (CXY) is ongoing, with the goal of exploiting the ability of molybdenum(IV) ketimide complexes (**3**) to undergo β -X elimination as a means of extruding organic nitriles (Y-CN) derived from molecular N₂.

2.3 Experimental Section

2.3.1 General Information

Information pertaining to the acquisition of solution NMR spectra and other general details are identical to those included in chapter 1. Additional information relevant to this research is as follows: synthesis of ¹⁵NMo(N[^tBu]Ar)₃ was described in chapter 1. TiCl₄·THF₂ was prepared following the method of Manzer.⁹⁵ PhHgCCl₂Br was prepared following the method of Seyferth.⁸⁸ α -Methylstyrene was distilled under vacuum from CaH₂, freeze-thaw degassed and stored over 4 Å molecular sieves prior to use. Fluorotrichloromethane (CFCl₃), carbon tetrachloride (CCl₄), 1,1,1-trichloromethane (MeCCl₃) and α,α,α -trichlorotoluene (PhCCl₃) were distilled (or vacuum distilled in the case of PhCCl₃), freeze-thaw degassed and stored over 4 Å molecular sieves prior to use.

2.3.2 Synthesis of Cl-Mo(N[^tBu]Ar)₃ (**1-Cl**) from NMo(N[^tBu]Ar)₃ (**2**)

A 50 mL schlenk flask containing TiCl₄·THF₂ (3 equiv, 0.224 g, 0.704 mmol) and THF (8 mL) was chilled to -35 °C. In a 20 mL scintillation vial, a suspension of LiAlH₄ (3 equiv, 0.027 g, 0.704 mmol) in THF (8 mL) was chilled to -35 °C. The dropwise addition of the LiAlH₄/THF suspension to the yellow suspension of TiCl₄·THF₂/THF resulted in a color change through pale green to dark brown with rapid effervescence. The flask was capped with a rubber septum and stirred at 0 °C in a salt-ice bath under a

flow of N₂ for 20 minutes. The ice bath was removed and the mixture was allowed to warm to 20 °C over 10 minutes. The flask was cooled again in a salt-ice bath. A solution of NMo(N[^tBu]Ar)₃ (0.150 g, 0.235 mmol) in THF (8 mL) was added *via* a syringe to the flask. This was followed immediately by the addition of haloform (3 equiv, 0.704 mmol) in THF (2 mL). The mixture was stirred for 30 minutes at 0 °C after which time solvent removal *in vacuo* yielded dark brown/black solids. The solids were triturated with hexanes (2 x 5 mL) and then extracted with copious amounts of pentane (3 x 25 mL). The brown-orange solution was filtered through Celite in scintered glass frit and the pentane solvent was removed *in vacuo*. The dark orange powder was dissolved in a minimum of cold pentane and filtered to collect a brown-orange powder identified by ¹H NMR spectroscopy to be Cl–Mo(N[^tBu]Ar)₃ (**1-Cl**). Removal of pentane from the filtrate yielded a pale brown powder identified by ¹H NMR spectroscopy to be NMo(N[^tBu]Ar)₃ (**2**).

An identical procedure was employed for each of the haloforms (isolated yield of **1-Cl** is indicated in parentheses); fluorotrichloromethane (CFCl₃) (0.037 g, 0.056 mmol, 24%), carbon tetrachloride (CCl₄) (0.040 g, 0.061 mmol, 26%), 1,1,1-trichloromethane (CH₃CCl₃) (0.036 g, 0.054 mmol, 23%) and α,α,α -trichlorotoluene (PhCCl₃) (0.037 g, 0.056 mmol, 24%).

2.3.3 Control reaction of NMo(N[^tBu]Ar)₃ (**2**) in the presence of LiAlH₄ and TiCl₄·THF₂

This reaction was carried out as described above using TiCl₄·THF₂ (3 equiv, 0.037 g, 0.12 mmol), LiAlH₄ (3 equiv, 0.005 g, 0.12 mmol) and NMo(N[^tBu]Ar)₃ (0.025 g, 0.235 mmol) in a total of 10 mL THF. ¹H NMR of the crude reaction mixture (THF-d₈) indicated that no deterioration of the NMo(N[^tBu]Ar)₃ had occurred. Increasing the temperature (25 °C) and the reaction time (up to 2 h) resulted in no deterioration in the NMo(N[^tBu]Ar)₃ (as observed by ¹H NMR).

2.3.4 NMR quantification of $\text{NMo}(\text{N}^t\text{BuAr})_3$ (**2**) conversion to $\text{Cl-Mo}(\text{N}^t\text{BuAr})_3$ (**1-Cl**)

These reactions were carried out as described above using $\text{TiCl}_4 \cdot \text{THF}_2$ (3 equiv, 0.090 g, 0.28 mmol), LiAlH_4 (3 equiv, 0.011 g, 0.028 mmol), $\text{NMo}(\text{N}^t\text{BuAr})_3$ (0.060 g, 0.094 mmol) and haloform (3 equiv, 0.704 mmol) in a total of 15 mL THF. Solvent was removed from the crude product mixture *in vacuo* and consumption of $\text{NMo}(\text{N}^t\text{BuAr})_3$ (**2**) was quantified by ^1H NMR (THF-d_8) versus an internal standard (Cp_2Fe ; δ 4.00 ppm, s, 10 H). For all four haloforms analysis of the crude product mixture revealed partial consumption of $\text{NMo}(\text{N}^t\text{BuAr})_3$ and the generation of $\text{Cl-Mo}(\text{N}^t\text{BuAr})_3$ (**1-Cl**). When CCl_4 and CFCl_3 were employed as the haloform a new diamagnetic product (**A**) was also obtained. ^1H NMR of product **A** (THF-d_8) δ : 6.57 (s, 3 H), 5.63 (s, 6 H), 1.99 (s, 18 H), 1.25 (s, 27 H).

Results

Haloform	2 (% remaining)	1-Cl (% yield)	Other products
CCl_4	23	32	A
CFCl_3	24	30	A
CH_3CCl_3	65	25	Yes
PhCCl_3	60	30	Yes

2.3.5 Analysis of volatile components produced in the reaction of $^{15}\text{NMo}(\text{N}^t\text{BuAr})_3$ (**2- ^{15}N**) with $\text{TiCl}_4 \cdot \text{THF}_2$, LiAlH_4 and CFCl_3

A 25 mL glass reaction vessel (fitted with a ground glass joint) was modified using glass-blowing techniques to enable the vacuum transfer of volatile materials from the main vessel into an NMR tube fitted with a ground glass joint. To the 25 mL vessel was added $\text{TiCl}_4 \cdot \text{THF}_2$ (3 equiv, 0.224 g, 0.704 mmol) and LiAlH_4 (3 equiv, 0.027 g, 0.704 mmol). Chilled ($-35\text{ }^\circ\text{C}$) THF (~ 2 mL) was added to the mixture of solids. The 25 mL vessel was capped with a rubber septum and the NMR tube was fitted with a gas

adaptor. The THF suspension was stirred at 0 °C in a salt-ice bath under a flow of N₂ for 20 minutes. A solution of ¹⁵NMo(N[^tBu]Ar)₃ (0.150 g, 0.235 mmol) in THF (~1 mL) was added via a syringe to the THF suspension. This was followed immediately by the addition of CFC₃ (3 equiv, 0.07 mL, 0.704 mmol). The mixture was stirred for 30 minutes at 0 °C after which time the THF suspension was frozen by immersion of the 25 mL vessel in liquid N₂ and the head space of the reactor was evacuated. Vacuum transfer of the volatiles into the NMR tube was achieved under a static vacuum. Once the transfer was complete the contents of the NMR tube were frozen (immersion in liquid N₂) and the tube was flame sealed. ¹⁹F NMR (282 MHz, THF-d₈, 20 °C) of the volatiles δ: 0.0 (CFC₃), -80.4 (d, *J* 55 Hz), -169.4 (t, *J* 49 Hz).

2.3.6 Analysis of volatile components produced in the reaction of NMo(N[^tBu]Ar)₃ (2) with TiCl₄·THF₂, LiAlH₄ and CH₃CCl₃

The reaction was carried out as described above in THF-d₈ solvent using CH₃CCl₃ (0.07 mL). ¹H NMR spectroscopy (300 MHz, THF-d₈, 20 °C) identified CH₃CCl₃ (δ 2.7 ppm), CH₂CHCl δ: 6.1 (m, CH₂CHCl), 5.5 (m, CH₂CHCl) and four other peaks that could not be assigned at δ 2.16 (s), 1.98 (m), 1.96(m) and 0.8 ppm (s).

2.3.7 Reaction of PhHgCCl₂Br with NMo(N[^tBu]Ar)₃ (2)

To a solution of NMo(N[^tBu]Ar)₃ (0.030 g, 0.047 mmol) in C₆D₆ (~0.8 mL) was added solid PhHgCCl₂Br (5 equiv, 0.103 g, 0.23 mmol). This solution was transferred to a J. Young tube and subsequently heated at 65 °C for 24 h. Analysis by ¹H NMR spectroscopy revealed complete consumption of NMo(N[^tBu]Ar)₃ and 11 new peaks in the diamagnetic region of the spectrum (relative ratios are indicated in parentheses) δ: 7.86 (0.9), 7.59 (1.8), 7.42 (4.4), 2.03 (18.5), 1.93-1.92 (15.3), 1.80 (5.2), 1.60 (10.1), 1.48 (15.1), 1.45 (27.0), 1.34 (6.3), 1.25 (8.8).

2.3.8 Reaction of PhHgBr with Cl–Mo(N[^tBu]Ar)₃ (1-Cl)

A mixture of Cl–Mo(N[^tBu]Ar)₃ (0.040 g, 0.06 mmol) and PhHgBr (0.022 g, 0.06 mmol) in C₆D₆ (~1 mL) was prepared in a vial and stirred at 25 °C for 19 h. The suspension was filtered to remove the insoluble PhHgBr and analyzed by ¹H NMR spectroscopy. No deterioration of Cl–Mo(N[^tBu]Ar)₃ (1-Cl) was observed. The same result was obtained when this reaction was repeated at 65 °C.

2.3.9 Reaction of PhHgBr with NMo(N[^tBu]Ar)₃ (2)

The reaction was carried out as described above using NMo(N[^tBu]Ar)₃ (0.040 g, 0.062 mmol) and PhHgBr (0.028 g, 0.062 mmol) in C₆D₆ (~1 mL). Analysis by ¹H NMR spectroscopy showed that no deterioration of NMo(N[^tBu]Ar)₃ (2) had occurred. The same result was obtained when this reaction was repeated at 65 °C.

2.3.10 Reaction of PhHgCCl₂Br with Cl–Mo(N[^tBu]Ar)₃ (1-Cl)

To a solution of Cl–Mo(N[^tBu]Ar)₃ (0.050 g, 0.076 mmol) in C₆D₆ (~0.8 mL) was added solid PhHgCCl₂Br (0.033 g, 0.076 mmol). This solution was transferred to a J. Young tube and allowed to stand at 25 °C for 40 h. Analysis by ¹H NMR spectroscopy revealed >85% consumption of Cl–Mo(N[^tBu]Ar)₃ together with 11 new peaks in the diamagnetic region of the spectrum (relative ratios are indicated in parentheses) δ : 7.86 (1.0), 7.59 (2.1), 7.42 (4.8), 2.03 (18.0), 1.93-1.92 (12.7), 1.80 (4.6), 1.60 (10.3), 1.48 (7.41), 1.45 (23.3), 1.34 (11.8), 1.25 (7.5).

2.3.11 Reaction of PhHgCCl₂Br with Mo(N[^tBu]Ar)₃ (1)

A mixture of Mo(N[^tBu]Ar)₃ (0.030 g, 0.048 mmol) and PhHgCCl₂Br (0.021 g, 0.048 mmol) in C₆D₆ (~0.8 mL) was prepared in a vial and stirred at 25 °C for 10 min before transferring to an NMR tube for analysis by ¹H NMR spectroscopy. Two

paramagnetic products were observed; ClMo(N[^tBu]Ar)₃ (**1-Cl**) and BrMo(N[^tBu]Ar)₃ (**1-Br**).

2.3.12 Reaction of PhHgCCl₂Br with Br–Mo(N[^tBu]Ar)₃ (**1-Br**)

A mixture of Br–Mo(N[^tBu]Ar)₃ (0.030 g, 0.043 mmol) and PhHgCCl₂Br (0.019 g, 0.043 mmol) in C₆D₆ (~0.8 mL) was prepared in a vial and stirred at 25 °C for 10 min before transferring to an NMR tube for analysis by ¹H NMR spectroscopy. Approximately 60% of the Br–Mo(N[^tBu]Ar)₃ remained and the generation of one other paramagnetic product – identified as complex **1-Cl** (20%) was observed. Eleven peaks in the diamagnetic region of the spectrum (accounting for *ca.* 20% of the products) were consistent with those observed in the reaction of **1-Cl** with PhHgCCl₂Br.

2.3.13 Syntheses of X–Mo(N[^tBu]Ar)₃ (**1-Cl**, **1-Br**) from Mo(N[^tBu]Ar)₃ (**1**)

A solution of Mo(N[^tBu]Ar)₃ (0.20g, 0.32 mmol) in Et₂O (6 mL) was chilled to –35 °C in a 20 mL scintillation vial. In a second vial, a solution of 10 equiv 1,2-dihaloethane (0.158 g, 3.20 mmol, 1,2 dichloroethane for **1-Cl**; 0.300 g, 3.2 mmol, 1,2 dibromoethane for **1-Br**) in Et₂O (2 mL) was chilled to –35 °C. Once cold, the 1,2-dihaloethane was added to the solution of Mo(N[^tBu]Ar)₃ and the mixture was stirred at 25 °C for 2 h. The orange-brown solution turned a darker brown color as it warmed to 25 °C. Solvent removal *in vacuo* gave an orange-brown powder that was dissolved in minimum Et₂O. Orange-brown solids were precipitated from solution upon addition of cold (–35 °C) pentane. These solids were isolated by filtration, washed with 2 mL cold pentane and dried *in vacuo* to yield 0.140 g (0.21 mmol, 66%) **1-Cl** and 0.155 g (0.22 mmol, 69%) **1-Br**. Both **1-Cl** and **1-Br** could be recrystallized from a concentrated solution of Et₂O stored at –35 °C for 2 days.

1-Cl: ¹H NMR (300 MHz, C₆D₆, 20 °C) δ : 24.17 (br s, *v*_{1/2} 76 Hz), –1.45 (s, *v*_{1/2} 8 Hz), –5.06 (s, *v*_{1/2} 14 Hz). Impurities included minor quantities (< 2% by NMR) of

$\text{NMo}(\text{N}[\text{tBu}]\text{Ar})_3$ and $\text{HN}[\text{tBu}]\text{Ar}$, both present from the synthesis of the starting material, $\text{Mo}(\text{N}[\text{tBu}]\text{Ar})_3$.

1-Br: ^1H NMR (300 MHz, C_6D_6 , 20 °C) δ : 17.30 (br s, $\nu_{1/2}$ 165 Hz), -0.435 (s, $\nu_{1/2}$ 12 Hz), -1.57 (br s, $\nu_{1/2}$ 87 Hz).

2.3.14 Thermal stability of **1-Cl**

A C_6D_6 (~0.8 mL) solution of $\text{Cl-Mo}(\text{N}[\text{tBu}]\text{Ar})_3$ (0.03 g) was stored at 25 °C in a sealed NMR tube. Analysis of this solution was carried out at frequent intervals over 30 h. After 30 h >85% of **1-Cl** had been consumed and a new diamagnetic product was observed. ^1H NMR (300 MHz, C_6D_6 , 20 °C) δ : 6.46 (s, 3 H), 6.41 (s, 6 H), 2.19 (s, 18 H), 1.18 (s, 27 H).

When this study was repeated in THF the rate of decomposition of **1-Cl** was reduced (>90% **1-Cl** remains after 20 h).

A C_6D_6 (~0.8 mL) solution of $\text{Cl-Mo}(\text{N}[\text{tBu}]\text{Ar})_3$ (0.03 g) was heated at 35 °C in an oil bath in a sealed NMR tube. Analysis of this solution was carried out at frequent intervals over 7 d. After 7 d >85% of **1-Cl** had been consumed. A new paramagnetic product is observed with resonances at δ : 28.2, -7.6 , -18.5 and -27 ppm. Peaks in the diamagnetic region of the spectrum are attributed to free amine $\text{HN}[\text{tBu}]\text{Ar}$, $\text{NMo}(\text{N}[\text{tBu}]\text{Ar})_3$ (<2%) and several other unidentified products.

2.3.15 One-electron reduction of $\text{Cl-Mo}(\text{N}[\text{tBu}]\text{Ar})_3$ (**1-Cl**) with magnesium

A solution of $\text{Cl-Mo}(\text{N}[\text{tBu}]\text{Ar})_3$ (0.150 g, 0.227 mmol) in THF (5 mL) was chilled to -35 °C and added to a stirred slurry of Mg powder (0.017 g, 10 equiv, 2.7 mmol) in THF (2 mL). The mixture was stirred at 25 °C for 2 h. A subtle darkening of the orange-brown solution was noted. THF was removed under a dynamic vacuum and the powder was then extracted with pentane. Filtration through Celite and removal of pentane *in vacuo* afforded an orange-brown powder, weight: 0.102 g (72%), identified by ^1H NMR as $\text{Mo}(\text{N}[\text{tBu}]\text{Ar})_3$ (**1**).

2.3.16 Alternate method for the one-electron reduction of Cl–Mo(N[^tBu]Ar)₃ (1-Cl)

A solution of Cl–Mo(N[^tBu]Ar)₃ (0.050 g, 0.076 mmol) in Et₂O (2 mL) was chilled to –35 °C. In a second vial a solution of Ti(N[^tBu]Ar)₃ (0.044 g, 0.076 mmol) in Et₂O (2 mL) was prepared and chilled to –35 °C. The Ti(N[^tBu]Ar)₃ solution was added to the Cl–Mo(N[^tBu]Ar)₃ solution and the mixture was stirred at 25 °C for 30 min. Removal of the solvent *in vacuo* yielded a dark orange powder. ¹H NMR showed that 2 new products were present in solution - Mo(N[^tBu]Ar)₃ (**1**) and Cl–Ti(N[^tBu]Ar)₃. ¹H NMR Cl–Ti(N[^tBu]Ar)₃: (300 MHz, C₆D₆, 20 °C) δ : 6.72 (s, 3 H, para), 6.32 (br s, 6 H, ortho), 2.21 (s, 18 H, ArMe), 1.40 (s, 27 H, NC(CH₃)₃).

Reactions performed using 0.150 g 4-Cl enabled isolation of pure Cl–Ti(N[^tBu]Ar)₃ by extraction of the orange powder with cold pentane and filtration to collect Cl–Ti(N[^tBu]Ar)₃. The filtrate contained 4-Cl as the major product and a small amount of Cl–Ti(N[^tBu]Ar)₃.

2.3.17 Attempted one-electron reduction of 1-Cl employing Na/Hg under argon

A solution of Cl–Mo(N[^tBu]Ar)₃ (0.070 g, 0.106 mmol) in THF (6 mL) was chilled to –35 °C. In a second vial a 0.04% sodium amalgam was prepared and 2 mL of chilled (–35 °C) THF was added. The solution of Cl–Mo(N[^tBu]Ar)₃ was added to the sodium amalgam and the mixture stirred for 7 h under an atmosphere of argon. The solution turned a darker brown color over the period of the reaction. The THF solution was decanted from the sodium amalgam and solvent was removed *in vacuo*. The greasy brown solids were extracted with pentane and filtered through Celite. Following removal of pentane under a dynamic vacuum the solids were analyzed by ¹H NMR spectroscopy. Complete consumption of 1-Cl was observed and the major product was free amine HN[^tBu]Ar. Resonances attributed to NMo(N[^tBu]Ar)₃ (**2**) were seen together with other unidentified products.

2.3.18 Attempted synthesis of $\text{NMo}(\text{N}[\text{tBu}]\text{Ar})_3$ (**2**) from $\text{Cl-Mo}(\text{N}[\text{tBu}]\text{Ar})_3$ (**1-Cl**)

A solution of $\text{Cl-Mo}(\text{N}[\text{tBu}]\text{Ar})_3$ (0.070 g, 0.106 mmol) in THF (6 mL) was chilled to $-35\text{ }^\circ\text{C}$. In a second vial a 0.04% sodium amalgam was prepared and 2 mL of chilled ($-35\text{ }^\circ\text{C}$) THF was added. The solution of $\text{Cl-Mo}(\text{N}[\text{tBu}]\text{Ar})_3$ was added to the sodium amalgam and the mixture stirred vigorously for 20 h under an atmosphere of N_2 . After *ca.* 45 min the solution had turned a purple color. The THF solution was decanted from the sodium amalgam and solvent was removed *in vacuo*. The greasy orange-brown solids were extracted with pentane and filtered through Celite. Following removal of pentane under a dynamic vacuum the solids were analyzed by ^1H NMR spectroscopy. Complete consumption of **1-Cl** was observed with peaks attributed to $\text{NMo}(\text{N}[\text{tBu}]\text{Ar})_3$ (**2**), free amine $\text{HN}[\text{tBu}]\text{Ar}$ and several other unidentified products.

References

-
- [1] Laplaza, C. E.; Cummins, C. C. *Science* **1995**, *268*, 861.
 [2] Laplaza, C. E.; Johnson, M. J. A.; Peters, J. C.; Odom, A. L.; Kim, E.; Cummins, C. C.; George, G. N.; Pickering, I. J. *J. Am. Chem. Soc.* **1996**, *118*, 8623.
 [3] Zanotti-Gerosa, A.; Solari, E.; Giannini, L.; Floriani, C.; Chiesi-Villa, A.; Rizzoli, C. *J. Am. Chem. Soc.* **1998**, *120*, 437.
 [4] Caselli, A.; Solari, E.; Scopelliti, R.; Floriani, C.; Re, N.; Rizzoli, C.; Chiesi-Villa, A. *J. Am. Chem. Soc.* **2000**, *122*, 3652.
 [5] Clentsmith, G. K. B.; Bates, V. M. E.; Hitchcock, P. B.; Cloke, F. G. N. *J. Am. Chem. Soc.* **1999**, *121*, 10444.
 [6] Pool, J. A.; Lobkovsky, E.; Chirik, P. J. *Nature* **2004**, *427*, 527.
 [7] Solari, E.; Da Silva, C.; Iacono, B.; Hesschenbrouck, J.; Scopelliti, R.; Floriani, C. *Angew. Chem. Int. Ed.* **2001**, *40*, 3907.
 [8] Kewaguchi, H.; Matsuo, T. *Angew. Chem. Int. Ed.* **2002**, *41*, 2792.
 [9] Peters, J. C.; Cherry, J-P. F.; Thomas, J. C.; Baraldo, L.; Mindiola, D. J.; Davis, W. M.; Cummins, C. C. *J. Am. Chem. Soc.* **1999**, *121*, 10053.
 [10] Tsai, Y-C.; Cummins, C. C. *Inorg. Chim. Acta.* **2003**, *345*, 63.
 [11] Neyman, K. M.; Nasluzov, V. A.; Hahn, J.; Landis, C. R.; Rösch, N. *Organometallics* **1997**, *16*, 995.
 [12] Cui, Q.; Musaev, D.G.; Svensson, M.; Sieber, S.; Morokuma, K. *J. Am. Chem. Soc.* **1995**, *117*, 12366.
 [13] Cummins, C. C. *Chem. Commun.* **1998**, 1777.
 [14] Holm, R. H. *Chem. Rev.* **1987**, *87*, 1401.
 [15] Lim, B. S.; Holm, R. H. *J. Am. Chem. Soc.* **2001**, *123*, 1920.
 [16] Woo, L. K. *Chem. Rev.* **1993**, *93*, 1125.

- [17] Laplaza, C. E.; Johnson, A. R.; Cummins, C. C. *J. Am. Chem. Soc.* **1996**, *118*, 709.
- [18] Johnson, M. J. A.; Lee, P. M.; Odom, A. L.; Davis, W. M.; Cummins, C. C. *Angew. Chem. Int. Ed.* **1997**, *36*, 87.
- [19] Agapie, T.; Odom, A. L.; Cummins, C. C. *Inorg. Chem.* **2000**, *39*, 174.
- [20] Henderickx, H.; Kwakkenbos, G.; Peters, A.; van der Spoel, J.; de Vries, K. *Chem. Commun.* **2003**, 2050.
- [21] Chatt, J.; Heaton, B. T. *J. Chem. Soc. A* **1971**, 705.
- [22] Bishop, M. W.; Chatt, J.; Dilworth, J. R.; Neaves, B. D.; Dahlstrom, P.; Hyde, J.; Zubieta, J. *J. Organomet. Chem.* **1981**, *213*, 109.
- [23] Dantona, R.; Schweda, E.; Strähle, J. Z. *Naturforsch. B* **1984**, *39*, 733.
- [24] Kafitz, W.; Weller, F.; Dehnicke, K. *Z. Anorg. Allg. Chem.* **1982**, *490*, 175.
- [25] Dehnicke, K.; Strähle, J. *Angew. Chem. Int. Ed.* **1992**, *31*, 955.
- [26] Refer to Chapter 1 for synthesis and characterization of several Lewis acid adducts of $\text{NMo}(\text{N}^t\text{BuAr})_3$.
- [27] Johnson, A. R. Ph.D. Thesis, Massachusetts Institute of Technology; Cambridge, MA: 1997.
- [28] Refer to Chapter 1 for synthesis and characterization of $\text{H}_2\text{C}=\text{NMo}(\text{N}^t\text{BuAr})_3$.
- [29] Williams, D. S.; Meyer, T. J.; White, P. S. *J. Am. Chem. Soc.* **1995**, *117*, 823.
- [30] Bochmann, M.; Wilson, L. M.; Hursthouse, M. B.; Motevall, M. *Organometallics* **1988**, *7*, 1148.
- [31] Diaconescu, P. L.; Cummins, C. C. *J. Am. Chem. Soc.* **2002**, *124*, 7660.
- [32] Figueroa, J. S.; Cummins, C. C. *J. Am. Chem. Soc.* **2003**, *125*, 4020.
- [33] Zhang, S.; Piers, W. E.; Gao, X.; Parvez, M. *J. Am. Chem. Soc.* **2000**, *122*, 5499.
- [34] Zhang, S.; Piers, W. E. *Organometallics* **2001**, *20*, 2088.
- [35] Mendiratta, A.; Cummins, C. C.; Kryatova, O. P.; Rybak-Akimova, E. V.; McDonough, J. E.; Hoff, C. D. *Inorg. Chem.* **2003**, *42*, 8621.
- [36] Tsai, Y. C.; Stephens, F. H.; Meyer, K.; Mendiratta, A.; Gheorghiu, M. D.; Cummins, C. C. *Organometallics* **2003**, *22*, 2902.
- [37] Brahms, D. L. S.; Dailey, W. P. *Chem. Rev.* **1996**, *96*, 1585.
- [38] Hine, J. *Divalent Carbon*; Ronald Press: New York, 1964.
- [39] Kirmse, W. *Carbene chemistry* Academic Press; New York: 1971.
- [40] Seyferth, D. *Organometallic compounds as precursors for fluorinated carbenes in Carbenes*, Vol. I; Jones, M.; Moss, R. A. Eds.; Wiley: New York, 1971, p. 101.
- [41] *Carbene chemistry: from fleeting intermediates to powerful reagents*; Bertrand, G. Ed.; Marcel Dekker: New York, 2002.
- [42] *Kinetics and spectroscopy of carbenes and biradicals* Platz, M. S. Ed.; Plenum Press: New York, 1990.
- [43] Grignard, V.; Bellet, E.; Courtot, C. *Ann. Chim. Applic.* **1920**, *12*, 364.
- [44] Kaupp, G.; Schmeyers, J.; Boy, J. *Chem. Eur. J.* **1998**, *4*, 2467.
- [45] Zhang, W.; Kraft, S.; Moore, J. S. *Chem. Commun.* **2003**, 832.
- [46] Moss, R. A. in *Carbenes*, Vol. I.; Jones, M.; Moss, R. A.; Eds.; Wiley: New York, 1973, p. 153.
- [47] Rondan, N. G.; Houk, K. N.; Moss, R. A. *J. Am. Chem. Soc.* **1980**, *102*, 1770.
- [48] Sevin, F.; McKee, M. L.; Shelvin, P. B. *J. Org. Chem.* **2004**, *69*, 382.
- [49] Das, D.; Whittenburg, S. L. *J. Mol. Structure: THEOCHEM.* **1999**, *492*, 175.

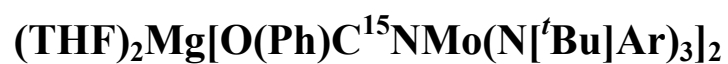
-
- [50] Gutsev, G. L.; Ziegler, T. *J. Phys. Chem.* **1991**, *95*, 7220.
- [51] *Carbenes*, Vol. II; Jones, M.; Moss, R. A. Eds.; Wiley: New York, 1975.
- [52] Wentrup, C. *Reactive Molecules*; Wiley: New York, 1984.
- [53] Schuster, G. B. *Adv. Phys. Org. Chem.* **1986**, *22*, 311 and references therein.
- [54] For a review of carbene selectivity, see: Moss, R. A. *Acc. Chem. Res.* **1980**, *13*, 58.
- [55] Carter, E. A.; Goddard, W. A., III. *J. Chem. Phys.* **1988**, *88*, 1752.
- [56] Shin, S. K.; Goddard, W. A., III; Beauchamp, J. L. *J. Phys. Chem.* **1990**, *94*, 6963.
- [57] Garcia, V. M.; Castell, O.; Reguero, M.; Caballol, R. *Mol. Phys.* **1996**, *87*, 1395.
- [58] Mendez, F.; Garcia-Garibay, M. A. *J. Org. Chem.* **1999**, *64*, 7061.
- [59] The pioneering work of Doering and Hoffmann demonstrated that carbenes could be trapped by olefins to form cyclopropanes: Doering, W. v. E.; Hoffmann, A. K. *J. Am. Chem. Soc.* **1954**, *76*, 6162.
- [60] Mechanism of carbene addition to olefins: Jones, W. M.; Brinker, U. H. in *Pericyclic Reactions*, Vol. I; Marchand, A. P.; Lehr, R. E. Eds.; Academic Press: New York, 1977, p. 109.
- [61] Dehmlow, E. V. *Tetrahedron Lett.* **1966**, *31*, 3763.
- [62] Jenneskens, L. W.; de Wolf, W. H.; Bickelhaupt, F. *Angew. Chem. Int. Ed.* **1985**, *27*, 585.
- [63] Mohamadi, F.; Still, W. C. *Tetrahedron Lett.* **1986**, *27*, 893.
- [64] Sustmann, R. *Tetrahedron Lett.* **1971**, *12*, 2717, 2721.
- [65] Houk, K. N. *Acc. Chem. Res.* **1975**, *8*, 361.
- [66] Bieler, S.; Kellner, K. *J. Organomet. Chem.* **1993**, *447*, 15.
- [67] Mayr, H.; Heigl, U. *Angew. Chem. Int. Ed.* **1985**, *24*, 579.
- [68] Seyferth, D.; Burlitch, J. M. *J. Am. Chem. Soc.* **1964**, *86*, 2730.
- [69] Seyferth, D. *Acc. Chem. Res.* **1972**, *5*, 65 and references therein.
- [70] Mueller, P. H.; Rondan, N. G.; Houk, K. N.; Harrison, J. F.; Hooper, D.; Willen, B. H.; Liebman, J. F. *J. Am. Chem. Soc.* **1981**, *103*, 5049.
- [71] Irikura, K. K.; Goddard, W. A., III; Beauchamp, J. L. *J. Am. Chem. Soc.* **1992**, *114*, 48.
- [72] Singlet-triplet energy gap in dichlorocarbene has been measured as 20.04 kcal mol⁻¹: reference 51.
- [73] Chlorofluorocarbene and dichlorocarbene: comparative reactivities in addition to olefins - Moss, R. A.; Gerstl, R. *J. Org. Chem.* **1967**, *32*, 2268.
- [74] Mukaiyama, T.; Shiono, M.; Watanabe, K.; Onaka, M. *Chem. Lett.* **1975**, 711.
- [75] Dolbier, W. R., Jr.; Burkholder, C. R. *Tetrahedron Lett.* **1988**, *29*, 6749.
- [76] Dolbier, W. R., Jr.; Burkholder, C. R. *J. Org. Chem.* **1990**, *55*, 589.
- [77] Cyanogen chloride has been shown to form addition complexes with inorganic halides such as TiCl₄: Dubois, C. *Bull. Soc. Chim. Fr.* **1978**, 143.
- [78] Kawai, K.; Kanesaka, I. *Spectrochim. Acta A* **1969**, *25*, 263.
- [79] Cha, J. S.; Brown, H. C. *J. Org. Chem.* **1993**, *58*, 4727.
- [80] Whipple, E. B.; Chiang, Y. *J. Chem. Phys.* **1964**, *40*, 713.
- [81] LaVilla, J. A.; Goodman, J. L. *J. Am. Chem. Soc.* **1989**, *111*, 6877.
- [82] ¹⁵N-¹H spin-spin coupling constant in ¹⁵N-acetonitrile: ³J_{NH} -1.34(2) Hz. Wilczek, M.; Kozminski, W.; Jackowski, K. *Chem. Phys. Lett.* **2002**, *358*, 263.
- [83] Seyferth, D.; Mueller, D. C. *J. Organomet. Chem.* **1970**, *25*, 293.

-
- [84] Seyferth, D.; Mueller, D. C. *J. Organomet. Chem.* **1971**, *28*, 325.
- [85] Seyferth, D.; Mueller, D. C. *J. Am. Chem. Soc.* **1971**, *93*, 3714.
- [86] Seyferth, D.; Mueller, D. C.; Lambert, R. L. *J. Am. Chem. Soc.* **1969**, *91*, 1562.
- [87] PhHgCCl₂F was demonstrated to extrude CFCl only upon refluxing a benzene solution of PhHgCCl₂F in the presence of an olefin for 48 h. The long reaction time and high temperature made this a less attractive route for the generation of CFCl compared to the titanium-mediated reduction of CFCl₃ described in section 2.2.3.
- [88] Seyferth, D.; Burlitch, J. M. *J. Organomet. Chem.* **1965**, *4*, 127.
- [89] In a typical reaction PhHgCCl₂Br (0.150 g, 0.340 mmol), α-methylstyrene (0.030 g, 0.254 mmol, 0.75 equiv) and ~0.8 mL C₆D₆ were added to sealed NMR tube that was heated to 65 °C in an oil bath. Solid PhHgBr was seen to precipitate from solution. The reaction was monitored by ¹H NMR spectroscopy.
- [90] Seyferth, D.; Burlitch, J. M.; Minasz, R. J.; Mui, J. Y.-P. Simmons, H. D.; Treiber, A. J.-H.; Dowd, S. R. *J. Am. Chem. Soc.* **1965**, *87*, 4259.
- [91] Seyferth, D.; Mui, J. Y. P.; Burlitch, J. M. *J. Am. Chem. Soc.* **1967**, *89*, 4953.
- [92] Fürstner, A.; Mathes, C.; Lehmann, C. W. *J. Am. Chem. Soc.* **1999**, *121*, 9453.
- [93] Neither of the previous reports provided spectroscopic information for **1**-Cl despite the crystallographic characterization of this complex included in Fürstner's article.
- [94] Agapie, T.; Diaconescu, P. L.; Mendiola, D. J.; Cummins, C. C. *Organometallics* **2002**, *21*, 1329.
- [95] Manzer, L. E. *Inorg. Synth.* **1982**, *21*, 135.

Chapter 3

Nitrogen atom transfer from dinitrogen into an organic nitrile

via the anionic ketimide complex



Nitrogen atom transfer from dinitrogen into an organic nitrile *via* the anionic ketimide complex $(\text{THF})_2\text{Mg}[\text{O}(\text{Ph})\text{C}^{15}\text{NMo}(\text{N}[\text{tBu}]\text{Ar})_3]_2$

3.1 Introduction

The potential for N-atom transfer from a dinitrogen-derived terminal nitride of molybdenum $\text{NMo}(\text{N}[\text{tBu}]\text{Ar})_3$ ($\text{Ar} = 3,5\text{-C}_6\text{H}_3(\text{CH}_3)_2$) (**1**)^{1,2} has been investigated by two distinct routes. In the second chapter of this thesis, the generation of dihalocarbenes in the presence of complex **1** was described. The focus of this chapter is an alternate method for the activation of complex **1**.

Generation of molybdenum(IV) ketimide compounds with the general formula $(\text{RR}'\text{CN})\text{Mo}(\text{N}[\text{tBu}]\text{Ar})_3$ is an attractive synthetic target due to the known β -elimination chemistry of these complexes.³ While the addition of divalent carbon (CX_2) to **1** could provide a ketimide complex $(\text{X}_2\text{CN})\text{Mo}(\text{N}[\text{tBu}]\text{Ar})_3$ in a single step, there exist significant limitations to this method of activating the metal-nitride functionality.

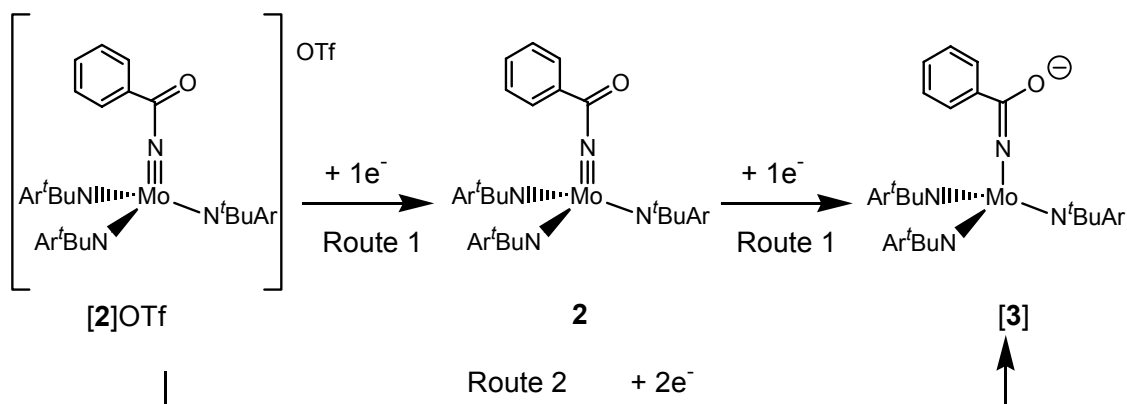
Synthesis of the benzoylimido complex $[\text{PhC}(\text{O})\text{NMo}(\text{N}[\text{tBu}]\text{Ar})_3]\text{OTf}$ [**2**]**OTf** (described in chapter 1) represents the addition of a two-coordinate carbocation $[\text{C}(\text{O})\text{Ph}]^+$ to the terminally-bound N-atom in **1**. We proposed that upon two-electron reduction of [**2**]**OTf**, an anionic ketimide complex of formula $[\text{O}(\text{Ph})\text{C}^{15}\text{NMo}(\text{N}[\text{tBu}]\text{Ar})_3]^-$ might be synthesized. Subsequent functionalization of the negatively charged oxygen atom could be used to furnish a substituent on the ketimide carbon that would be unstable with respect to β -elimination. β -Elimination from a complex of formula $\text{RO}(\text{Ph})\text{C}^{15}\text{NMo}(\text{N}[\text{tBu}]\text{Ar})_3$ would afford one equivalent of benzonitrile (wherein the nitrogen atom is derived from molecular N_2) and generate the molybdenum(IV) species, $\text{RO-Mo}(\text{N}[\text{tBu}]\text{Ar})_3$. The regeneration of $\text{Mo}(\text{N}[\text{tBu}]\text{Ar})_3$ from $\text{RO-Mo}(\text{N}[\text{tBu}]\text{Ar})_3$ could be achieved by a one-electron reduction, in a similar manner to the reductive chemistry of $\text{Cl-Mo}(\text{N}[\text{tBu}]\text{Ar})_3$, described in chapter 2.

The one- and two-electron reduction chemistry of [2]OTf has been investigated and the results are presented herein. Analysis of electronic structure for the anionic ketimide complex (THF)₂Mg[O(Ph)C¹⁵NMo(N[^tBu]Ar)₃]₂ [3]₂Mg(THF)₂ has been carried out using ¹⁵N solid state CP/MAS NMR spectroscopy. Syntheses of ketimide complexes RO(Ph)C¹⁵NMo(N[^tBu]Ar)₃ (4 and 5) and investigation of the potential for N-atom transfer from these complexes will be described.

3.2 Results and Discussion

3.2.1 One and two-electron reduction chemistry of [PhC(O)¹⁵NMo(N[^tBu]Ar)₃]SO₃CF₃ [2]OTf

The synthesis of an anionic ketimide complex of formula [O(Ph)C¹⁵NMo(N[^tBu]Ar)₃]⁻ [3] from [2]OTf was investigated *via* two different strategies. The first of these routes required an initial one-electron reduction to form the neutral molybdenum(V) complex PhC(O)¹⁵NMo(N[^tBu]Ar)₃ (2). Subsequent one-electron reduction of complex 2 would result in generation of the desired anionic ketimide complex [O(Ph)C¹⁵NMo(N[^tBu]Ar)₃]⁻ [3] (Scheme 1, route 1).



Scheme 1. One and two-electron reduction routes to the anionic ketimide complex [O(Ph)C¹⁵NMo(N[^tBu]Ar)₃]⁻ [3].

Reaction of [2]OTf with one-electron reductants such as Na/Hg amalgam and lithium metal resulted in the formation of significant amounts of free amine HN[^tBu]Ar₃. In the reaction of [2]OTf with Ti(N[^tBu]Ar)₃ (1.0 equiv), TfO–Ti(N[^tBu]Ar)₃ was isolated in high yield. In the reaction of [2]OTf with one equivalent of cobaltocene (Cp₂Co), cobaltocenium triflate [Cp₂Co]OTf was isolated *via* pentane extraction of the product mixture followed by filtration. Analysis of the filtrate by ¹H NMR spectroscopy showed that a small amount of ligand was generated together with a new diamagnetic product (A). Product A contained no resonances that could be assigned to the phenyl substituent of the –C(O)Ph fragment. Subsequent experiments that were carried out to probe the thermal stability of complex 2 showed the formation of product A together with multiplet resonances assigned to *iso*-butylene.⁴ From these data, we conclude that the neutral imido complex 2 is unstable with respect to radical decomposition pathways, thereby prohibiting its isolation en route to the anionic ketimide complex [3].

The two-electron reduction of [2]OTf was attempted with magnesium sand (Mg⁰), calcium (Ca⁰) and mercury amalgams of these two metals. Reactions of [2]OTf with Mg⁰ or Ca⁰ (in THF solvent) resulted in no obvious color change after 1 h at 25 °C. Since complex [2]OTf is thermally unstable in THF solution, decomposing to a single (unidentified) diamagnetic product (A) upon standing at 25 °C, it is preferable to effect the reduction rapidly and at low temperature in order to limit this decomposition. The inhomogeneous nature of the Mg⁰ and Ca⁰ reductions of [2]OTf require long reaction times which result in unfavorable decomposition of the benzoylimido complex [2]OTf.

Reduction of [2]OTf with Mg/Hg and Ca/Hg amalgams in cold (–35 °C) THF resulted in a color change from red-orange to black after *ca.* 5 min at 25 °C and upon work up, a dark solid was isolated. Characterization by ¹H NMR spectroscopy showed that together with a number of diamagnetic products, a significant amount of free amine (HN[^tBu]Ar) was present. Other resonances in the ¹H NMR spectra indicated that a new diamagnetic molybdenum-containing product had been generated. Distinctive resonances included two broad singlets at *ca.* 3.7 and 1.8 ppm, attributed to a coordinated

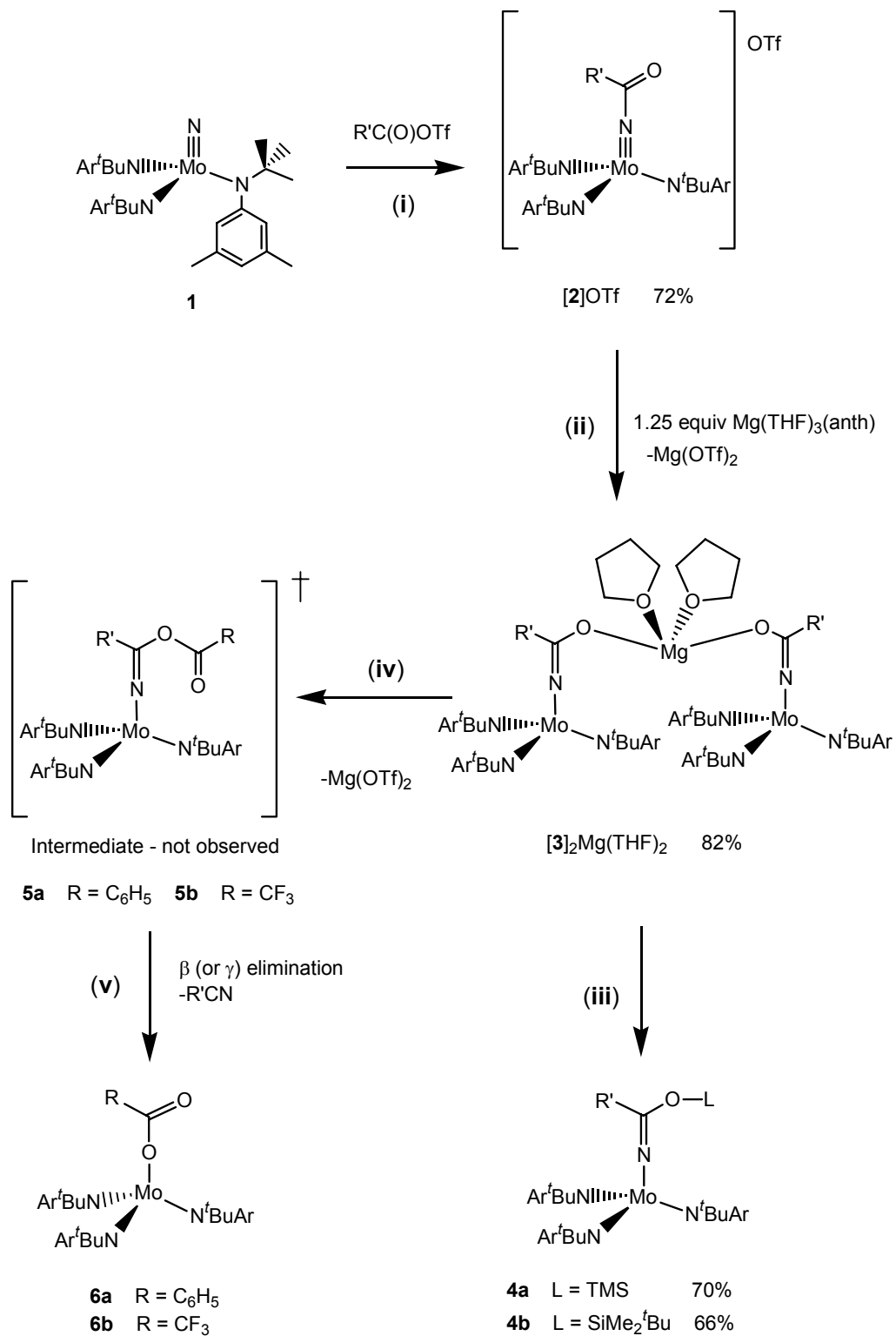
THF molecule, and peaks at *ca.* 2.2 and 1.4 ppm attributed to the aryl-methyl (18 H) and *t*-butyl (27 H) protons of the amide ligands.

The two-electron reduction of [2]OTf (Scheme 1, route 2) is smoothly accomplished using 1.25 equiv magnesium anthracene ($\text{Mg}(\text{THF})_3(\text{anth})$).⁵ Upon addition of a THF suspension of magnesium anthracene to a thawing THF solution of [2]OTf a color change from red-orange to black was observed.⁶ Removal of THF *in vacuo* and extraction with thawing pentane (to remove anthracene and magnesium salts) enabled the isolation of $(\text{THF})_2\text{Mg}[\text{O}(\text{Ph})\text{C}^{15}\text{NMo}(\text{N}[\text{tBu}]\text{Ar})_3]_2$ [3]₂Mg(THF)₂ as a black microcrystalline powder. The following information was obtained *via* inspection of the ¹H, ¹³C, and ¹⁹F solution NMR spectra and ¹⁵N solid state spectrum of [3]₂Mg(THF)₂:

- Integration of the ¹H NMR spectrum indicates a single THF molecule of solvation per molybdenum center.
- The ketimide carbon (N=C) was located in the ¹³C NMR spectrum as a doublet (¹J_{NC} 2.3 Hz) at 137.4 ppm.
- The ¹⁹F NMR spectrum of [3]₂Mg(THF)₂ revealed no resonances after 128 scans.
- The ¹⁵N isotropic chemical shift (δ_{iso}) tensor determined from solid state CP/MAS spectra (obtained at spinning rates of 2 kHz and 2.7 kHz) is 419 ppm.

While complex [3]₂Mg(THF)₂ has not been characterized by X-ray crystallography, the NMR data indicates that the product is a magnesium-bridged dimer of the desired anionic ketimide complex. Two molecules of THF solvate the magnesium; one THF per molybdenum (Scheme 2, reaction (ii)). The absence of a resonance in the ¹⁹F NMR spectrum suggests the reaction proceeds with loss of 0.5 equivalents Mg(OTf)₂ per molybdenum.

The resonance of the ketimide carbon in [3]₂Mg(THF)₂ was readily assigned due to the ¹⁵N-¹³C one-bond coupling, which split this resonance into a well defined doublet. The magnitude of the coupling (¹J_{N-C} 2.3 Hz) is in the range reported for organic ketimines.^{7,8} The ¹³C chemical shift of the ketimide resonance (137.4 ppm) is similar to



Scheme 2. Synthesis of the anionic ketimide complex $[3]_2Mg(THF)_2$ ($R' = C_6H_5$) and functionalization to form neutral ketimide complexes **4** and **5**.

that measured for the ketimide complex $\text{H}_2\text{C}^{15}\text{NMo}(\text{N}[\text{tBu}]\text{Ar})_3$ (described in chapter 1) at 138.9 ppm (d, $^1J_{N-C}$ 5.78 Hz).

The ^{15}N isotropic chemical shift (δ_{iso}) tensor for complex $[\mathbf{3}]_2\text{Mg}(\text{THF})_2$ (419 ppm) is shifted upfield by 48 ppm with respect to δ_{iso} measured for the benzoylimido complex $[\mathbf{2}]\text{OTf}$ (467 ppm) and is similar to that measured for the ketimide complex $\text{H}_2\text{C}^{15}\text{NMo}(\text{N}[\text{tBu}]\text{Ar})_3$ (455 ppm). A complete description of the ^{15}N solid state NMR spectrum obtained for complex $[\mathbf{3}]_2\text{Mg}(\text{THF})_2$ is described in section 3.2.2.

Attempts to recrystallize complex $[\mathbf{3}]_2\text{Mg}(\text{THF})_2$ *via* encryption of the magnesium counter ion with either 12-crown-4 or 18-crown-6 resulted in decomposition to a number of products including $\text{NMo}(\text{N}[\text{tBu}]\text{Ar})_3$ and free amine $\text{HN}[\text{tBu}]\text{Ar}$. This observation indicates that coordination of the magnesium counter ion, between two equivalents of the anionic ketimide, provides a stabilizing interaction.

3.2.2 ^{15}N Solid state CP/MAS NMR spectroscopy of $(\text{THF})_2\text{Mg}[\text{O}(\text{Ph})\text{C}^{15}\text{NMo}(\text{N}[\text{tBu}]\text{Ar})_3]_2$ $[\mathbf{3}]_2\text{Mg}(\text{THF})_2$

Analysis of electronic structure and bonding in the terminal molybdenum nitride complex $^{15}\text{NMo}(\text{N}[\text{tBu}]\text{Ar})_3]_2$ (**1**) and various ^{15}N -labeled derivatives was described in chapter 1. The combined use of ^{15}N solid state NMR spectroscopy and density functional calculations offered insight into the ways in which functionalization of the terminal N-atom modified the electronic structure. The anionic ketimide complex $[\mathbf{3}]_2\text{Mg}(\text{THF})_2$ and derivatives that may be generated upon functionalization of the negatively charged O-atom, provide a unique opportunity to examine electronic structure in a range of complexes that are activated, to a greater or lesser extent, toward removal of the dinitrogen-derived N-atom.

Measurement of the ^{15}N solid state CP/MAS NMR spectrum of complex $[\mathbf{3}]_2\text{Mg}(\text{THF})_2$ was carried out in order to probe experimentally the electronic structure at nitrogen. The principal components of the chemical shift tensor were extracted from the

experimental data using the SIMPSON general simulation program.⁹ The experimental and simulated ^{15}N solid state CP/MAS NMR spectra of $[\mathbf{3}]_2\text{Mg}(\text{THF})_2$ are presented in Figure 1. The principal components of the chemical shift tensor are listed in Table 1.

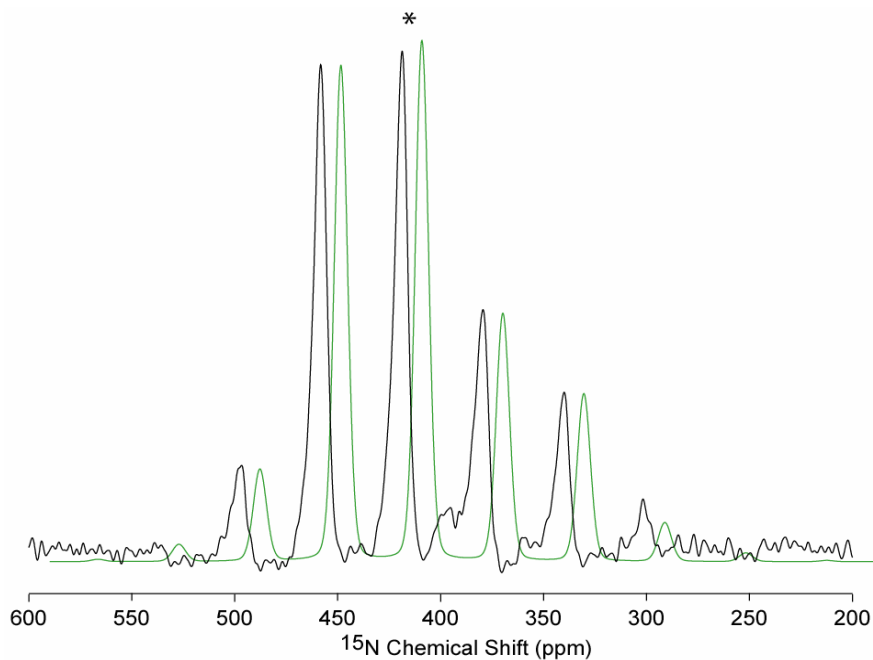


Figure 1. Experimental (—) and simulated (—) ^{15}N solid state CP/MAS NMR spectra for complex $[\mathbf{3}]_2\text{Mg}(\text{THF})_2$. The experimental spectrum was acquired at a spinning rate of 2 kHz. The simulated spectrum is offset with respect to the experimental spectrum for clarity. The isotropic peak (δ_{iso}) is indicated by an asterisk.

	δ_{iso} (ppm)	δ_{11} (ppm)	δ_{22} (ppm)	δ_{33} (ppm)	Ω (ppm)	κ
Experiment	419	539	407	312	227	0.166

Table 1. Experimental principal components of the ^{15}N chemical shift tensor for complex $[\mathbf{3}]_2\text{Mg}(\text{THF})_2$. The span of the chemical shift anisotropy is defined as $\Omega = \delta_{11} - \delta_{33}$ and the skew (κ) is defined as $[3(\delta_{22} - \delta_{\text{iso}})/(\delta_{11} - \delta_{33})]$.

The ^{15}N solid state CP/MAS NMR spectrum of complex $[\mathbf{3}]_2\text{Mg}(\text{THF})_2$ displays a number of interesting features. First, the very narrow span ($\Omega = 227$ ppm) of the

spectrum is in direct contrast with many of the ^{15}N -labeled Lewis acid and imido derivatives of complex **1** (chapter 1) whose spans were in the range of 391 ppm to 1186 ppm. Comparison of the δ_{nn} values obtained for $[\mathbf{3}]_2\text{Mg}(\text{THF})_2$, with those reported in chapter 1, reveals that the small span is the result of both a (relatively) upfield value of δ_{11} and downfield value of δ_{33} .¹⁰

The rhombic nature of the chemical shift anisotropy ($\delta_{11} \neq \delta_{22} \neq \delta_{33}$) is indicative of the non-axially symmetric geometry at the N-atom of complex $[\mathbf{3}]_2\text{Mg}(\text{THF})_2$. The axial symmetry of complex **1** (and most of its Lewis acid and imido derivatives) is reflected in the value of the skew ($\kappa = 1$). The deviation of complex $[\mathbf{3}]_2\text{Mg}(\text{THF})_2$ from axial symmetry is highlighted by its skew value of 0.166.

The unique features of the spectrum obtained for $[\mathbf{3}]_2\text{Mg}(\text{THF})_2$ should enable an accurate prediction of the geometry of this complex by quantitative comparison of the calculated values of the chemical shielding tensor (for model complexes displaying differing optimized geometries) with the tensor values measured experimentally. An understanding of the orbital interactions that influence the magnitude of the principal components of the chemical shift tensor can be obtained from analysis of the NMR output file of a density functional calculation. Computational analysis of complex $[\mathbf{3}]_2\text{Mg}(\text{THF})_2$ is currently under investigation.

3.2.3 Reactions of $(\text{THF})_2\text{Mg}[\text{O}(\text{Ph})\text{C}^{15}\text{NMo}(\text{N}[\text{tBu}]\text{Ar})_3]_2$ $[\mathbf{3}]_2\text{Mg}(\text{THF})_2$ with electrophiles

Functionalization of the negatively charged O-atom in the anionic ketimide complex $[\mathbf{3}]_2\text{Mg}(\text{THF})_2$ may be used in the synthesis of ketimide complexes $\text{RO}(\text{Ph})\text{C}^{15}\text{NMo}(\text{N}[\text{tBu}]\text{Ar})_3$. The choice of electrophile employed in these reactions is important since the substituent on the ketimide carbon (RO-) may be stable toward β -elimination or undergo β -elimination to generate molybdenum(IV) species $\text{RO}-\text{Mo}(\text{N}[\text{tBu}]\text{Ar})_3$ with the concomitant formation of one equivalent of PhCN^{15} . The syntheses of neutral ketimide complexes (**4**), which are stable with respect to β -

elimination, are described in section 3.2.3.1. Reactions of complex $[\mathbf{3}]_2\text{Mg}(\text{THF})_2$ that form ketimide complexes (**5**), which are unstable with respect to β -elimination, are described in section 3.2.3.2.

3.2.3.1 Syntheses of ketimide complexes $\text{RO}(\text{Ph})\text{C}^{15}\text{NMo}(\text{N}[\text{tBu}]\text{Ar})_3$ (**4**)

Initial attempts to functionalize the anionic ketimide complex $[\mathbf{3}]_2\text{Mg}(\text{THF})_2$ focused on the use of mild, halogen-containing electrophiles such as trimethylsilyl chloride ($\text{Me}_3\text{Si}-\text{Cl}$), methyl iodide (CH_3I), tosyl chloride ($(\text{CH}_3)_2\text{C}_6\text{H}_4\text{SO}_2\text{Cl}$) and $\text{Cl}-\text{Ti}(\text{N}[\text{tBu}]\text{Ar})_3$. The addition of 2.0 equivalents of electrophile (one equiv per molybdenum, in cold pentane) to a thawing pentane solution of complex $[\mathbf{3}]_2\text{Mg}(\text{THF})_2$ (Scheme 2, reaction (iii)) resulted in a color change from black to forest green after approximately 2 min. Work up after 10 min and analysis of the product mixture by ^1H NMR spectroscopy showed the complete consumption of complex $[\mathbf{3}]_2\text{Mg}(\text{THF})_2$ and the formation of a number of diamagnetic products. For the electrophiles listed above, these diamagnetic materials included $^{15}\text{NMo}(\text{N}[\text{tBu}]\text{Ar})_3$, free amine ($\text{HN}[\text{tBu}]\text{Ar}$) and at least one other diamagnetic molybdenum-containing product.

In the reaction of complex $[\mathbf{3}]_2\text{Mg}(\text{THF})_2$ with 2.0 equiv $\text{Me}_3\text{Si}-\text{Cl}$, resonances at 2.22, 1.30 and 0.28 ppm were assigned to the aryl-methyl (18 H), *t*-butyl (27 H) and trimethylsilyl (9 H) groups of the desired ketimide complex $\text{Me}_3\text{SiO}(\text{Ph})\text{CNMo}(\text{N}[\text{tBu}]\text{Ar})_3$ (**4a**). Similarly, in the reaction of complex $[\mathbf{3}]_2\text{Mg}(\text{THF})_2$ with 2.0 equiv CH_3I , resonances at 3.77, 2.19 and 1.30 ppm were assigned to the methoxy (3 H), aryl-methyl (18 H) and *t*-butyl (27 H) groups of the desired ketimide complex $\text{MeO}(\text{Ph})\text{CNMo}(\text{N}[\text{tBu}]\text{Ar})_3$ (**4b**). Steps were taken to find other electrophiles that would more cleanly deliver $\text{R}_3\text{Si}-$ and $\text{Me}-$ groups to the O-atom of the ketimide ligand.

Syntheses of siloxy-ketimide complexes $\text{RMe}_2\text{SiO}(\text{Ph})\text{CNMo}(\text{N}[\text{tBu}]\text{Ar})_3$ (**4a** R = Me; **4b** R = *t*Bu) were achieved *via* reaction of complex $[\mathbf{3}]_2\text{Mg}(\text{THF})_2$ with 2.0 equiv $\text{RMe}_2\text{Si}-\text{OTf}$ in thawing pentane. Upon stirring at 25 °C for 2 min a color change from

black to forest green was observed. After 10 min, work up of the reaction mixture enabled isolation of the siloxy-ketimide product (**4a** or **4b**) as a greasy dark green solid. Two distinct absorptions are observed in the UV-visible spectrum of complex **4a** at 432 nm and 624 nm (Figure 2). An almost identical UV-visible spectrum is observed for complex **4b**, in which absorption maxima are located at 429 nm and 625 nm.

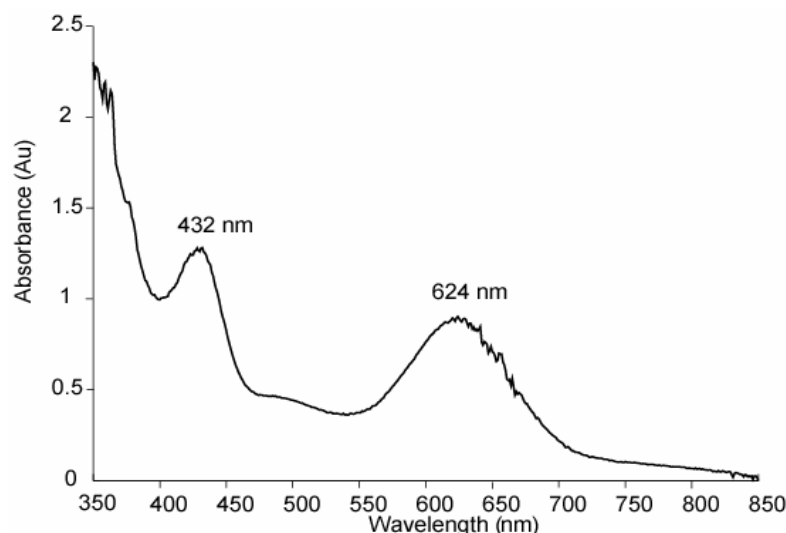


Figure 2. UV-Visible spectrum of $\text{Me}_3\text{SiO}(\text{Ph})\text{C}^{15}\text{NMo}(\text{N}[\text{tBu}]\text{Ar})_3$ (**4a**) (toluene, 25 °C).

For complex **4a** the ^{13}C resonance of the ketimide carbon was located at 137.5 ppm. The ^{15}N - ^{13}C one-bond coupling could not be determined from ^{13}C spectra of the ^{15}N -labeled isotopomer of complex **4a** due to overlap of this resonance with a broad peak at 137.4 ppm (assigned to the meta-carbon atoms of the amide aryl groups). Similarly, for complex **4b**, the ketimide ^{13}C resonance overlapped with a broad singlet assigned to the meta-carbon atoms of the ligand preventing accurate measurement of the ^{15}N - ^{13}C one-bond coupling constant for the ^{15}N labeled isotopomer.

Synthesis of the methoxy-ketimide complex $\text{MeO}(\text{Ph})\text{CNMo}(\text{N}[\text{tBu}]\text{Ar})_3$ (**4c**) was attempted using methyl tosylate and methyl triflate (MeOTf). While a diamagnetic molybdenum-containing compound, attributed to complex **4c**, was present in the product mixture, a number of other species including complex **1** and free amine ($\text{HN}[\text{tBu}]\text{Ar}$) were identified. A clean, high-yielding route to complex **4c** remains a synthetic target.

3.2.3.2 Syntheses of ketimide complexes $\text{RC}(\text{O})\text{O}(\text{Ph})\text{C}^{15}\text{NMo}(\text{N}[\text{tBu}]\text{Ar})_3$ (**5a** and **5b**)

Reactions of complex $[\mathbf{3}]_2\text{Mg}(\text{THF})_2$ with electrophiles such as benzoyl chloride, benzoyl triflate (BzOTf) and trifluoroacetic anhydride ($(\text{CF}_3\text{CO})_2\text{O}$) have been investigated in an effort to generate ketimide complexes $\text{RC}(\text{O})\text{O}(\text{Ph})\text{C}^{15}\text{NMo}(\text{N}[\text{tBu}]\text{Ar})_3$ (**5a** R = Ph, **5b** R = CF_3 , Scheme 2, reaction (iv)) wherein the substituent on the ketimide carbon is unstable with respect to β -elimination (Scheme 2, reaction (v)).

Precedent for the β -elimination chemistry of ketimide complex **5a** comes from the work of Mendiratta.¹¹ Recent research has shown that upon reaction of (η^2 -PhCN)– $\text{Mo}(\text{N}[\text{tBu}]\text{Ar})_3$ with benzoyl peroxide (PhCO_2)₂, a molybdenum(IV) benzoate complex $\text{PhC}(\text{O})\text{OMo}(\text{N}[\text{tBu}]\text{Ar})_3$ (**6a**) and one equivalent of benzonitrile (PhCN) can be isolated. It is proposed that the generation of complex **6a** proceeds *via* ketimide complex **5a**, which is formed upon radical addition of $[\text{PhC}(\text{O})\text{O}]^\bullet$ to the carbon atom of the η^2 -coordinated nitrile (PhCN). Complex **5a** rapidly undergoes β -elimination to form a molybdenum(IV) benzoate complex (**6a**) and one equivalent of PhCN. Kinetic studies designed to probe the rate of β -OC(O)Ph elimination by complex **5a** are in progress.

Reaction of complex $[\mathbf{3}]_2\text{Mg}(\text{THF})_2$ with benzoyl chloride resulted in formation of complex **1** and free amine ($\text{HN}[\text{tBu}]\text{Ar}$). This observation was consistent with experiments described in section 3.2.3.1 in which attempts to deliver alkyl or silyl groups by means of halogen-containing electrophiles resulted in the generation of **1** and significant amounts of free amine.

Reaction of complex $[\mathbf{3}]_2\text{Mg}(\text{THF})_2$ with benzoyl triflate (2.0 equiv) resulted in a color change from black to dark green. Upon work up, analysis of the brown-pink solid (¹H NMR spectroscopy) showed that the product mixture comprised complexes **1** and **6a** together with a small amount of free amine. Complex **6a** is readily identified by ¹H

NMR spectroscopy as a result of a distinctive, broad resonance located at 4.27 ppm, assigned to the *t*-butyl protons of the amide ligands.

^{15}N Solution NMR spectroscopy¹² was used to determine the fate of the dinitrogen-derived N-atom upon formation of complex **6a**. Three resonances were located in the ^{15}N NMR spectrum at 838.9, 449.8 and 261.5 ppm (Figure 3).

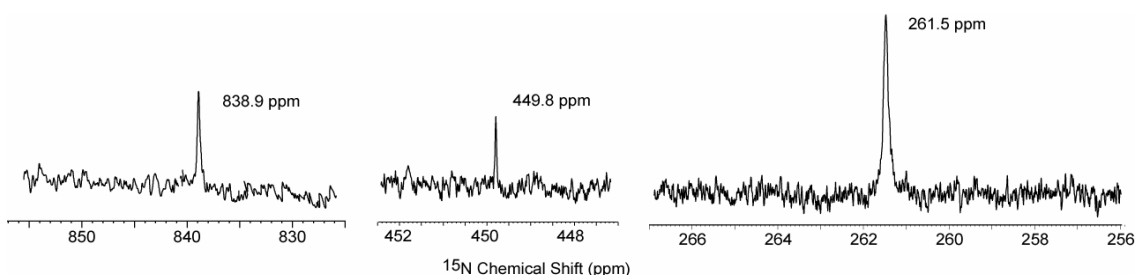


Figure 3. ^{15}N Solution NMR spectrum of the reaction between complex $[\mathbf{3}]\text{Mg}(\text{THF})_2$ and benzoyl triflate.

The major peak in the ^{15}N solution NMR spectrum (261.5 ppm) is assigned to PhCN^{15} .¹³ The most downfield resonance (838.9 ppm) can be assigned to complex **1**.¹⁴ The identity of the ^{15}N -containing species responsible for the signal at 449.8 ppm has not been determined. This signal might be attributed to the trimer of benzonitrile $[\text{PhCN}]_3$, whose formation is known to be catalyzed by Lewis acids.¹⁵ Density functional calculations are being used to determine the ^{15}N isotropic chemical shift of $[\text{PhCN}^{15}]_3$ since this parameter could not be found in an extensive search of the literature. Alternatively, the resonance at 449.8 ppm could be attributed to a molybdenum(IV) ketimide complex ($\text{R}_2\text{CNMo}(\text{N}[\text{tBu}]\text{Ar})_3$). Density functional calculations are also in progress on a number of plausible molybdenum(IV) ketimide complexes.

Gas chromatography (GC-MS) was used to confirm our assignment of the ^{15}N solution NMR spectrum. GC-MS data, obtained from analysis of the reaction between complex $[\mathbf{3}]_2\text{Mg}(\text{THF})_2$ and benzoyl triflate (2.0 equiv), displayed an intense signal assigned to $[\text{PhCN}^{15}]^+$ for which the parent ion formula weight was 104.¹⁶

Reaction of $[\mathbf{3}]_2\text{Mg}(\text{THF})_2$ with trifluoroacetic anhydride $((\text{CF}_3\text{CO})_2\text{O}$, 2.0 equiv) in thawing pentane resulted in a color change from black to brown-orange and the isolation of a brown-orange product. The major product of this reaction was $\text{CF}_3\text{C}(\text{O})\text{OMo}(\text{N}[\text{tBu}]\text{Ar})_3$ (**6b**), whose ^1H NMR spectrum contains a distinctive, broad singlet at 10.26 ppm (assigned to the *t*-butyl (27 H) protons of the amide ligands). Complex **6b** was identified by comparison with an independently prepared sample[†]. Complex **1** and free amine were amongst the compounds identified in the crude product mixture.

^{15}N Solution NMR spectroscopy was used to determine the fate of the dinitrogen-derived N-atom. Three signals at 839 ppm (complex **1**), 450 ppm and 261 ppm (PhCN^{15}) were located in the ^{15}N spectrum of the crude product mixture. The yield of PhCN^{15} was determined to be 43% by GC-MS.

3.3 Concluding remarks

Activation of the terminal molybdenum nitride complex $^{15}\text{NMo}(\text{N}[\text{tBu}]\text{Ar})_3$ (**1**) has been used to mediate N-atom transfer from dinitrogen into an organic nitrile. Synthesis of the benzoylimido complex $[\text{PhC}(\text{O})^{15}\text{NMo}(\text{N}[\text{tBu}]\text{Ar})_3]\text{OTf}$ [**2**]OTf and its subsequent two-electron reduction, provided the anionic ketimide complex $(\text{THF})_2\text{Mg}[\text{O}(\text{Ph})\text{C}^{15}\text{NMo}(\text{N}[\text{tBu}]\text{Ar})_3]_2$ [**3**] $_2\text{Mg}(\text{THF})_2$ in high yield. Reactions of complex [**3**] $_2\text{Mg}(\text{THF})_2$ with electrophiles (R–OTf) enabled the formation of ketimide complexes $\text{RO}(\text{Ph})\text{C}^{15}\text{NMo}(\text{N}[\text{tBu}]\text{Ar})_3$, wherein the potential for β -elimination of the ketimide substituent (RO-) may be controlled by judicious choice of the electrophile. Reactions of [**3**] $_2\text{Mg}(\text{THF})_2$ with benzoyl triflate or trifluoroacetic anhydride resulted in the syntheses of molybdenum(IV) complexes $\text{RO–Mo}(\text{N}[\text{tBu}]\text{Ar})_3$ (**6a** R = PhCO; **6b** R = CF_3CO) together with the concomitant formation of one equivalent PhCN^{15} . Selective ^{15}N -labeling of benzonitrile was demonstrated unequivocally by the combined use of ^{15}N solution NMR studies and GC-MS measurements.

[†] Reaction of $\text{Mo}(\text{N}[\text{tBu}]\text{Ar})_3$ with $\frac{1}{3}$ equivalents thallium(III) trifluoroacetate ($\text{Tl}(\text{O}_2\text{CCF}_3)_3$) resulted in the clean formation of complex **6b**. See experimental section for further details.

The nitrogen atom transfer route described herein represents only the second example of the activation of complex **1** toward N-atom transfer into an organic molecule¹⁷ and one of few existing examples of N-atom transfer[†] (into an organic molecule) from a terminal transition-metal nitride complex.^{18–22} Furthermore, examples of the synthesis of nitrogen-containing organic molecules from N₂ are limited.^{23–26} The advantage of the work described herein, over that previously reported, is two-fold. First, there exists the potential for catalytic application of complex **1** in N-atom transfer, since the molybdenum(IV) species formed upon β -elimination from ketimide complexes **5a** and **5b** contains three intact *tris*-amide ligands. The regeneration of Mo(N[^tBu]Ar)₃ from the molybdenum(IV) complexes **6a** and **6b** is currently under investigation in our laboratories.

Secondly, the selective ¹⁵N-labeling of organic nitriles can be achieved by the use of the ¹⁵N-labeled isotopomer of complex [3]₂Mg(THF)₂. Syntheses of complexes [2]OTf and [3]₂Mg(THF)₂ in their ¹⁵N-labeled forms, may be achieved *via* the use of ¹⁵NMo(N[^tBu]Ar)₃ (**1**). Complex **1** is readily prepared as its ¹⁵N-labeled isotopomer through the use of ¹⁵N-isotopically-enriched dinitrogen.[‡] The scope of this reaction, with respect to the generation of other organic nitriles is currently under investigation.

3.4 Experimental Section

General details, solution state ¹H, ¹³C and ¹⁹F NMR parameters and ¹⁵N solid-state NMR parameters are identical to those included in chapter 1 (sections 1.5.1 and 1.5.3). For information pertaining to the simulation of solid state spectra using the SIMPSON program refer to chapter 1, section 1.5.4. The benzoylimido complex [PhC(O)NMo(N[^tBu]Ar)₃]SO₃CF₃ [2]OTf was prepared by the method outlined in chapter 1. Magnesium anthracene [Mg(THF)₃(anth)] was prepared by the method of Freeman and Hutchinson.⁵ GC-MS experiments were carried out on an Agilent 6890N GC system fitted with a Restek Rtx-1 column (crossbond, 100% dimethyl polysiloxane,

[†] In the references cited the N-atom of the terminal transition-metal nitride complex is not derived from N₂.

[‡] ¹⁵N₂ is currently the most inexpensive source of this isotope.

capillary: 30.0 m x 250 μm x 1.00 μm) in combination with an Agilent 5973 mass selective detector. ^{15}N solution NMR spectra were acquired on a Bruker DRX600 spectrometer operating at 600 MHz for ^1H (60 MHz for ^{15}N) and equipped with a triple resonance ($^1\text{H}/^{13}\text{C}/^{15}\text{N}$) probe. Proton decoupling was not applied during the acquisition of ^{15}N solution spectra.

3.4.1 One-electron reduction of $[\text{PhC}(\text{O})\text{NMo}(\text{N}[\text{tBu}]\text{Ar})_3]\text{SO}_3\text{CF}_3$ [2]OTf with cobaltocene

To a thawing solution of $[\text{PhC}(\text{O})\text{NMo}(\text{N}[\text{tBu}]\text{Ar})_3]\text{SO}_3\text{CF}_3$ [2]OTf (0.075 g, 0.084 mmol) in THF (4 mL) was added a cold ($-35\text{ }^\circ\text{C}$) THF (2 mL) solution of cobaltocene (Cp_2Co , 1.1 eq, 0.017 g, 0.092 mmol). Upon addition, a color change from red-orange to dark brown was noted. The solution was stirred and allowed to warm to room temperature over 30 min before solvent was removed under a dynamic vacuum. The greasy brown solids were triturated with hexanes and then extracted with cold pentane. Filtration through a glass frit enabled isolation of pale brown solids identified as $[\text{Cp}_2\text{Co}]\text{OTf}$ (^1H , ^{19}F NMR). Solvent removal from the filtrate yielded a greasy brown solid. Analysis of this solid by ^1H NMR spectroscopy showed the formation of one major diamagnetic product (**A**) together with a small amount (*ca.* 5%) of free amine ($\text{HN}[\text{tBu}]\text{Ar}$). Product **A** ^1H NMR spectrum: (300 MHz, C_6D_6 , $20\text{ }^\circ\text{C}$) δ : 6.43 (3 H), 6.40 (6 H), 2.25 (18 H), 1.34 (27 H).

3.4.2 Thermal Stability of $[\text{PhC}(\text{O})\text{NMo}(\text{N}[\text{tBu}]\text{Ar})_3]\text{SO}_3\text{CF}_3$ [2]OTf

A solution of $[\text{PhC}(\text{O})\text{NMo}(\text{N}[\text{tBu}]\text{Ar})_3]\text{SO}_3\text{CF}_3$ ([2]OTf, 0.030g, 0.034 mmol) in CDCl_3 (0.6 mL) was prepared in a vial and transferred to a J. Young tube. The sample was stored at $25\text{ }^\circ\text{C}$ for 18 h after which time the solution had turned a dark brown-orange color. ^1H NMR spectroscopy indicated the complete consumption of [2]OTf and the formation of a new diamagnetic product with the following resonances in the ^1H NMR spectrum: (300 MHz, CDCl_3 , $20\text{ }^\circ\text{C}$) δ : 6.65 (3 H), 6.62 (6 H), 2.27 (18 H), 1.35 (27 H). Multiplet resonances at δ 4.67 and 1.74 ppm were assigned to *iso*-butylene. ^{19}F

NMR (283 MHz, CDCl₃, 20 °C) δ : -78.18, -78.45 ppm (ratio 1:9). Repetition of this experiment in THF, resulted in decomposition of [2]OTf to the products listed for reaction in CDCl₃.

3.4.3 Synthesis of (THF)₂Mg[O(Ph)C¹⁵NMo(N[^tBu]Ar)₃]₂ [3]₂Mg(THF)₂

A solution of [PhC(O)¹⁵NMo(N[^tBu]Ar)₃]SO₃CF₃ [2]OTf (0.670 g, 0.750 mmol) in THF (20 mL) was chilled to -35 °C in a 50 mL flask. In a vial, a solution of magnesium anthracene [Mg(THF)₃(anthracene)] (1.25 equiv, 0.395 g, 0.938 mmol) in THF (15 mL) was chilled to -35 °C. The magnesium anthracene solution was added to the 50 mL flask with vigorous stirring and after *ca.* 1 min a color change from red-orange to black was observed. The solution was stirred at 25 °C for 10 min after which time the solution was filtered through Celite and THF solvent was removed *in vacuo* to yield a sticky black solid. The solid was triturated with hexanes (10 mL) and solvent was removed *in vacuo* to yield a black powder. The powder was extracted with pentane, filtered through Celite and following solvent removal under a dynamic vacuum, a black microcrystalline powder was isolated: [3]₂Mg(THF)₂ 0.518 g (0.615 mmol, 82%). ¹H NMR (500 MHz, C₆D₆, 20 °C) δ : 7.24 (m, 2 H, Ph), 6.98 (br s, 6 H, ortho), 6.78 (t, 2 H, Ph-para), 6.68 (s, 3 H, para), 3.71 (m, 4 H, THF), 2.24 (s, 18 H, ArCH₃), 1.78 (m, 4 H, THF), 1.45 (br s, 27 H, NC(CH₃)₃). ¹³C NMR (125 MHz, C₆D₆, 20 °C) δ : 154.8 (ipso), 137.4 (d, ¹J_{NC} 2.3 Hz, N=C), 137.0 (meta), 128.7 (ortho), 127.5 (Ph), 126.0 (Ph), 125.98 (para), 125.3 (Ph), 70.44 (THF), 63.06 (NC(CH₃)₃), 32.27 (NC(CH₃)₃), 25.43 (THF), 22.02 (ArCH₃). UV-visible spectrum (toluene, 20 °C) λ_{\max} : 477 nm, 726 nm.

This reaction is amenable to scale-up and has been performed using 1.9 g [2]OTf.

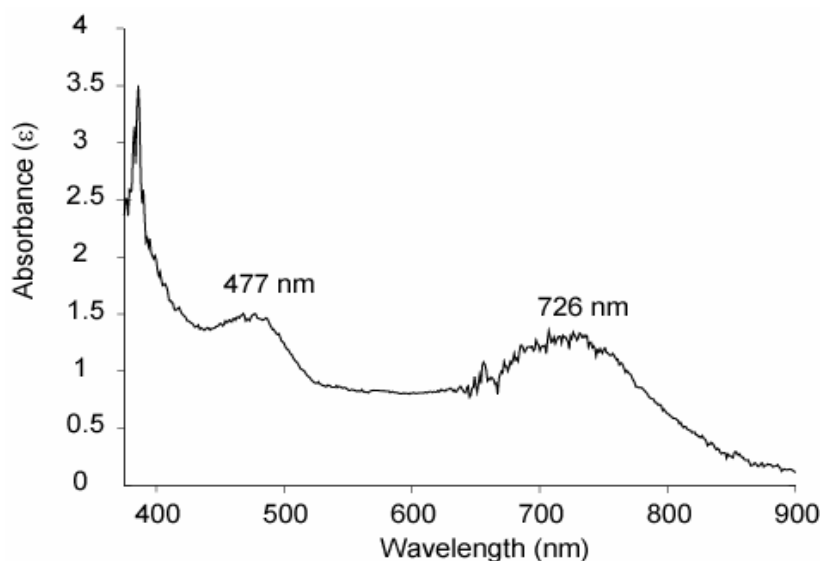


Figure 4. UV-visible spectrum of complex $[3]_2\text{Mg}(\text{THF})_2$ (toluene, 25 °C).

3.4.4 Synthesis of $\text{Me}_3\text{SiO}(\text{Ph})\text{CNMo}(\text{N}[\text{tBu}]\text{Ar})_3$ (**4a**) and $\text{tBuMe}_2\text{SiO}(\text{Ph})\text{CNMo}(\text{N}[\text{tBu}]\text{Ar})_3$ (**4b**)

A solution of $(\text{THF})_2\text{Mg}[\text{O}(\text{Ph})\text{CNMo}(\text{N}[\text{tBu}]\text{Ar})_3]_2$ (0.150 g, 0.091 mmol) in pentane (10 mL) was chilled to $-35\text{ }^\circ\text{C}$ in a 20 mL vial. In a second vial, a solution of the electrophile (Me_3SiOTf , 2.0 equiv, 0.040 g, 0.181 mmol; $\text{tBuMe}_2\text{SiOTf}$, 2.0 equiv, 0.048 g, 0.181 mmol) in pentane (6 mL) was chilled to $-35\text{ }^\circ\text{C}$. 2 mL of the solution containing the electrophile was added to the first vial and both solutions were frozen (in a liquid nitrogen-cooled cold well) before the addition of a further 2 mL of the solution containing the electrophile. The solutions were frozen again before the final 2 mL of electrophile solution was added. This mixture was then allowed to stir at 25 °C. After *ca.* 2 min a color change from black to forest green was observed. The solution was stirred at 25 °C for 10 min after which time the solution was filtered through Celite and pentane solvent was removed *in vacuo* to yield a greasy forest green solid: $\text{Me}_3\text{SiO}(\text{Ph})\text{CNMo}(\text{N}[\text{tBu}]\text{Ar})_3$ (**4a**) 0.105 g (0.128 mmol, 70%); $\text{tBuMe}_2\text{SiO}(\text{Ph})\text{CNMo}(\text{N}[\text{tBu}]\text{Ar})_3$ (**4b**) 0.098 g (0.114 mmol, 63%).

Me₃SiO(Ph)CNMo(N[^tBu]Ar)₃ (4a) ¹H NMR (500 MHz, C₆D₆, 20 °C) δ : 7.10 (m, 2 H, Ph), 6.82 (br s, 6 H, ortho), 6.78 (m, 1 H, Ph), 6.64 (s, 3 H, para), 6.6 (m, 2 H, Ph), 2.22 (s, 18 H, ArCH₃), 1.30 (s, 27 H, NC(CH₃)₃), 0.278 (s, 9 H, Si(CH₃)₃). ¹³C NMR (125 MHz, C₆D₆, 20 °C) δ : 151.1 (ipso), 147.8 (Ph), 137.5 (N=C), 137.4 (meta), 130.7 (para), 129.3 (ortho), 127.1 (Ph), 126.7 (Ph), 125.9 (Ph), 121.0 (Ph), 116.3 (Ph), 63.28 (NC(CH₃)₃), 31.83 (br s, $v_{1/2}$ 10 Hz, NC(CH₃)₃), 21.88 (ArCH₃), 2.47 (Si(CH₃)₃). UV-visible spectrum (toluene, 20 °C) λ_{\max} : 432 nm, 624 nm.

^tBuMe₂SiO(Ph)CNMo(N[^tBu]Ar)₃ (4b) ¹H NMR (500 MHz, C₆D₆, 20 °C) δ : 6.69 (br s, 6 H, ortho), 6.55 (br s, 3 H, para) [due to overlap of the very broad ortho and para resonances with the Ph resonances, the chemical shifts of these 5 protons are not assigned], 2.18 (s, 18 H, ArCH₃), 1.40 (br s, 27 H, NC(CH₃)₃), 1.15 (s, 9 H, SiMe₂C(CH₃)₃), 0.143 (s, 6 H, Si(CH₃)₂^tBu). ¹³C NMR (125 MHz, C₆D₆, 20 °C) δ : 137.5 (N=C), 137.4 (br s, meta), 130.7 (para), 129.3 (ortho), 127.1 (Ph), 125.9 (Ph), 125.3 (Ph), 121.2 (Ph), 116.5 (Ph), 61.73 (NC(CH₃)₃), 32.32 (br s, NC(CH₃)₃), 27.17 (SiMe₂C(CH₃)₃), 21.99 (ArCH₃), 2.30 (Si(CH₃)₃). UV-visible spectrum (toluene, 20 °C) λ_{\max} : 429 nm, 625 nm.

3.4.5 Reaction of (THF)₂Mg[O(Ph)C¹⁵NMo(N[^tBu]Ar)₃]₂ [3]₂Mg(THF)₂ with PhC(O)OTf

A pentane (15 mL) solution of (THF)₂Mg[O(Ph)C¹⁵NMo(N[^tBu]Ar)₃]₂ (0.250 g, 0.151 mmol) was frozen in a 50 mL flask by storage in a liquid nitrogen-cooled cold well. In a 20 mL vial a pentane (10 mL) solution of PhC(O)OTf (0.95 equiv, 0.068 g, 0.287 mmol) was chilled to -35 °C. The PhC(O)OTf solution was added drop-wise over 5 min to the thawing solution in the 50 mL flask. After stirring at 25 °C for *ca.* 2 min a color change from black to dark blue-green was observed. The solution was stirred for a total of 15 min before filtering through Celite to give a brown-pink filtrate. Solvent removal *in vacuo* yielded a greasy brown-pink solid. A number of products were observed in the ¹H NMR of the product mixture. These included ¹⁵NMo(N[^tBu]Ar)₃, HN[^tBu]Ar and PhC(O)OMo(N[^tBu]Ar)₃ (**6a**). Product **6a** was identified by comparison

with an independently prepared sample.¹¹ ¹H NMR for compound **6a** (300 MHz, C₆D₆, 20 °C) δ : 7.65 (m, 2 H, Ph), 7.34 (m, 2 H, Ph), 6.16 (t, 1 H, Ph), 5.66 (br s, 6 H, ortho), 4.82 (s, 3 H, para), 4.27 (br s, 27 H, NC(CH₃)₃), 1.69 (s, 18 H, ArCH₃). ¹⁵N NMR (60 MHz, C₆D₆, 20 °C) δ : 838.9 ppm (¹⁵NMo(N[^tBu]Ar)₃, **1**), 449.8 ppm (not assigned), 261.5 ppm (PhCN¹⁵). GC-MS confirmed the assignment of PhCN¹⁵.

3.4.6 Reaction of (THF)₂Mg[O(Ph)C¹⁵NMo(N[^tBu]Ar)₃]₂ [3]₂Mg(THF)₂ with (CF₃CO)₂O

A pentane (8 mL) solution of (THF)₂Mg[O(Ph)C¹⁵NMo(N[^tBu]Ar)₃]₂ (0.155 g, 0.187 mmol) was frozen in a 20 mL vial by storage in a liquid nitrogen-cooled cold well. In a second 20 mL vial a pentane (5 mL) solution of (CF₃CO)₂O (0.95 equiv, 0.037 g, 0.0178 mmol) was chilled to -35 °C. The (CF₃CO)₂O solution was added drop-wise over 5 min to the thawing solution of [3]₂Mg(THF)₂. After stirring at 25 °C for *ca.* 2 min a color change from black to brown-orange was observed. The solution was stirred for a total of 10 min before filtering through Celite to give a brown-orange filtrate. Solvent removal *in vacuo* yielded a greasy brown-orange solid. The crude product mixture was dissolved in 1.5 mL C₆D₆ and analyzed by ¹H NMR spectroscopy and GC-MS (see Appendix 4 for GC-MS data). Products observed in the ¹H NMR included ¹⁵NMo(N[^tBu]Ar)₃, HN[^tBu]Ar and CF₃C(O)OMo(N[^tBu]Ar)₃ (**6b**). Product **6b** was the major product and was identified by comparison with an independently prepared sample. ¹⁵N NMR (60 MHz, C₆D₆, 20 °C) δ : 838.9 ppm (¹⁵NMo(N[^tBu]Ar)₃, **1**), 449.8 ppm (not assigned), 261.5 ppm (PhCN¹⁵). Yield of PhCN¹⁵: 43% (GC-MS).

3.4.7 Synthesis of CF₃C(O)OMo(N[^tBu]Ar)₃ (**6b**)

An Et₂O (6 mL) solution of Mo(N[^tBu]Ar)₃ (0.137 g, 0.219 mmol) was chilled to -35 °C in a 20 mL vial. In a second vial an Et₂O (3 mL) solution of Tl(O₂CCF₃)₃ (0.33 equiv, 0.040 g, 0.073 mmol) was chilled to -35 °C. Upon addition of Tl(O₂CCF₃)₃ to the solution of Mo(N[^tBu]Ar)₃ a color change from orange-brown to red was observed. The solution was stirred for a total of 20 min before filtering through Celite to yield a dark

red-orange filtrate. Solvent removal *in vacuo* gave a red-orange solid identified as complex **6b** 0.128 g (0.173 mmol, 79%). ¹H NMR (300 MHz, C₆D₆, 20 °C) δ : 10.31 (br s, $\nu_{1/2}$ 59 Hz, 27 H, NC(CH₃)₃), 3.38 (br s, $\nu_{1/2}$ 82 Hz, 6 H, ortho), 1.37 (s, 3 H, para), 0.664 (s, 18 H, ArCH₃). ¹⁹F NMR (282 MHz, CD₂Cl₂, 20 °C) δ : -73.9 ppm (br s)

References

-
- [1] Laplaza, C. E.; Cummins, C. C. *Science* **1995**, *268*, 861.
- [2] Laplaza, C. E.; Johnson, M. J. A.; Peters, J. C.; Odom, A. L.; Kim, E.; Cummins, C. C.; George, G. N.; Pickering, I. J. *J. Am. Chem. Soc.* **1996**, *118*, 8623.
- [3] Mendiratta, A.; Cummins, C. C.; Kryatova, O. P.; Rybak-Akimova, E. V.; McDonough, J. E.; Hoff, C. D. *Inorg. Chem.* **2003**, *42*, 8621.
- [4] Weydert, M.; Brennan, J. G.; Andersen, R. A.; Bergman, R. G. *Organometallics* **1995**, *14*, 3942.
- [5] Freeman, P. K.; Hutchinson, L. L. *J. Org. Chem.* **1983**, *48*, 879.
- [6] See Experimental Section for a UV-visible spectrum of [3]₂Mg(THF)₂.
- [7] Schulman, J. M.; Venanzi, T. *J. Am. Chem. Soc.* **1976**, *98*, 4701.
- [8] Schulman, J. M.; Venanzi, T. *J. Am. Chem. Soc.* **1976**, *98*, 6739.
- [9] For details of parameters used in the acquisition of solid state NMR spectra and the simulation of solid state spectra using the SIMPSON program, see chapter 1, sections 1.5.3 and 1.5.4.
- [10] Typically, for complexes included in chapter 1, a reduction in the span of the CSA resulted from a reduced paramagnetic contribution to δ_{11} (i.e. a more upfield shift). Variation in the magnitude of δ_{33} was usually much less significant.
- [11] A. Mendiratta; unpublished results.
- [12] von Philipsborn, W.; Müller, R. *Angew. Chem. Int. Ed.* **1986**, *25*, 383.
- [13] Literature value of the ¹⁵N isotropic chemical shift for PhCN¹⁵ (CDCl₃) is 256.7 ppm (referenced to NH₃ at 0.0 ppm): Witanowski, M.; Stefaniak, L.; Webb, G. A. *Ann. Rep. NMR Spec.* Vol. 25; Webb, G. A. Ed.; Academic Press; London, 1993, p. 214.
- [14] Reported ¹⁵N isotropic chemical shift for complex **1** δ 840 ppm (referenced to NH₃ at 0.0 ppm). See reference 2.
- [15] Diaz-Ortiz, A.; de la Hoz, A.; Moreno, A.; Sanchez-Migallon, A.; Valiente, G. *Green Chem.* **2002**, *4*, 339.
- [16] See Appendix 4 for GC-MS chromatograms of PhCN¹⁴ (a solution in C₆D₆ prepared as a calibration standard) and the crude product mixture isolated following reaction of complex [3]Mg with TFAA (sample diluted in C₆D₆).
- [17] First example of N-atom transfer from complex **1**: Henderickx, H.; Kwakkenbos, G.; Peters, A.; van der Spoel, J.; de Vries, K. *Chem. Commun.* **2003**, 2050.
- [18] Groves, J. T.; Takahashi, T. *J. Am. Chem. Soc.* **1983**, *105*, 2073.
- [19] Groves, J. T.; Takahashi, T.; Butler, W. M. *Inorg. Chem.* **1983**, *22*, 884.
- [20] Du Bois, J.; Hong, J.; Carreira, E. M.; Day, M. W. *J. Am. Chem. Soc.* **1996**, *118*, 915.

-
- [21] Du Bois, J.; Tomooka, C. S.; Hong, J.; Carreira, E. M. *Acc. Chem. Res.* **1997**, *30*, 364.
- [22] Chisholm, M. H.; Delbridge, E. E.; Kidwell, A. R.; Quinlan, K. B. *Chem. Commun.* **2003**, 126.
- [23] Korobkov, I.; Gambrotta, S.; Yap, G. P. A. *Angew. Chem. Int. Ed.* **2003**, *42*, 4958.
- [24] Fryzuk, M. D.; Johnson, S. A. *Coord. Chem. Rev.* **2000**, *200*, 379.
- [25] Hidai, M. *Coord. Chem. Rev.* **1999**, *185*, 99.
- [26] Gambarotta, S. *Inorganic Chemistry Highlights*; Meyer, G.; Naumann, D.; Wesemann, L. Eds.; Wiley-VCH; Weinheim: 2002.

Appendix 1: Tables of selected bond lengths and angles

A 1.1 Bond lengths [Å] and angles [°] for 1-BF₃.

Mo(1)-N(4)	1.678(4)	C(33)-C(331)	1.513(7)
Mo(1)-N(2)	1.946(4)	C(34)-C(35)	1.390(8)
Mo(1)-N(1)	1.943(4)	C(35)-C(36)	1.392(7)
Mo(1)-N(3)	1.945(4)	C(35)-C(351)	1.500(7)
F(1)-B(1)	1.366(7)	C(37)-C(310)	1.520(7)
N(1)-C(11)	1.458(6)	C(37)-C(39)	1.517(7)
N(1)-C(17)	1.511(6)	C(37)-C(38)	1.527(7)
B(1)-F(2)	1.372(7)	N(4)-Mo(1)-N(2)	106.36(17)
B(1)-F(3)	1.376(7)	N(4)-Mo(1)-N(1)	105.42(17)
B(1)-N(4)	1.609(7)	N(2)-Mo(1)-N(1)	112.45(17)
Cl(1)-C(41)	1.771(11)	N(4)-Mo(1)-N(3)	104.80(17)
N(2)-C(21)	1.455(6)	N(2)-Mo(1)-N(3)	112.86(16)
N(2)-C(27)	1.519(6)	N(1)-Mo(1)-N(3)	114.02(16)
Cl(2)-C(41)	1.653(10)	C(11)-N(1)-C(17)	115.2(4)
N(3)-C(31)	1.458(6)	C(11)-N(1)-Mo(1)	113.1(3)
N(3)-C(37)	1.517(6)	C(17)-N(1)-Mo(1)	130.8(3)
C(11)-C(12)	1.395(7)	F(1)-B(1)-F(2)	111.5(5)
C(11)-C(16)	1.392(7)	F(1)-B(1)-F(3)	110.7(5)
C(12)-C(13)	1.387(7)	F(2)-B(1)-F(3)	111.4(5)
C(13)-C(14)	1.388(8)	F(1)-B(1)-N(4)	108.0(4)
C(13)-C(131)	1.498(8)	F(2)-B(1)-N(4)	107.6(4)
C(14)-C(15)	1.391(8)	F(3)-B(1)-N(4)	107.4(4)
C(15)-C(16)	1.403(7)	C(21)-N(2)-C(27)	116.3(4)
C(15)-C(151)	1.507(8)	C(21)-N(2)-Mo(1)	112.3(3)
C(17)-C(110)	1.511(8)	C(27)-N(2)-Mo(1)	130.5(3)
C(17)-C(18)	1.512(8)	C(31)-N(3)-C(37)	114.8(4)
C(17)-C(19)	1.542(8)	C(31)-N(3)-Mo(1)	113.1(3)
C(21)-C(26)	1.398(7)	C(37)-N(3)-Mo(1)	130.6(3)
C(21)-C(22)	1.389(7)	B(1)-N(4)-Mo(1)	177.6(4)
C(22)-C(23)	1.388(7)	C(12)-C(11)-C(16)	119.6(5)
C(23)-C(24)	1.387(8)	C(12)-C(11)-N(1)	120.8(4)
C(23)-C(231)	1.507(8)	C(16)-C(11)-N(1)	119.6(4)
C(24)-C(25)	1.383(7)	C(13)-C(12)-C(11)	121.5(5)
C(25)-C(26)	1.402(7)	C(12)-C(13)-C(14)	117.8(5)
C(25)-C(251)	1.503(7)	C(12)-C(13)-C(131)	120.9(5)
C(27)-C(29)	1.496(8)	C(14)-C(13)-C(131)	121.4(5)
C(27)-C(28)	1.504(8)	C(15)-C(14)-C(13)	122.6(5)
C(27)-C(210)	1.503(7)	C(14)-C(15)-C(16)	118.3(5)
C(31)-C(36)	1.387(7)	C(14)-C(15)-C(151)	122.0(5)
C(31)-C(32)	1.395(7)	C(16)-C(15)-C(151)	119.6(5)
C(32)-C(33)	1.400(7)	C(11)-C(16)-C(15)	120.2(5)
C(33)-C(34)	1.385(8)	C(110)-C(17)-N(1)	110.3(4)

C(110)-C(17)-C(18)	109.6(5)	C(28)-C(27)-N(2)	109.3(4)
N(1)-C(17)-C(18)	110.7(5)	C(210)-C(27)-N(2)	109.7(4)
C(110)-C(17)-C(19)	106.9(5)	C(36)-C(31)-C(32)	119.8(5)
N(1)-C(17)-C(19)	107.9(4)	C(36)-C(31)-N(3)	121.0(4)
C(18)-C(17)-C(19)	111.3(6)	C(32)-C(31)-N(3)	119.2(4)
C(26)-C(21)-C(22)	119.3(5)	C(31)-C(32)-C(33)	119.8(5)
C(26)-C(21)-N(2)	118.8(4)	C(34)-C(33)-C(32)	119.1(5)
C(22)-C(21)-N(2)	121.9(4)	C(34)-C(33)-C(331)	121.7(5)
C(23)-C(22)-C(21)	121.3(5)	C(32)-C(33)-C(331)	119.2(5)
C(22)-C(23)-C(24)	118.3(5)	C(33)-C(34)-C(35)	121.8(5)
C(22)-C(23)-C(231)	120.8(5)	C(36)-C(35)-C(34)	118.4(5)
C(24)-C(23)-C(231)	120.9(5)	C(36)-C(35)-C(351)	120.9(5)
C(25)-C(24)-C(23)	122.4(5)	C(34)-C(35)-C(351)	120.7(5)
C(24)-C(25)-C(26)	118.4(5)	C(31)-C(36)-C(35)	121.1(5)
C(24)-C(25)-C(251)	121.3(5)	C(310)-C(37)-N(3)	110.5(4)
C(26)-C(25)-C(251)	120.3(5)	C(310)-C(37)-C(39)	109.7(4)
C(21)-C(26)-C(25)	120.3(5)	N(3)-C(37)-C(39)	109.5(4)
C(29)-C(27)-C(28)	111.1(6)	C(310)-C(37)-C(38)	110.0(5)
C(29)-C(27)-C(210)	108.8(5)	N(3)-C(37)-C(38)	108.4(4)
C(28)-C(27)-C(210)	108.0(5)	C(39)-C(37)-C(38)	108.6(5)
C(29)-C(27)-N(2)	110.0(4)	Cl(2)-C(41)-Cl(1)	110.6(5)

A 1.2 Bond lengths [\AA] and angles [$^\circ$] for 1-GeCl₂

Mo(1)-N(4)	1.700(4)	C(1)-C(4)	1.526(9)
Mo(1)-N(3)	1.942(4)	C(5)-C(6)	1.407(15)
Mo(1)-N(2)	1.942(5)	C(5)-C(10)	1.448(12)
Mo(1)-N(1)	1.945(5)	C(6)-C(7)	1.407(15)
Ge(1)-Cl(1)	1.572(3)	C(7)-C(8)	1.415(17)
Ge(1)-N(4)	2.069(4)	C(7)-C(11)	1.452(14)
Ge(1)-Cl(2)	2.264(2)	C(8)-C(9)	1.351(17)
Ge(1')-Cl(1')	1.565(4)	C(9)-C(10)	1.478(13)
Ge(1')-N(4)	2.069(4)	C(9)-C(12)	1.507(14)
Ge(1')-Cl(2)	2.267(2)	C(5')-C(6')	1.393(16)
N(1)-C(1)	1.510(7)	C(5')-C(10)	1.474(13)
N(1)-C(5')	1.593(12)	C(6')-C(7')	1.417(16)
N(1)-C(5)	1.598(11)	C(7')-C(8')	1.399(18)
N(2)-C(13)	1.516(7)	C(7')-C(23)	1.554(15)
N(2)-C(17)	1.587(11)	C(8')-C(9')	1.376(19)
N(2)-C(17')	1.597(11)	C(9')-C(10)	1.472(14)
N(3)-C(25)	1.510(6)	C(9')-C(12)	1.493(15)
N(3)-C(29)	1.566(12)	C(11)-C(31')	1.487(14)
N(3)-C(29')	1.571(12)	C(13)-C(16)	1.512(8)
C(1)-C(3)	1.510(8)	C(13)-C(14)	1.521(9)
C(1)-C(2)	1.518(8)	C(13)-C(15)	1.529(9)
		C(17)-C(18)	1.396(16)

C(17)-C(22)	1.474(13)	Ge(1)-Cl(2)-Ge(1')	20.42(4)
C(18)-C(19)	1.426(16)	C(1)-N(1)-C(5')	112.6(5)
C(19)-C(20)	1.411(19)	C(1)-N(1)-C(5)	109.1(5)
C(19)-C(23)	1.559(15)	C(5')-N(1)-C(5)	69.3(6)
C(20)-C(21)	1.37(2)	C(1)-N(1)-Mo(1)	130.8(3)
C(21)-C(22)	1.465(15)	C(5')-N(1)-Mo(1)	107.1(5)
C(21)-C(24)	1.494(15)	C(5)-N(1)-Mo(1)	111.3(4)
C(17')-C(18')	1.407(15)	C(13)-N(2)-C(17)	112.0(5)
C(17')-C(22)	1.459(12)	C(13)-N(2)-C(17')	108.2(5)
C(18')-C(19')	1.416(15)	C(17)-N(2)-C(17')	69.4(6)
C(19')-C(20')	1.407(17)	C(13)-N(2)-Mo(1)	130.9(4)
C(19')-C(35)	1.451(14)	C(17)-N(2)-Mo(1)	108.2(5)
C(20')-C(21')	1.362(17)	C(17')-N(2)-Mo(1)	111.5(4)
C(21')-C(22)	1.489(13)	C(25)-N(3)-C(29)	111.0(5)
C(21')-C(24)	1.492(14)	C(25)-N(3)-C(29')	110.4(5)
C(25)-C(27)	1.526(8)	C(29)-N(3)-C(29')	67.8(6)
C(25)-C(26)	1.525(7)	C(25)-N(3)-Mo(1)	131.5(3)
C(25)-C(28)	1.528(8)	C(29)-N(3)-Mo(1)	109.3(4)
C(29)-C(30)	1.390(15)	C(29')-N(3)-Mo(1)	109.1(4)
C(29)-C(34)	1.470(12)	Mo(1)-N(4)-Ge(1')	167.8(3)
C(30)-C(31)	1.414(15)	Mo(1)-N(4)-Ge(1)	168.1(3)
C(31)-C(32)	1.406(17)	Ge(1')-N(4)-Ge(1)	22.39(6)
C(31)-C(35)	1.477(14)	N(1)-C(1)-C(3)	110.4(5)
C(32)-C(33)	1.376(17)	N(1)-C(1)-C(2)	109.1(5)
C(33)-C(34)	1.469(13)	C(3)-C(1)-C(2)	110.1(5)
C(33)-C(36)	1.478(14)	N(1)-C(1)-C(4)	109.8(5)
C(29')-C(30')	1.390(15)	C(3)-C(1)-C(4)	108.2(5)
C(29')-C(34)	1.476(13)	C(2)-C(1)-C(4)	109.2(6)
C(30')-C(31')	1.404(16)	C(6)-C(5)-C(10)	125.4(9)
C(31')-C(32')	1.420(18)	C(6)-C(5)-N(1)	127.2(9)
C(32')-C(33')	1.380(18)	C(10)-C(5)-N(1)	107.4(7)
C(33')-C(34)	1.462(13)	C(5)-C(6)-C(7)	119.2(10)
C(33')-C(36)	1.495(14)	C(6)-C(7)-C(8)	118.5(11)
		C(6)-C(7)-C(11)	118.3(10)
N(4)-Mo(1)-N(3)	105.76(19)	C(8)-C(7)-C(11)	123.1(10)
N(4)-Mo(1)-N(2)	106.5(2)	C(9)-C(8)-C(7)	121.4(11)
N(3)-Mo(1)-N(2)	111.7(2)	C(8)-C(9)-C(10)	124.9(10)
N(4)-Mo(1)-N(1)	106.1(2)	C(8)-C(9)-C(12)	117.0(10)
N(3)-Mo(1)-N(1)	112.1(2)	C(10)-C(9)-C(12)	117.9(9)
N(2)-Mo(1)-N(1)	114.0(3)	C(6')-C(5')-C(10)	124.8(9)
Cl(1)-Ge(1)-N(4)	122.43(18)	C(6')-C(5')-N(1)	128.2(9)
Cl(1)-Ge(1)-Cl(2)	123.84(16)	C(10)-C(5')-N(1)	106.4(8)
N(4)-Ge(1)-Cl(2)	94.72(13)	C(5')-C(6')-C(7')	119.1(11)
Cl(1')-Ge(1')-N(4)	122.70(18)	C(8')-C(7')-C(6')	120.0(12)
Cl(1')-Ge(1')-Cl(2)	123.99(15)	C(8')-C(7')-C(23)	120.2(10)
N(4)-Ge(1')-Cl(2)	94.67(13)	C(6')-C(7')-C(23)	119.8(11)

C(9')-C(8')-C(7')	120.1(11)	C(7')-C(23)-C(19)	48.0(6)
C(8')-C(9')-C(10)	125.1(11)	C(21')-C(24)-C(21)	61.0(8)
C(8')-C(9')-C(12)	115.4(11)	N(3)-C(25)-C(27)	108.8(5)
C(10)-C(9')-C(12)	119.2(10)	N(3)-C(25)-C(26)	109.8(4)
C(5)-C(10)-C(9')	171.1(9)	C(27)-C(25)-C(26)	109.6(5)
C(5)-C(10)-C(9)	110.4(8)	N(3)-C(25)-C(28)	109.0(5)
C(9')-C(10)-C(9)	61.7(7)	C(27)-C(25)-C(28)	109.8(5)
C(5)-C(10)-C(5')	76.8(6)	C(26)-C(25)-C(28)	109.9(5)
C(9')-C(10)-C(5')	110.5(8)	C(30)-C(29)-C(34)	123.1(9)
C(9)-C(10)-C(5')	170.4(8)	C(30)-C(29)-N(3)	127.0(9)
C(7)-C(11)-C(31')	48.0(7)	C(34)-C(29)-N(3)	109.9(7)
C(9')-C(12)-C(9)	60.6(7)	C(29)-C(30)-C(31)	119.8(11)
C(16)-C(13)-N(2)	109.1(5)	C(32)-C(31)-C(30)	119.3(11)
C(16)-C(13)-C(14)	110.1(6)	C(32)-C(31)-C(35)	116.5(10)
N(2)-C(13)-C(14)	109.5(5)	C(30)-C(31)-C(35)	124.2(10)
C(16)-C(13)-C(15)	109.3(6)	C(33)-C(32)-C(31)	122.3(11)
N(2)-C(13)-C(15)	109.8(5)	C(32)-C(33)-C(34)	121.5(10)
C(14)-C(13)-C(15)	109.0(5)	C(32)-C(33)-C(36)	117.4(10)
C(18)-C(17)-C(22)	125.7(9)	C(34)-C(33)-C(36)	121.2(9)
C(18)-C(17)-N(2)	127.1(9)	C(30')-C(29')-C(34)	123.5(9)
C(22)-C(17)-N(2)	106.9(7)	C(30')-C(29')-N(3)	127.2(9)
C(17)-C(18)-C(19)	117.7(11)	C(34)-C(29')-N(3)	109.3(7)
C(20)-C(19)-C(18)	120.3(12)	C(29')-C(30')-C(31')	119.7(11)
C(20)-C(19)-C(23)	120.2(11)	C(30')-C(31')-C(32')	119.8(11)
C(18)-C(19)-C(23)	119.5(11)	C(30')-C(31')-C(11)	124.3(11)
C(21)-C(20)-C(19)	120.3(12)	C(32')-C(31')-C(11)	115.9(10)
C(20)-C(21)-C(22)	124.9(11)	C(33')-C(32')-C(31')	121.0(11)
C(20)-C(21)-C(24)	115.7(11)	C(32')-C(33')-C(34)	122.7(11)
C(22)-C(21)-C(24)	119.1(11)	C(32')-C(33')-C(36)	116.9(10)
C(18')-C(17')-C(22)	125.3(9)	C(34)-C(33')-C(36)	120.5(10)
C(18')-C(17')-N(2)	127.6(9)	C(33')-C(34)-C(33)	59.5(7)
C(22)-C(17')-N(2)	107.1(7)	C(33')-C(34)-C(29)	173.0(8)
C(17')-C(18')-C(19')	119.0(11)	C(33)-C(34)-C(29)	114.1(8)
C(20')-C(19')-C(18')	119.3(11)	C(33')-C(34)-C(29')	113.3(8)
C(20')-C(19')-C(35)	122.3(10)	C(33)-C(34)-C(29')	172.1(8)
C(18')-C(19')-C(35)	118.4(10)	C(29)-C(34)-C(29')	72.9(6)
C(21')-C(20')-C(19')	121.1(11)	C(19')-C(35)-C(31)	48.4(7)
C(20')-C(21')-C(22)	124.7(10)	C(33)-C(36)-C(33')	58.6(7)
C(20')-C(21')-C(24)	117.4(10)		
C(22)-C(21')-C(24)	117.7(9)		
C(17')-C(22)-C(21)	171.2(9)		
C(17')-C(22)-C(17)	76.4(6)		
C(21)-C(22)-C(17)	110.9(8)		
C(17')-C(22)-C(21')	110.5(8)		
C(21)-C(22)-C(21')	61.7(8)		
C(17)-C(22)-C(21')	170.0(8)		

A 1.3 Bond lengths [\AA] and angles [$^\circ$] for 1-SnCl₂

Mo(1)-N(4)	1.692(5)	C(13)-C(16)	1.523(10)
Mo(1)-N(3)	1.941(6)	C(13)-C(15)	1.551(11)
Mo(1)-N(2)	1.948(6)	C(17)-C(18)	1.381(19)
Mo(1)-N(1)	1.946(6)	C(17)-C(22)	1.458(14)
Sn(1)-Sn(1')	0.9226(12)	C(18)-C(19)	1.418(19)
Sn(1)-Cl(1')	1.630(4)	C(19)-C(20)	1.39(2)
Sn(1)-N(4)	2.266(5)	C(19)-C(23)	1.550(17)
Sn(1)-Cl(2)	2.417(2)	C(20)-C(21)	1.39(2)
Sn(1)-Cl(1)	2.417(4)	C(21)-C(24)	1.459(17)
Cl(1')-Sn(1')	2.438(4)	C(21)-C(22)	1.452(17)
Sn(1')-Cl(1)	1.610(4)	C(17')-C(18')	1.403(19)
Sn(1')-N(4)	2.271(5)	C(17')-C(22)	1.425(15)
Sn(1')-Cl(2)	2.421(2)	C(18')-C(19')	1.428(18)
N(1)-C(1)	1.512(8)	C(19')-C(20')	1.42(2)
N(1)-C(5')	1.574(15)	C(19')-C(35)	1.448(19)
N(1)-C(5)	1.555(13)	C(20')-C(21')	1.38(2)
N(2)-C(13)	1.494(9)	C(21')-C(24)	1.428(19)
N(2)-C(17)	1.562(14)	C(21')-C(22)	1.470(16)
N(2)-C(17')	1.588(13)	C(25)-C(27)	1.508(10)
N(3)-C(25)	1.512(8)	C(25)-C(28)	1.532(9)
N(3)-C(29)	1.549(12)	C(25)-C(26)	1.526(9)
N(3)-C(29')	1.566(14)	C(29)-C(30)	1.403(18)
C(1)-C(3)	1.493(11)	C(29)-C(34)	1.437(15)
C(1)-C(2)	1.516(10)	C(30)-C(31)	1.404(17)
C(1)-C(4)	1.537(11)	C(31)-C(32)	1.39(2)
C(5)-C(6)	1.388(17)	C(31)-C(35)	1.515(15)
C(5)-C(10)	1.444(14)	C(32)-C(33)	1.35(2)
C(6)-C(7)	1.414(17)	C(33)-C(34)	1.453(15)
C(7)-C(8)	1.41(2)	C(33)-C(36)	1.477(16)
C(7)-C(11)	1.465(16)	C(29')-C(30')	1.36(2)
C(8)-C(9)	1.40(2)	C(29')-C(34)	1.466(15)
C(9)-C(12)	1.455(17)	C(30')-C(31')	1.43(2)
C(9)-C(10)	1.454(15)	C(31')-C(32')	1.43(2)
C(5')-C(6')	1.40(2)	C(32')-C(33')	1.36(2)
C(5')-C(10)	1.475(15)	C(33')-C(34)	1.462(17)
C(6')-C(7')	1.40(2)	C(33')-C(36)	1.471(15)
C(7')-C(8')	1.38(2)	N(4)-Mo(1)-N(3)	105.1(2)
C(7')-C(23)	1.545(19)	N(4)-Mo(1)-N(2)	106.2(2)
C(8')-C(9')	1.41(3)	N(3)-Mo(1)-N(2)	112.2(3)
C(9')-C(12)	1.415(18)	N(4)-Mo(1)-N(1)	106.0(2)
C(9')-C(10)	1.484(19)	N(3)-Mo(1)-N(1)	112.4(3)
C(11)-C(31')	1.500(17)	N(2)-Mo(1)-N(1)	114.1(3)
C(13)-C(14)	1.496(10)	Sn(1')-Sn(1)-Cl(1')	144.10(19)
		Sn(1')-Sn(1)-N(4)	78.57(16)
		Cl(1')-Sn(1)-N(4)	119.51(19)

Sn(1')-Sn(1)-Cl(2)	79.28(11)	C(2)-C(1)-C(4)	109.0(7)
Cl(1')-Sn(1)-Cl(2)	126.65(15)	C(6)-C(5)-C(10)	123.4(10)
N(4)-Sn(1)-Cl(2)	91.68(14)	C(6)-C(5)-N(1)	127.5(10)
Sn(1')-Sn(1)-Cl(1)	23.12(13)	C(10)-C(5)-N(1)	109.1(9)
Cl(1')-Sn(1)-Cl(1)	120.98(18)	C(5)-C(6)-C(7)	120.9(12)
N(4)-Sn(1)-Cl(1)	92.40(17)	C(8)-C(7)-C(6)	117.8(13)
Cl(2)-Sn(1)-Cl(1)	97.26(13)	C(8)-C(7)-C(11)	122.6(11)
Sn(1)-Cl(1')-Sn(1')	12.82(7)	C(6)-C(7)-C(11)	119.6(12)
Sn(1)-Sn(1')-Cl(1)	143.9(2)	C(9)-C(8)-C(7)	122.1(12)
Sn(1)-Sn(1')-N(4)	77.96(16)	C(8)-C(9)-C(12)	117.7(12)
Cl(1)-Sn(1')-N(4)	120.27(19)	C(8)-C(9)-C(10)	121.5(12)
Sn(1)-Sn(1')-Cl(2)	78.73(11)	C(12)-C(9)-C(10)	120.9(12)
Cl(1)-Sn(1')-Cl(2)	127.14(17)	C(6')-C(5')-C(10)	123.7(12)
N(4)-Sn(1')-Cl(2)	91.44(14)	C(6')-C(5')-N(1)	129.4(12)
Sn(1)-Sn(1')-Cl(1')	23.08(12)	C(10)-C(5')-N(1)	106.6(9)
Cl(1)-Sn(1')-Cl(1')	120.79(19)	C(5')-C(6')-C(7')	119.7(14)
N(4)-Sn(1')-Cl(1')	91.69(16)	C(8')-C(7')-C(6')	120.6(16)
Cl(2)-Sn(1')-Cl(1')	96.78(12)	C(8')-C(7')-C(23)	119.0(14)
Sn(1')-Cl(1)-Sn(1)	13.01(7)	C(6')-C(7')-C(23)	120.3(14)
Sn(1)-Cl(2)-Sn(1')	21.99(3)	C(7')-C(8')-C(9')	121.4(16)
C(1)-N(1)-C(5')	111.3(6)	C(8')-C(9')-C(12)	116.4(15)
C(1)-N(1)-C(5)	109.5(6)	C(8')-C(9')-C(10)	122.0(14)
C(5')-N(1)-C(5)	69.2(7)	C(12)-C(9')-C(10)	121.5(14)
C(1)-N(1)-Mo(1)	130.7(4)	C(5)-C(10)-C(9)	114.2(10)
C(5')-N(1)-Mo(1)	107.9(6)	C(5)-C(10)-C(9')	170.2(11)
C(5)-N(1)-Mo(1)	111.7(5)	C(9)-C(10)-C(9')	57.7(9)
C(13)-N(2)-C(17)	112.0(7)	C(5)-C(10)-C(5')	75.0(8)
C(13)-N(2)-C(17')	108.9(7)	C(9)-C(10)-C(5')	169.0(10)
C(17)-N(2)-C(17')	68.2(7)	C(9')-C(10)-C(5')	112.5(10)
C(13)-N(2)-Mo(1)	131.0(4)	C(7)-C(11)-C(31')	51.5(9)
C(17)-N(2)-Mo(1)	108.4(6)	C(9')-C(12)-C(9)	59.2(10)
C(17')-N(2)-Mo(1)	111.1(6)	C(14)-C(13)-N(2)	110.9(6)
C(25)-N(3)-C(29)	111.0(6)	C(14)-C(13)-C(16)	109.8(7)
C(25)-N(3)-C(29')	110.9(7)	N(2)-C(13)-C(16)	109.9(6)
C(29)-N(3)-C(29')	67.8(7)	C(14)-C(13)-C(15)	107.6(6)
C(25)-N(3)-Mo(1)	130.7(4)	N(2)-C(13)-C(15)	109.3(7)
C(29)-N(3)-Mo(1)	110.4(6)	C(16)-C(13)-C(15)	109.2(7)
C(29')-N(3)-Mo(1)	108.7(6)	C(18)-C(17)-C(22)	124.1(11)
Mo(1)-N(4)-Sn(1)	168.0(3)	C(18)-C(17)-N(2)	127.8(11)
Mo(1)-N(4)-Sn(1')	167.1(3)	C(22)-C(17)-N(2)	107.8(9)
Sn(1)-N(4)-Sn(1')	23.47(6)	C(17)-C(18)-C(19)	120.1(12)
C(3)-C(1)-N(1)	110.0(6)	C(20)-C(19)-C(18)	118.5(13)
C(3)-C(1)-C(2)	109.6(7)	C(20)-C(19)-C(23)	120.2(13)
N(1)-C(1)-C(2)	109.7(6)	C(18)-C(19)-C(23)	121.3(12)
C(3)-C(1)-C(4)	109.0(7)	C(19)-C(20)-C(21)	121.5(14)
N(1)-C(1)-C(4)	109.6(6)	C(20)-C(21)-C(24)	115.6(13)

C(20)-C(21)-C(22)	123.2(13)	C(32')-C(33')-C(34)	122.2(12)
C(24)-C(21)-C(22)	121.0(13)	C(32')-C(33')-C(36)	117.2(13)
C(18')-C(17')-C(22)	125.4(11)	C(34)-C(33')-C(36)	120.6(11)
C(18')-C(17')-N(2)	126.5(11)	C(29)-C(34)-C(33)	113.8(9)
C(22)-C(17')-N(2)	108.1(9)	C(29)-C(34)-C(33')	171.5(9)
C(17')-C(18')-C(19')	119.4(14)	C(33)-C(34)-C(33')	59.4(8)
C(18')-C(19')-C(20')	116.5(15)	C(29)-C(34)-C(29')	73.5(7)
C(18')-C(19')-C(35)	118.8(14)	C(33)-C(34)-C(29')	171.1(10)
C(20')-C(19')-C(35)	124.7(12)	C(33')-C(34)-C(29')	112.9(9)
C(21')-C(20')-C(19')	124.1(13)	C(19')-C(35)-C(31)	50.9(8)
C(20')-C(21')-C(24)	117.1(12)	C(33)-C(36)-C(33')	58.6(8)
C(20')-C(21')-C(22)	120.9(14)		
C(24)-C(21')-C(22)	121.9(13)		
C(17')-C(22)-C(21')	113.5(10)		
C(17')-C(22)-C(17)	75.6(8)		
C(21')-C(22)-C(17)	168.5(10)		
C(17')-C(22)-C(21)	169.6(10)		
C(21')-C(22)-C(21)	57.9(10)		
C(17)-C(22)-C(21)	112.3(10)		
C(7')-C(23)-C(19)	51.6(8)		
C(21')-C(24)-C(21)	58.7(9)		
C(27)-C(25)-N(3)	109.6(6)		
C(27)-C(25)-C(28)	110.1(6)		
N(3)-C(25)-C(28)	108.8(6)		
C(27)-C(25)-C(26)	109.4(6)		
N(3)-C(25)-C(26)	109.8(5)		
C(28)-C(25)-C(26)	109.2(6)		
C(30)-C(29)-C(34)	123.7(10)		
C(30)-C(29)-N(3)	125.9(11)		
C(34)-C(29)-N(3)	110.3(9)		
C(31)-C(30)-C(29)	119.3(12)		
C(32)-C(31)-C(30)	117.7(12)		
C(32)-C(31)-C(35)	119.5(11)		
C(30)-C(31)-C(35)	122.8(12)		
C(33)-C(32)-C(31)	124.1(12)		
C(32)-C(33)-C(34)	121.2(12)		
C(32)-C(33)-C(36)	118.0(12)		
C(34)-C(33)-C(36)	120.8(11)		
C(30')-C(29')-C(34)	124.7(11)		
C(30')-C(29')-N(3)	127.4(12)		
C(34)-C(29')-N(3)	107.9(10)		
C(29')-C(30')-C(31')	120.4(14)		
C(32')-C(31')-C(30')	116.8(13)		
C(32')-C(31')-C(11)	118.0(12)		
C(30')-C(31')-C(11)	125.2(13)		
C(33')-C(32')-C(31')	123.1(14)		

A 1.4 Bond lengths [Å] and angles [°]
for [2b]OTf.

Mo(1)-N(2)	1.715(6)	C(21)#1-Si(1)-C(21)#2	111.23(15)
Mo(1)-N(1)	1.936(3)	O(1)-S(1)-O(1)#1	114.47(16)
Mo(1)-N(1)#1	1.936(3)	O(1)-S(1)-O(1)#2	114.43(16)
Mo(1)-N(1)#2	1.936(3)	O(1)#1-S(1)-O(1)#2	114.43(16)
N(1)-C(17)	1.510(5)	O(1)-S(1)-C(31)	103.9(2)
N(1)-C(11)	1.466(5)	O(1)#1-S(1)-C(31)	103.9(2)
Si(1)-N(2)	1.795(6)	O(1)#2-S(1)-C(31)	103.9(2)
Si(1)-C(21)	1.848(4)	Mo(1)-N(2)-Si(1)	179.94(13)
Si(1)-C(21)#1	1.848(4)	C(12)-C(11)-C(16)	120.0(4)
Si(1)-C(21)#2	1.847(4)	C(12)-C(11)-N(1)	120.5(4)
F(1)-C(31)	1.289(5)	C(16)-C(11)-N(1)	119.5(4)
O(1)-S(1)	1.405(4)	C(11)-C(12)-C(13)	121.3(4)
S(1)-O(1)#1	1.405(4)	C(14)-C(13)-C(12)	117.8(4)
S(1)-O(1)#2	1.406(4)	C(14)-C(13)-C(131)	121.8(4)
S(1)-C(31)	1.801(9)	C(12)-C(13)-C(131)	120.4(4)
C(11)-C(12)	1.374(6)	C(15)-C(14)-C(13)	121.6(4)
C(11)-C(16)	1.385(6)	C(14)-C(15)-C(16)	119.3(4)
C(12)-C(13)	1.393(6)	C(14)-C(15)-C(151)	120.4(4)
C(13)-C(14)	1.397(6)	C(16)-C(15)-C(151)	120.3(4)
C(13)-C(131)	1.517(6)	C(15)-C(16)-C(11)	120.0(4)
C(14)-C(15)	1.376(6)	N(1)-C(17)-C(110)	108.7(3)
C(15)-C(16)	1.394(6)	N(1)-C(17)-C(18)	111.1(3)
C(15)-C(151)	1.518(6)	C(110)-C(17)-C(18)	107.7(4)
C(17)-C(110)	1.540(6)	N(1)-C(17)-C(19)	110.2(3)
C(17)-C(18)	1.517(6)	C(110)-C(17)-C(19)	109.5(4)
C(17)-C(19)	1.527(6)	C(18)-C(17)-C(19)	109.7(4)
C(31)-F(1)#1	1.291(5)	F(1)#1-C(31)-F(1)#2	105.6(5)
C(31)-F(1)#2	1.291(5)	F(1)#1-C(31)-F(1)	105.8(5)
N(2)-Mo(1)-N(1)	108.08(10)	F(1)#2-C(31)-F(1)	105.8(5)
N(2)-Mo(1)-N(1)#1	108.02(10)	F(1)#1-C(31)-S(1)	113.0(4)
N(1)-Mo(1)-N(1)#1	110.84(9)	F(1)#2-C(31)-S(1)	113.0(4)
N(2)-Mo(1)-N(1)#2	108.08(10)	F(1)-C(31)-S(1)	113.1(4)
N(1)-Mo(1)-N(1)#2	110.85(9)		
N(1)#1-Mo(1)-N(1)#2	110.84(9)		
C(17)-N(1)-C(11)	115.6(3)		
C(17)-N(1)-Mo(1)	129.0(3)		
C(11)-N(1)-Mo(1)	114.4(2)		
N(2)-Si(1)-C(21)	107.65(16)		
N(2)-Si(1)-C(21)#1	107.67(16)		
C(21)-Si(1)-C(21)#1	111.22(15)		
N(2)-Si(1)-C(21)#2	107.63(16)		
C(21)-Si(1)-C(21)#2	111.25(15)		

A 1.5 Bond lengths [\AA] and angles [$^\circ$]
for [2c]OTf

Mo(1)-N(4)	1.739(3)	C(23)-C(24)	1.393(6)
Mo(1)-N(1)	1.928(3)	C(23)-C(231)	1.506(6)
Mo(1)-N(2)	1.935(3)	C(24)-C(25)	1.379(6)
Mo(1)-N(3)	1.938(3)	C(25)-C(26)	1.409(5)
N(1)-C(11)	1.463(5)	C(25)-C(251)	1.518(6)
N(1)-C(17)	1.537(5)	C(27)-C(29)	1.525(6)
O(1)-C(41)	1.204(5)	C(27)-C(210)	1.524(6)
S(1)-O(3)	1.371(5)	C(27)-C(28)	1.534(5)
S(1)-O(4)	1.402(4)	C(31)-C(32)	1.387(5)
S(1)-O(2)	1.455(7)	C(31)-C(36)	1.395(6)
S(1)-C(5)	1.77(2)	C(32)-C(33)	1.399(6)
F(1)-C(5)	1.355(18)	C(33)-C(34)	1.398(6)
C(5)-F(2)	1.29(2)	C(33)-C(331)	1.504(6)
C(5)-F(3)	1.362(17)	C(34)-C(35)	1.382(6)
S(1A)-O(3)	1.301(9)	C(35)-C(36)	1.393(5)
S(1A)-O(2A)	1.388(17)	C(35)-C(351)	1.508(6)
S(1A)-O(4)	1.435(9)	C(37)-C(310)	1.521(6)
S(1A)-C(5A)	1.89(6)	C(37)-C(38)	1.528(5)
F(1A)-C(5A)	1.32(7)	C(37)-C(39)	1.532(6)
C(5A)-F(3)	1.12(7)	C(41)-C(42)	1.479(6)
C(5A)-F(2)	1.33(7)	C(42)-C(43)	1.384(6)
N(2)-C(21)	1.459(5)	C(42)-C(47)	1.392(6)
N(2)-C(27)	1.531(5)	C(43)-C(44)	1.380(6)
N(3)-C(31)	1.452(5)	C(44)-C(45)	1.380(6)
N(3)-C(37)	1.527(5)	C(45)-C(46)	1.377(7)
N(4)-C(41)	1.422(5)	C(46)-C(47)	1.377(6)
O(5)-C(64)	1.424(6)	C(61)-C(62)	1.486(7)
O(5)-C(61)	1.440(6)	C(62)-C(63)	1.513(7)
C(11)-C(12)	1.385(6)	C(63)-C(64)	1.507(7)
C(11)-C(16)	1.386(5)	N(4)-Mo(1)-N(1)	107.03(13)
C(12)-C(13)	1.383(6)	N(4)-Mo(1)-N(2)	109.17(14)
C(13)-C(14)	1.393(6)	N(1)-Mo(1)-N(2)	109.75(13)
C(13)-C(131)	1.519(6)	N(4)-Mo(1)-N(3)	108.88(14)
C(14)-C(15)	1.367(6)	N(1)-Mo(1)-N(3)	108.37(13)
C(15)-C(16)	1.400(6)	N(2)-Mo(1)-N(3)	113.42(13)
C(15)-C(151)	1.517(6)	C(11)-N(1)-C(17)	115.6(3)
C(17)-C(110)	1.504(6)	C(11)-N(1)-Mo(1)	115.3(2)
C(17)-C(19)	1.523(6)	C(17)-N(1)-Mo(1)	128.5(2)
C(17)-C(18)	1.536(6)	O(3)-S(1)-O(4)	121.0(3)
C(21)-C(26)	1.383(5)	O(3)-S(1)-O(2)	112.1(4)
C(21)-C(22)	1.392(5)	O(4)-S(1)-O(2)	111.3(3)
C(22)-C(23)	1.389(5)	O(3)-S(1)-C(5)	105.5(7)
		O(4)-S(1)-C(5)	103.8(6)
		O(2)-S(1)-C(5)	100.2(6)
		F(2)-C(5)-F(1)	104.0(14)

F(2)-C(5)-F(3)	108.4(11)	N(1)-C(17)-C(18)	107.3(3)
F(1)-C(5)-F(3)	102.6(14)	C(26)-C(21)-C(22)	120.2(4)
F(2)-C(5)-S(1)	115.4(14)	C(26)-C(21)-N(2)	119.6(3)
F(1)-C(5)-S(1)	111.8(10)	C(22)-C(21)-N(2)	120.2(3)
F(3)-C(5)-S(1)	113.5(13)	C(21)-C(22)-C(23)	120.6(4)
O(3)-S(1A)-O(2A)	96.3(9)	C(24)-C(23)-C(22)	118.4(4)
O(3)-S(1A)-O(4)	123.7(7)	C(24)-C(23)-C(231)	121.6(4)
O(2A)-S(1A)-O(4)	112.6(9)	C(22)-C(23)-C(231)	120.0(4)
O(3)-S(1A)-C(5A)	110(2)	C(25)-C(24)-C(23)	122.2(4)
O(2A)-S(1A)-C(5A)	99(3)	C(24)-C(25)-C(26)	118.5(4)
O(4)-S(1A)-C(5A)	111(2)	C(24)-C(25)-C(251)	121.2(4)
F(3)-C(5A)-F(1A)	108(4)	C(26)-C(25)-C(251)	120.2(4)
F(3)-C(5A)-F(2)	123(6)	C(21)-C(26)-C(25)	120.1(4)
F(1A)-C(5A)-F(2)	102(5)	C(29)-C(27)-C(210)	109.4(4)
F(3)-C(5A)-S(1A)	114(4)	C(29)-C(27)-N(2)	110.5(3)
F(1A)-C(5A)-S(1A)	102(4)	C(210)-C(27)-N(2)	109.1(3)
F(2)-C(5A)-S(1A)	105(3)	C(29)-C(27)-C(28)	109.1(3)
C(21)-N(2)-C(27)	113.9(3)	C(210)-C(27)-C(28)	110.5(3)
C(21)-N(2)-Mo(1)	115.0(2)	N(2)-C(27)-C(28)	108.4(3)
C(27)-N(2)-Mo(1)	130.4(2)	C(32)-C(31)-C(36)	120.7(4)
C(5)-F(2)-C(5A)	28(3)	C(32)-C(31)-N(3)	120.3(4)
C(31)-N(3)-C(37)	115.0(3)	C(36)-C(31)-N(3)	119.0(3)
C(31)-N(3)-Mo(1)	114.2(2)	C(31)-C(32)-C(33)	120.1(4)
C(37)-N(3)-Mo(1)	130.6(2)	C(32)-C(33)-C(34)	118.2(4)
S(1A)-O(3)-S(1)	29.1(3)	C(32)-C(33)-C(331)	120.4(4)
C(5A)-F(3)-C(5)	27(3)	C(34)-C(33)-C(331)	121.4(4)
C(41)-N(4)-Mo(1)	175.7(3)	C(35)-C(34)-C(33)	122.3(4)
S(1)-O(4)-S(1A)	27.4(3)	C(34)-C(35)-C(36)	118.7(4)
C(64)-O(5)-C(61)	108.5(4)	C(34)-C(35)-C(351)	121.1(4)
C(12)-C(11)-C(16)	119.8(4)	C(36)-C(35)-C(351)	120.2(4)
C(12)-C(11)-N(1)	120.3(4)	C(31)-C(36)-C(35)	120.0(4)
C(16)-C(11)-N(1)	119.9(4)	C(310)-C(37)-N(3)	108.7(3)
C(11)-C(12)-C(13)	120.8(4)	C(310)-C(37)-C(38)	109.9(3)
C(12)-C(13)-C(14)	118.4(4)	N(3)-C(37)-C(38)	109.8(3)
C(12)-C(13)-C(131)	120.8(4)	C(310)-C(37)-C(39)	109.1(3)
C(14)-C(13)-C(131)	120.8(4)	N(3)-C(37)-C(39)	109.8(3)
C(15)-C(14)-C(13)	122.0(4)	C(38)-C(37)-C(39)	109.5(3)
C(14)-C(15)-C(16)	118.9(4)	O(1)-C(41)-N(4)	118.7(4)
C(14)-C(15)-C(151)	121.2(4)	O(1)-C(41)-C(42)	123.9(4)
C(16)-C(15)-C(151)	119.9(4)	N(4)-C(41)-C(42)	117.4(4)
C(11)-C(16)-C(15)	120.1(4)	C(43)-C(42)-C(47)	118.9(4)
C(110)-C(17)-C(19)	109.4(4)	C(43)-C(42)-C(41)	123.6(4)
C(110)-C(17)-N(1)	110.2(3)	C(47)-C(42)-C(41)	117.5(4)
C(19)-C(17)-N(1)	110.1(4)	C(44)-C(43)-C(42)	120.8(4)
C(110)-C(17)-C(18)	108.2(4)	C(43)-C(44)-C(45)	119.7(5)
C(19)-C(17)-C(18)	111.5(4)	C(46)-C(45)-C(44)	120.0(4)

C(45)-C(46)-C(47)	120.5(4)	C(64)-C(63)-C(62)	102.5(4)
C(46)-C(47)-C(42)	120.1(4)	O(5)-C(64)-C(63)	106.3(5)
O(5)-C(61)-C(62)	106.7(4)		
C(61)-C(62)-C(63)	101.0(4)		

A 1.6 Bond lengths [Å] and angles [°] for [2d]I.

Mo(1)-N(2)	1.708(9)	C(11)-N(1)-C(17)	115.8(4)
Mo(1)-N(1)#1	1.939(4)	C(11)-N(1)-Mo(1)	113.2(3)
Mo(1)-N(1)	1.939(4)	C(17)-N(1)-Mo(1)	129.6(3)
Mo(1)-N(1)#2	1.939(4)	C(21)-N(2)-Mo(1)	180.0(4)
N(1)-C(11)	1.453(6)	C(12)-C(11)-C(16)	120.9(5)
N(1)-C(17)	1.508(6)	C(12)-C(11)-N(1)	119.9(5)
Cl(1)-C(31)	1.671(8)	C(16)-C(11)-N(1)	119.2(5)
N(2)-C(21)	1.457(15)	C(11)-C(12)-C(13)	120.4(6)
C(11)-C(12)	1.380(7)	C(14)-C(13)-C(12)	118.6(6)
C(11)-C(16)	1.384(8)	C(14)-C(13)-C(131)	121.0(6)
C(12)-C(13)	1.391(8)	C(12)-C(13)-C(131)	120.4(7)
C(13)-C(14)	1.390(9)	C(15)-C(14)-C(13)	121.0(6)
C(13)-C(131)	1.521(9)	C(14)-C(15)-C(16)	120.1(6)
C(14)-C(15)	1.378(8)	C(14)-C(15)-C(151)	119.4(6)
C(15)-C(16)	1.392(8)	C(16)-C(15)-C(151)	120.5(6)
C(15)-C(151)	1.526(9)	C(11)-C(16)-C(15)	119.0(5)
C(17)-C(19)	1.517(8)	N(1)-C(17)-C(19)	110.9(4)
C(17)-C(110)	1.515(10)	N(1)-C(17)-C(110)	108.7(5)
C(17)-C(18)	1.521(9)	C(19)-C(17)-C(110)	110.2(5)
C(21)-C(22)	1.48(3)	N(1)-C(17)-C(18)	109.8(4)
C(21)-C(22)#2	1.48(3)	C(19)-C(17)-C(18)	108.8(6)
C(21)-C(22)#1	1.48(3)	C(110)-C(17)-C(18)	108.4(7)
C(31)-Cl(1)#3	1.671(8)	N(2)-C(21)-C(22)	112.3(12)
C(31)-Cl(1)#4	1.671(8)	N(2)-C(21)-C(22)#2	112.3(12)
		C(22)-C(21)-C(22)#2	106.5(13)
N(2)-Mo(1)-N(1)#1	106.44(12)	N(2)-C(21)-C(22)#1	112.3(12)
N(2)-Mo(1)-N(1)	106.44(12)	C(22)-C(21)-C(22)#1	106.5(13)
N(1)#1-Mo(1)-N(1)	112.32(11)	C(22)#2-C(21)-C(22)#1	106.5(13)
N(2)-Mo(1)-N(1)#2	106.44(12)	Cl(1)#3-C(31)-Cl(1)	100.9(6)
N(1)#1-Mo(1)-N(1)#2	112.32(11)	Cl(1)#3-C(31)-Cl(1)#4	100.9(6)
N(1)-Mo(1)-N(1)#2	112.32(11)	Cl(1)-C(31)-Cl(1)#4	100.9(6)

A 1.7 Bond lengths [Å] and angles [°] for 3.

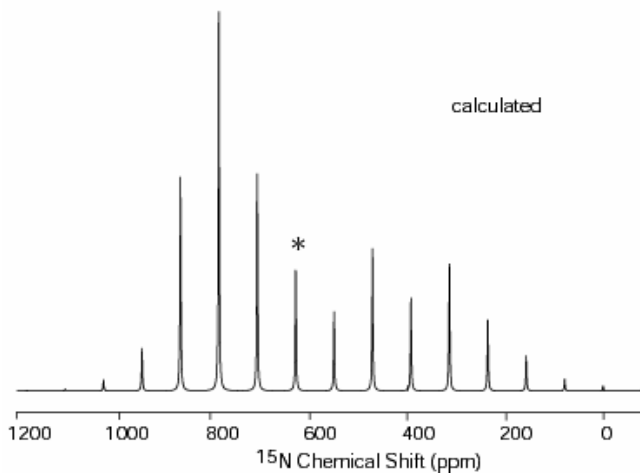
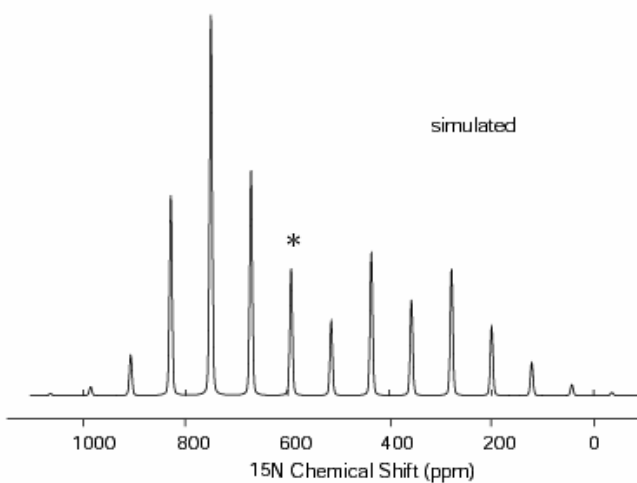
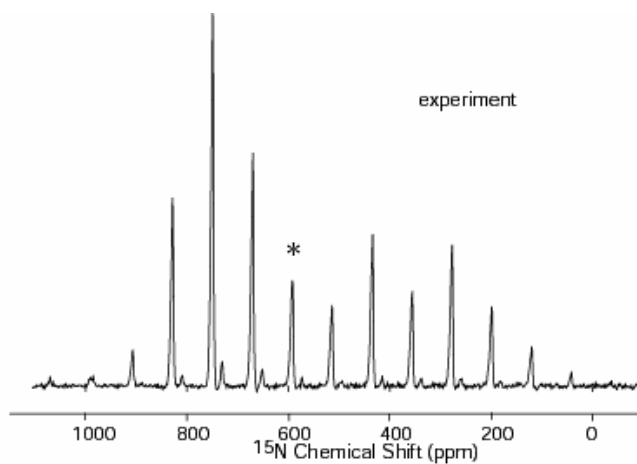
Mo(1)-N(4)	1.777(4)	N(1)-C(17)	1.498(7)
Mo(1)-N(2)	1.963(4)	N(2)-C(21)	1.458(6)
Mo(1)-N(3)	1.968(4)	N(2)-C(27)	1.497(6)
Mo(1)-N(1)	1.971(4)	N(3)-C(31)	1.439(7)
N(1)-C(11)	1.441(7)	N(3)-C(37)	1.501(7)
		N(4)-C(41)	1.300(7)

C(11)-C(12)	1.378(8)	C(25)-C(26)	1.392(8)
C(11)-C(16)	1.397(8)	C(25)-C(251)	1.505(8)
C(12)-C(13)	1.407(7)	C(27)-C(28)	1.500(9)
C(13)-C(14)	1.385(8)	C(27)-C(210)	1.509(8)
C(13)-C(131)	1.500(8)	C(27)-C(29)	1.529(8)
C(14)-C(15)	1.404(9)	C(31)-C(36)	1.383(7)
C(15)-C(16)	1.402(8)	C(31)-C(32)	1.415(8)
C(15)-C(151)	1.500(9)	C(32)-C(33)	1.369(8)
C(17)-C(18)	1.515(8)	C(33)-C(34)	1.408(9)
C(17)-C(19)	1.521(8)	C(33)-C(331)	1.507(9)
C(17)-C(110)	1.535(8)	C(34)-C(35)	1.386(8)
C(21)-C(26)	1.388(8)	C(35)-C(36)	1.388(8)
C(21)-C(22)	1.388(7)	C(35)-C(351)	1.520(9)
C(22)-C(23)	1.373(8)	C(37)-C(310)	1.514(8)
C(23)-C(24)	1.399(8)	C(37)-C(38)	1.538(8)
C(23)-C(231)	1.506(8)	C(37)-C(39)	1.558(8)
C(24)-C(25)	1.390(8)		
N(4)-Mo(1)-N(2)	101.27(18)	N(1)-C(17)-C(18)	108.0(4)
N(4)-Mo(1)-N(3)	102.56(18)	N(1)-C(17)-C(19)	110.6(5)
N(2)-Mo(1)-N(3)	111.50(17)	C(18)-C(17)-C(19)	109.8(5)
N(4)-Mo(1)-N(1)	101.36(19)	N(1)-C(17)-C(110)	110.2(4)
N(2)-Mo(1)-N(1)	120.10(18)	C(18)-C(17)-C(110)	108.5(5)
N(3)-Mo(1)-N(1)	116.33(18)	C(19)-C(17)-C(110)	109.8(5)
C(11)-N(1)-C(17)	116.9(4)	C(26)-C(21)-C(22)	118.8(5)
C(11)-N(1)-Mo(1)	110.9(3)		
C(17)-N(1)-Mo(1)	131.3(3)	C(26)-C(21)-N(2)	121.3(4)
C(21)-N(2)-C(27)	115.8(4)	C(22)-C(21)-N(2)	119.9(4)
C(21)-N(2)-Mo(1)	109.5(3)	C(23)-C(22)-C(21)	121.3(5)
C(27)-N(2)-Mo(1)	134.1(3)	C(22)-C(23)-C(24)	118.9(5)
C(31)-N(3)-C(37)	117.6(4)	C(22)-C(23)-C(231)	121.2(5)
C(31)-N(3)-Mo(1)	111.8(3)	C(24)-C(23)-C(231)	119.9(5)
C(37)-N(3)-Mo(1)	129.5(3)	C(25)-C(24)-C(23)	121.5(5)
C(41)-N(4)-Mo(1)	178.0(4)	C(24)-C(25)-C(26)	117.8(5)
C(12)-C(11)-C(16)	120.1(5)	C(24)-C(25)-C(251)	121.0(5)
C(12)-C(11)-N(1)	121.8(5)	C(26)-C(25)-C(251)	121.2(5)
C(16)-C(11)-N(1)	118.1(5)	C(21)-C(26)-C(25)	121.7(5)
C(11)-C(12)-C(13)	121.2(5)	N(2)-C(27)-C(28)	111.1(4)
C(14)-C(13)-C(12)	118.6(5)	N(2)-C(27)-C(210)	109.0(4)
C(14)-C(13)-C(131)	121.2(5)	C(28)-C(27)-C(210)	109.3(5)
C(12)-C(13)-C(131)	120.2(5)	N(2)-C(27)-C(29)	109.3(4)
C(13)-C(14)-C(15)	121.0(5)	C(28)-C(27)-C(29)	111.2(6)
C(14)-C(15)-C(16)	119.4(5)	C(210)-C(27)-C(29)	106.8(5)
C(14)-C(15)-C(151)	121.4(5)	C(36)-C(31)-C(32)	118.1(5)
C(16)-C(15)-C(151)	119.2(6)	C(36)-C(31)-N(3)	121.5(5)
C(11)-C(16)-C(15)	119.7(5)	C(32)-C(31)-N(3)	120.4(5)

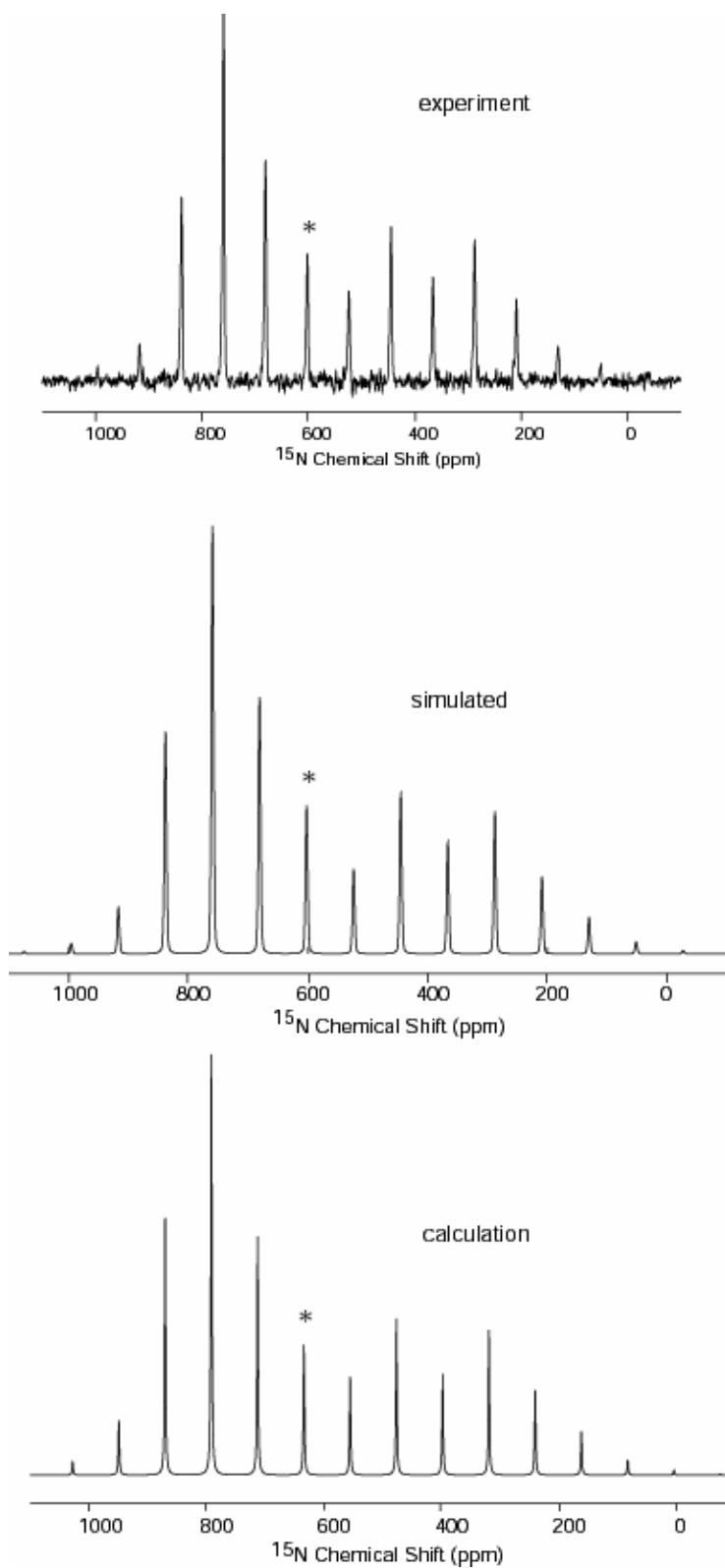
C(33)-C(32)-C(31)	121.7(5)	C(35)-C(36)-C(31)	121.9(5)
C(32)-C(33)-C(34)	118.1(5)	N(3)-C(37)-C(310)	111.6(4)
C(32)-C(33)-C(331)	121.5(6)	N(3)-C(37)-C(38)	107.7(5)
C(34)-C(33)-C(331)	120.4(5)	C(310)-C(37)-C(38)	109.9(5)
C(35)-C(34)-C(33)	121.8(5)	N(3)-C(37)-C(39)	109.9(4)
C(34)-C(35)-C(36)	118.3(5)	C(310)-C(37)-C(39)	109.9(5)
C(34)-C(35)-C(351)	120.1(5)	C(38)-C(37)-C(39)	107.8(5)
C(36)-C(35)-C(351)	121.5(5)		

Appendix 2(a): Representative ^{15}N solid state NMR spectra for Lewis acid complexes (1-LA)

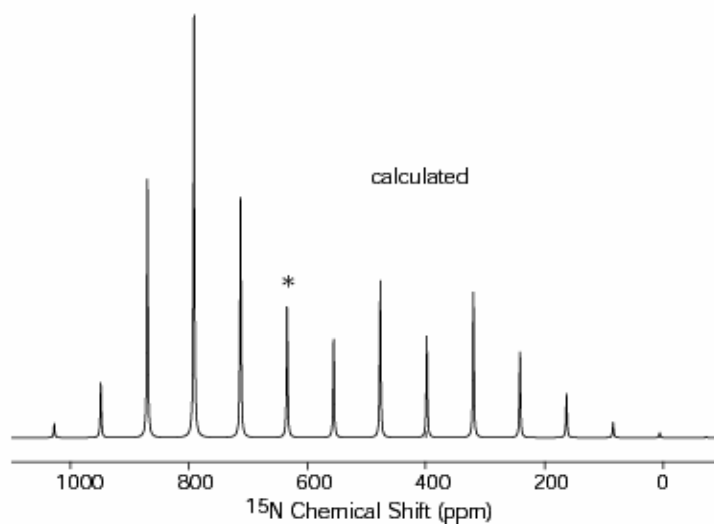
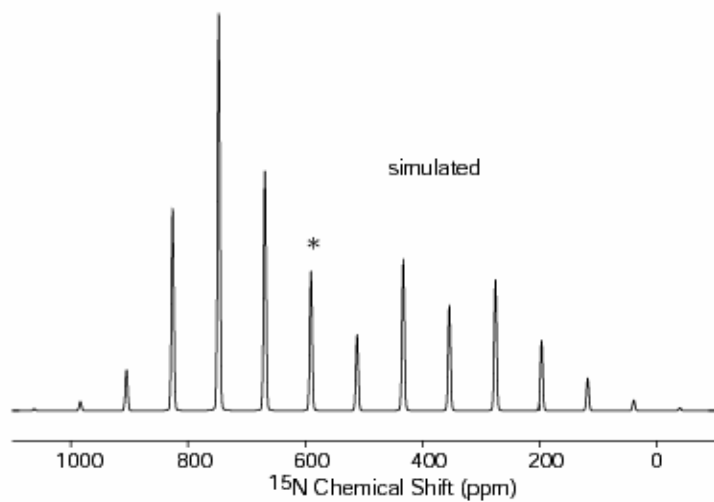
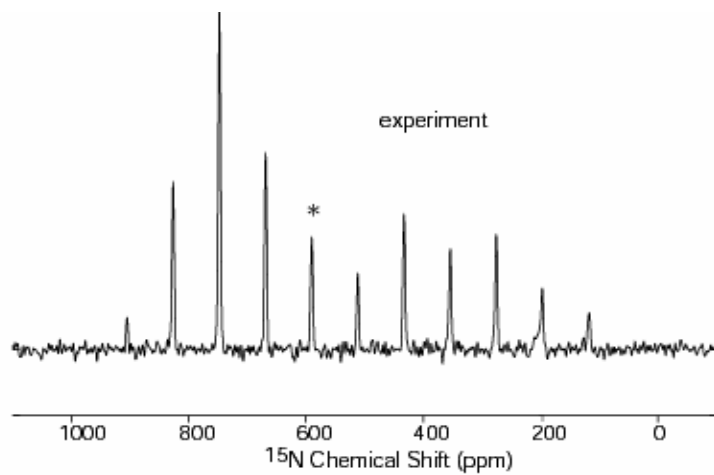
A 2(a).1 Experimental, simulated and calculated ^{15}N CPMAS spectra for $\text{F}_3\text{B}-^{15}\text{NMo}(\text{N}[\text{Bu}]\text{Ar})_3, 1-\text{BF}_3$ (Calculated spectrum of 1m-BF₃)



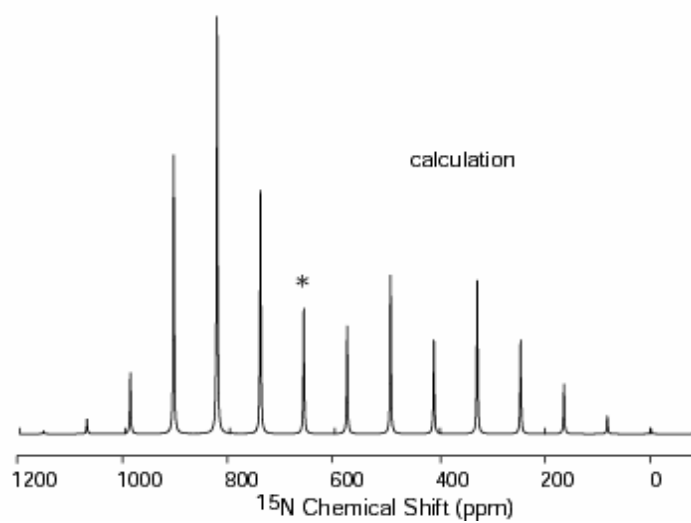
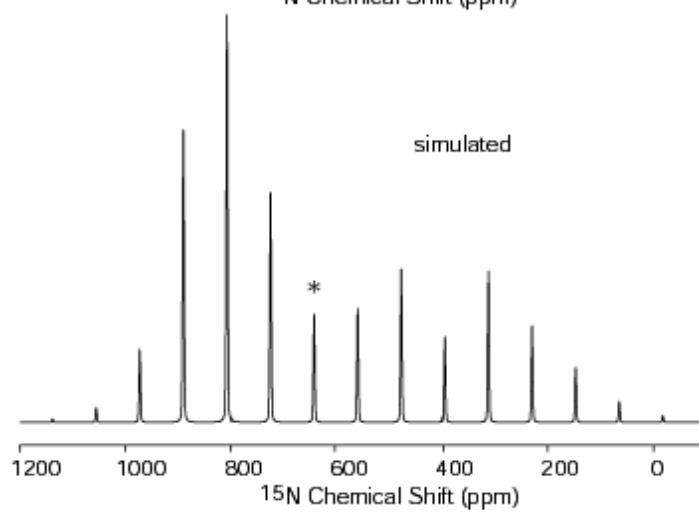
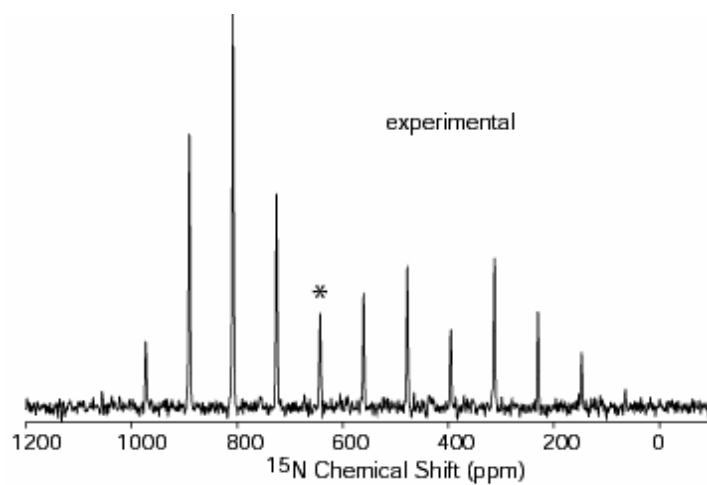
A 2(a).2 Experimental, simulated and calculated ^{15}N CPMAS spectra for $\text{Cl}_3\text{Al}-^{15}\text{NMo}(\text{N}[\text{tBu}]\text{Ar})_3, 1-\text{AlCl}_3$ (Calculated spectrum of $1\text{m}-\text{AlCl}_3$)



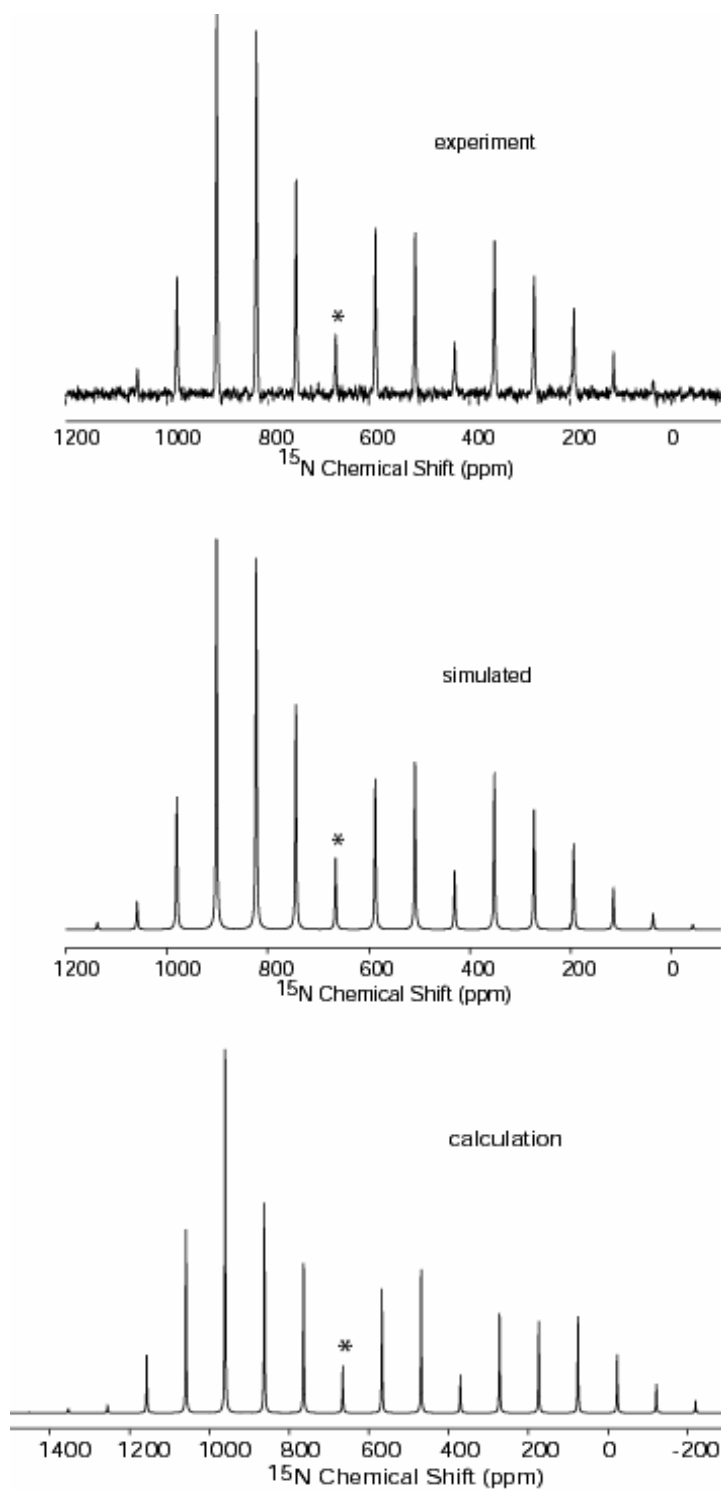
A 2(a).3 Experimental, simulated and calculated ^{15}N CPMAS spectra for $\text{Cl}_3\text{Ga}-^{15}\text{NMo}(\text{N}[\text{tBu}]\text{Ar})_3, 1-\text{GaCl}_3$ (Calculated spectrum of 1m-GaCl_3)



A 2(a).4 Experimental, simulated and calculated ^{15}N CPMAS spectra for $\text{Cl}_2\text{Ge}-^{15}\text{NMo}(\text{N}[\text{Bu}]\text{Ar})_3, 1-\text{GeCl}_2$ (Calculated spectrum of 1m-GeCl_2)

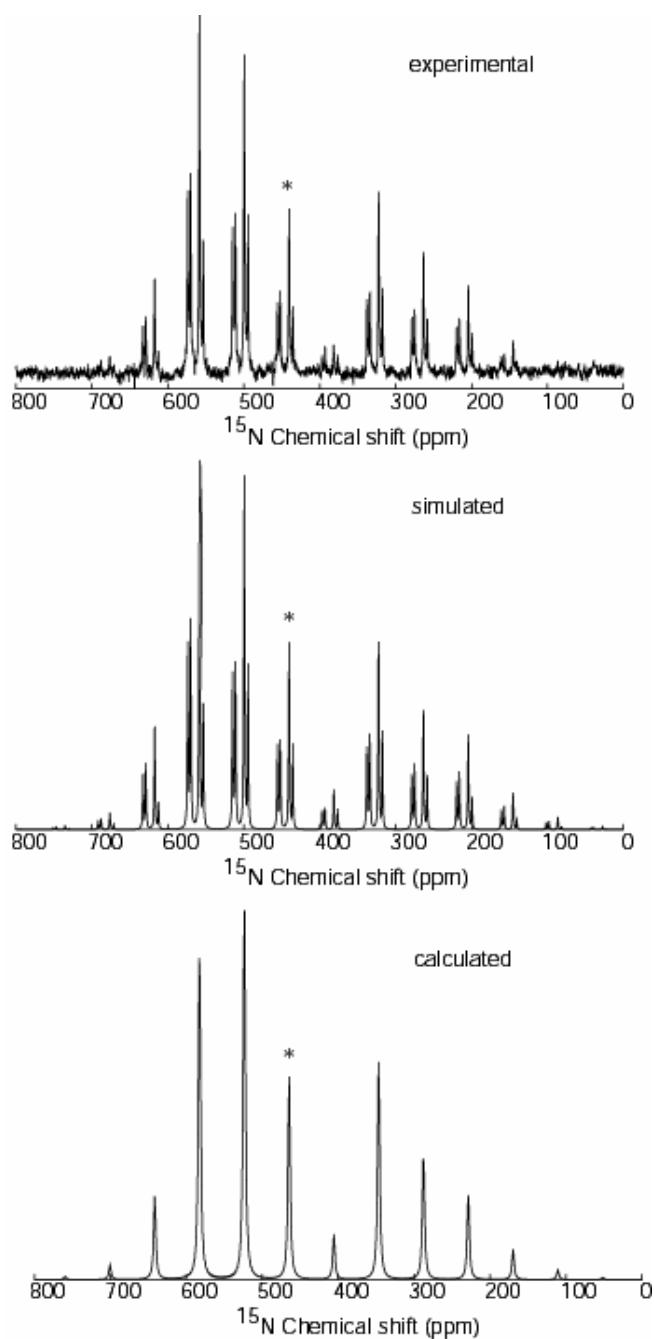


A 2(a).5 Experimental, simulated and calculated ^{15}N CPMAS spectra for $\text{Cl}_2\text{Sn}-^{15}\text{NMo}(\text{N}[\text{tBu}]\text{Ar})_3, 1-\text{SnCl}_2$ (Calculated spectrum of 1m-SnCl_2)

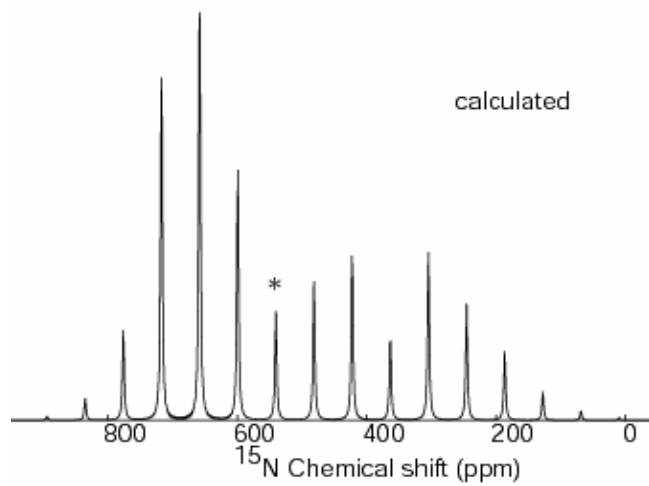
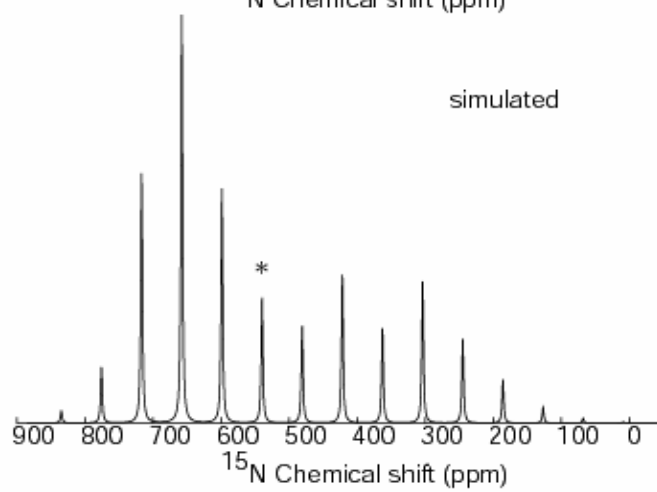
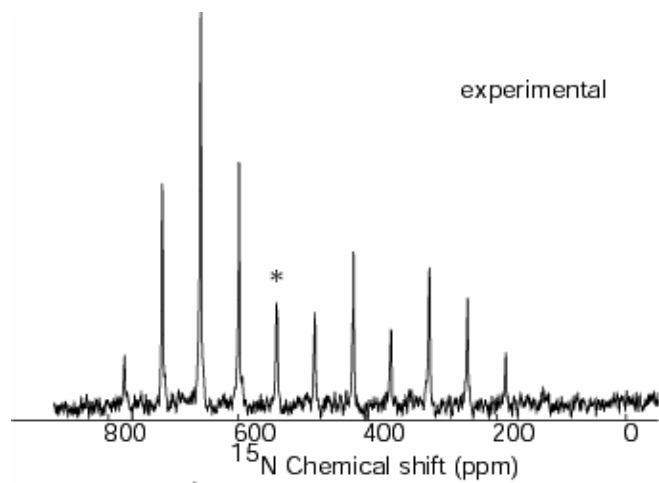


Appendix 2(b): Representative ^{15}N solid state NMR spectra for imido complexes (2)

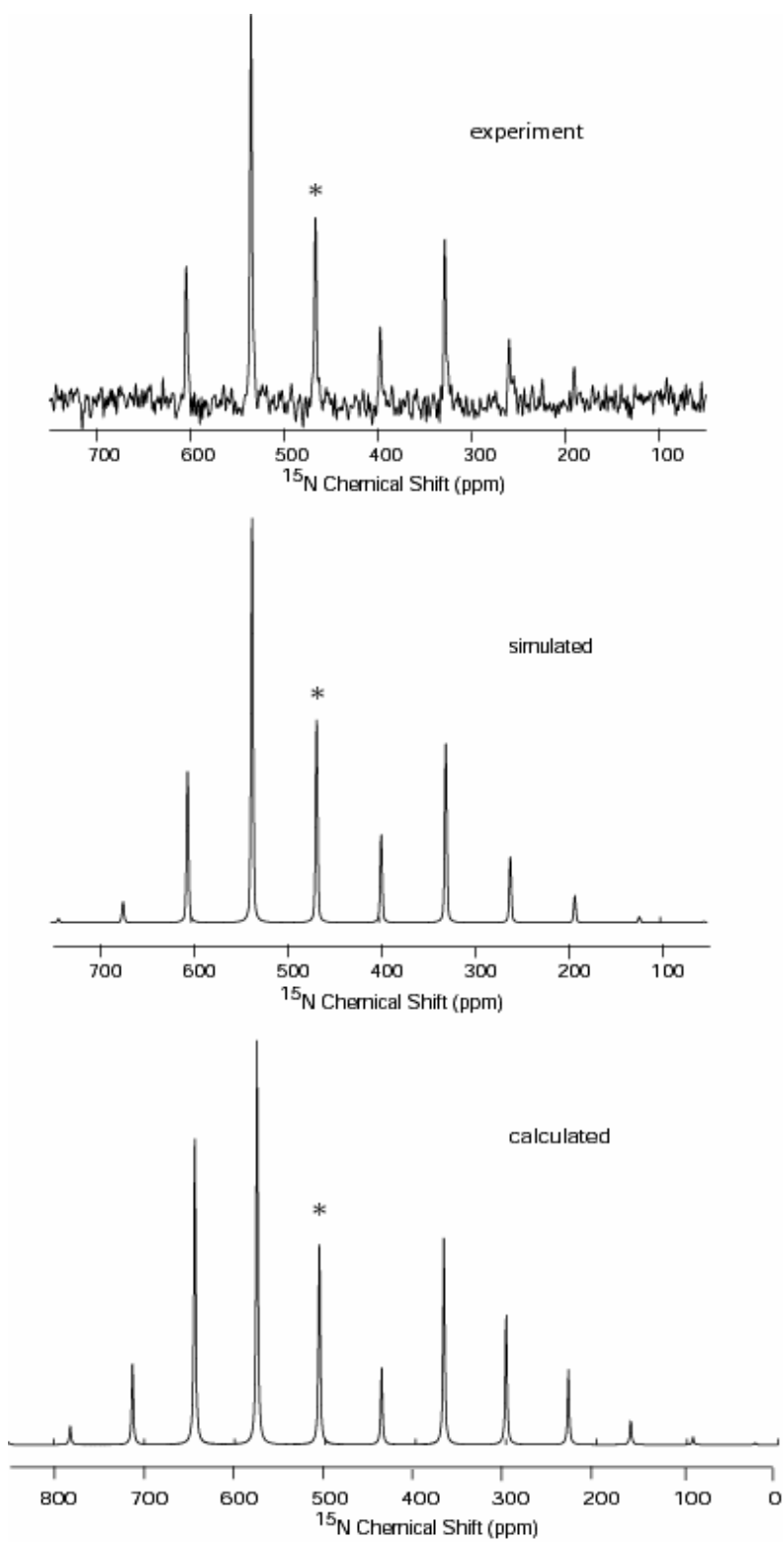
A 2(b).1 Experimental, simulated and calculated ^{15}N CPMAS spectra for $[\text{CH}_3^{15}\text{NMo}(\text{N}[\text{tBu}]\text{Ar})_3\text{I}]$ [2a]I (Calculated spectrum of [2a-m]I)



A 2(b).2 Experimental, simulated and calculated ^{15}N CPMAS spectra for $[(\text{CH}_3)_3\text{Si}^{15}\text{NMo}(\text{N}[\text{tBu}]\text{Ar})_3]\text{OTf}$ [2b]OTf (Calculated spectrum of [2b-m]OTf)



A 2(b).3 Experimental, simulated and calculated ^{15}N CPMAS spectra for $[\text{PhC}(\text{O})^{15}\text{NMo}(\text{N}[\text{tBu}]\text{Ar})_3\text{OTf} [2\text{c}]\text{OTf}$ (Calculated spectrum of $[2\text{c-m}]\text{OTf}$)



Appendix 3: Density Functional Theory Calculations

A 3.1 Representative input file for $^{15}\text{NMo}(\text{NH}_2)_3$, 1-m

```

#! /bin/sh

nohup $ADFBIN/adf <<EOR > adf.out
Title NMo_nh2_3

SYMMETRY nosym

ATOMS
  N      0.000000      0.000000      0.000000
Mo      0.000000      0.000000      1.660000
  N      1.912533      0.000000      2.172462
  N      -0.956267      1.656302      2.172462
  N      -0.956267     -1.656302      2.172462
  H      -1.378108      2.234788      1.462907
  H      -1.021252      1.921025      3.142906
  H      2.624437      0.076083      1.462907
  H      2.174282     -0.076083      3.142906
  H      -1.246329     -2.310871      1.462907
  H      -1.153031     -1.844942      3.142906
END

BASIS
  type TZ2P
  core none
END

GEOMETRY
  sp
END
RELATIVISTIC ZORA SpinOrbit

charge 0

XC
  LDA VWN
  GGA Becke Perdew
END

SCF
  DIIS
END

end input
EOR

```

A 3.2 Optimized geometry for $^{15}\text{NMo}(\text{NH}_2)_3$, 1m

```

N      0.000273     -0.000374      0.011827
Mo     -0.000112      0.000273      1.663469
N      1.904387      0.001685      2.159868

```

N	-0.955178	1.648290	2.159832
N	-0.948821	-1.651117	2.160007
H	-1.338378	2.317686	1.496960
H	-1.111237	1.966529	3.116064
H	2.675064	-0.002888	1.497448
H	2.257033	-0.022920	3.116079
H	-1.337223	-2.317045	1.496870
H	-1.143554	-1.946794	3.116252

A 3.3 Optimized geometry for F₃BNMo(NH₂)₃, 1m-BF₃

N	0.055495	0.007750	-0.002036
Mo	0.014467	0.000346	1.668265
N	-0.938570	-1.633336	2.138379
N	1.890153	0.000863	2.195411
N	-0.941169	1.631122	2.141964
H	-1.307640	2.299598	1.463613
H	-1.127416	1.938423	3.097018
H	2.668475	0.015517	1.537721
H	2.225972	-0.023338	3.158685
H	-1.310270	-2.300994	1.465841
H	-1.142815	-1.925394	3.094738
B	0.121545	0.061459	-1.684336
F	-0.532909	-1.086355	-2.091417
F	-0.541676	1.230918	-2.011937
F	1.470440	0.074212	-1.970352

A 3.4 Optimized geometry for Cl₃BNMo(NH₂)₃, 1m-BCl₃

N	1.856833	0.013810	2.142056
Mo	-0.025622	0.000975	1.658484
N	-0.003417	0.013894	-0.022729
B	0.017057	0.023563	-1.575637
Cl	-0.852866	-1.528951	-2.085917
N	-0.958547	-1.647112	2.095398
N	-0.992537	1.622956	2.120111
Cl	-0.884369	1.563417	-2.068912
Cl	1.809448	0.044282	-2.039936
H	-1.195106	1.932316	3.071591
H	-1.365918	2.277411	1.433577
H	2.216841	0.010418	3.097216
H	2.616805	0.027227	1.462452
H	-1.152840	-1.975766	3.042116
H	-1.320506	-2.297174	1.398619

A 3.5 Optimized geometry for Cl₂GeNMo(NH₂)₃, 1m-GeCl₂

N	-0.022949	-0.004136	-0.088800
Mo	0.011369	-0.063509	1.579132
Ge	-0.069608	0.046318	-2.251946
N	1.913421	-0.072831	2.000406
N	-0.918341	1.539364	2.211796
N	-0.911241	-1.720499	2.030103
H	2.645265	-0.078075	1.288222
H	2.312484	-0.117016	2.937949

H	-1.337200	2.259385	1.627844
H	-1.045218	1.765189	3.199206
H	-1.273365	-2.376245	1.336611
H	-1.057547	-2.071485	2.976756
Cl	2.181962	-0.284597	-2.370218
Cl	-0.859892	-2.083020	-2.393800

A 3.6 Optimized geometry for $\text{Cl}_2\text{SnNMo}(\text{NH}_2)_3$, 1m-SnCl₂

N	-0.038458	-0.011444	-0.015785
Mo	0.011478	-0.061378	1.650534
Sn	-0.100824	0.100367	-2.364838
N	1.917010	-0.065721	2.057303
N	-0.921311	1.547179	2.265199
N	-0.899743	-1.720955	2.118474
H	2.639607	-0.076642	1.341929
H	2.323608	-0.107213	2.991527
H	-1.347381	2.252689	1.665470
H	-1.046961	1.793486	3.247350
H	-1.259866	-2.376183	1.430648
H	-1.039955	-2.071784	3.065891
Cl	2.321613	-0.285994	-2.393610
Cl	-0.933213	-2.205652	-2.451313

A 3.7 Optimized geometry for $[\text{CH}_3\text{NMo}(\text{NH}_2)_3]^+$, [2a-m]

N	-0.013631	0.027029	0.068536
Mo	0.006004	-0.005736	1.768658
N	-0.882425	1.603491	2.358478
N	1.872727	-0.052408	2.256183
N	-0.946544	-1.609842	2.262356
C	-0.008810	0.015270	-1.364944
H	-0.550994	-0.870484	-1.725931
H	-0.498680	0.923492	-1.743952
H	1.028584	-0.018969	-1.727635
H	2.664490	-0.066032	1.613458
H	2.200365	-0.065857	3.225793
H	-1.282964	2.340504	1.779276
H	-1.005327	1.824483	3.351333
H	-1.359898	-2.289497	1.623846
H	-1.103059	-1.892110	3.233608

A 3.8 Optimized geometry for $[(\text{CH}_3)_3\text{SiNMo}(\text{NH}_2)_3]^+$, [2b-m]

N	0.0017	0.0017	0.0057
N	-0.9267	-1.6058	2.2509
N	1.8538	-0.0001	2.2522
N	-0.9277	1.6053	2.2515
Mo	0.0001	0.0001	1.7022
H	-1.3360	2.2976	1.6245
H	-1.0637	1.8820	3.2267
H	2.6580	0.0080	1.6258
H	2.1607	-0.0230	3.2275
H	-1.3218	-2.3060	1.6242
H	-1.0990	-1.8612	3.2261

H	1.9097	0.0327	-3.3935
H	2.3403	0.9130	-1.9134
H	2.3443	-0.8748	-1.9311
H	-0.9233	-1.6196	-3.4186
H	-0.3792	-2.4560	-1.9505
H	-1.9282	-1.5635	-1.9566
H	-0.9407	1.6589	-3.3947
H	-1.9360	1.5828	-1.9268
H	-0.3893	2.4797	-1.9207
Si	0.0087	0.0125	-1.8270
C	-0.8912	-1.5567	-2.3193
C	-0.9013	1.5832	-2.2964
C	1.8240	0.0216	-2.2953

A 3.9 Optimized geometry for $[\text{PhC}(\text{O})\text{NMo}(\text{NH}_2)_3]^+$, [2c-m]

N	0.006488	-0.031329	-0.031230
Mo	-0.046566	0.010830	1.673002
N	-1.020312	1.599339	2.155442
N	-0.935293	-1.602091	2.234423
N	1.799633	0.078068	2.245918
H	-1.399579	2.291733	1.506786
H	-1.176526	1.888064	3.125143
H	-1.273449	-2.326754	1.599284
H	-1.206577	-1.811033	3.198749
H	2.597641	0.254694	1.635004
H	2.098413	0.034847	3.223086
O	-0.808032	0.522041	-2.098564
C	0.041318	-0.097053	-1.506359
C	1.120792	-0.929996	-2.050439
C	1.197294	-1.041195	-3.453566
C	2.205645	-1.805356	-4.028301
C	3.145352	-2.453397	-3.217204
C	3.071785	-2.349041	-1.824411
C	2.058087	-1.597985	-1.238761
H	0.462881	-0.524447	-4.067591
H	2.264188	-1.896159	-5.111712
H	3.937463	-3.044539	-3.672437
H	3.802447	-2.854809	-1.196411
H	1.996506	-1.530713	-0.153598

A 3.10 Optimized geometry for $\text{H}_2\text{CNMo}(\text{N}[\text{CH}_3]\text{Ph})_3$, 3m-C₃

C	-0.077798	-0.257055	-0.038200
C	-0.031999	-0.266111	1.357612
C	1.196032	-0.215979	2.022227
C	2.397091	-0.137091	1.296317
C	2.341596	-0.145010	-0.108812
C	1.114180	-0.203656	-0.769349
N	3.649450	-0.024830	1.976530
C	4.408522	-1.266709	2.125422
H	3.783652	-2.060915	2.572254
H	-0.953355	-0.307249	1.934987
H	1.085788	-0.194670	-1.857172
Mo	4.196791	1.793376	2.566630
N	3.906512	3.338402	1.351623

C	2.678616	4.053519	1.492425
C	2.655306	5.338405	2.073518
C	1.452262	6.012970	2.264934
C	0.242117	5.424285	1.879087
C	0.254899	4.157211	1.294443
C	1.460779	3.477763	1.095909
H	1.456683	6.999378	2.728970
H	-0.678053	3.693222	0.976784
C	4.972265	4.071132	0.655715
H	5.849984	3.427178	0.572071
H	5.272142	4.996058	1.169654
H	4.635766	4.344882	-0.357539
N	3.946981	2.304822	4.453100
C	2.687282	1.915718	5.012771
C	1.515200	2.633063	4.726838
C	0.280895	2.199749	5.219961
C	0.201841	1.059652	6.021163
C	1.369400	0.351176	6.331218
C	2.599806	0.774752	5.833550
H	-0.618805	2.764296	4.979452
H	1.317429	-0.540888	6.954515
C	4.884392	2.935050	5.384884
H	5.063941	2.314298	6.277737
H	5.839980	3.102506	4.876756
H	4.491828	3.908252	5.727739
N	5.974661	1.703245	2.544632
C	7.270734	1.601269	2.578634
H	5.269914	-1.095308	2.783988
H	4.784256	-1.634983	1.152866
H	3.589806	5.792541	2.401914
H	7.893169	2.487155	2.736733
H	-0.697735	5.954755	2.029670
H	1.578281	3.532683	4.114427
H	7.756901	0.631275	2.435788
H	3.508289	0.213250	6.053851
H	1.467995	2.498356	0.618149
H	-0.760666	0.722790	6.406168
H	1.237377	-0.221393	3.112327
H	3.272657	-0.078260	-0.671586
H	-1.036140	-0.288964	-0.555934

A 3.11 Optimized geometry for $\text{H}_2\text{CNMo}(\text{N}[\text{CH}_3]\text{Ph})_3$, 3m- C_s

N	0.0150	-0.2453	0.1226
N	-0.6464	1.3580	-2.2606
N	-0.0782	-1.8161	-2.3580
N	2.4391	0.2599	-1.7866
C	0.0065	-0.2773	1.4173
C	-0.4002	1.8949	-3.6083
C	-1.7724	1.9172	-1.5765
C	-1.5803	2.9769	-0.6789
C	-2.6575	3.5174	0.0232
C	-3.9461	3.0113	-0.1647
C	-4.1476	1.9667	-1.0716
C	-3.0696	1.4254	-1.7759
C	-1.1195	-2.6814	-1.7854

C	0.1379	-1.9925	-3.7671
C	1.3452	-2.5334	-4.2386
C	1.5752	-2.6874	-5.6076
C	0.6032	-2.3018	-6.5338
C	-0.6067	-1.7715	-6.0776
C	-0.8407	-1.6237	-4.7097
C	3.4590	-0.7907	-1.7309
C	2.9031	1.5991	-1.8239
C	3.8055	2.0443	-2.8105
C	4.1895	3.3837	-2.8681
C	3.6873	4.3097	-1.9477
C	2.8060	3.8747	-0.9555
C	2.4272	2.5336	-0.8857
H	0.9295	-0.1563	1.9955
H	-0.9359	-0.4230	1.9558
H	0.4598	1.3821	-4.0634
H	-1.2708	1.7536	-4.2698
H	-0.1648	2.9699	-3.5652
H	-2.4905	4.3355	0.7241
H	-5.1508	1.5632	-1.2313
H	-1.1224	-2.5531	-0.6992
H	-2.1267	-2.4405	-2.1654
H	-0.9137	-3.7369	-2.0239
H	-1.3697	-1.4643	-6.7925
H	2.5170	-3.1145	-5.9525
H	2.9711	-1.7583	-1.5649
H	4.0356	-0.8644	-2.6667
H	4.1647	-0.6170	-0.9023
H	2.4235	4.5785	-0.2164
H	4.8767	3.7105	-3.6485
H	3.9861	5.3557	-2.0000
H	1.7695	2.1853	-0.0885
H	4.1828	1.3394	-3.5512
H	2.0984	-2.8397	-3.5148
H	-1.7846	-1.2072	-4.3586
H	0.7873	-2.4125	-7.6017
H	-4.7859	3.4277	0.3925
H	-0.5715	3.3610	-0.5359
H	-3.2246	0.6057	-2.4784
Mo	0.4881	-0.0833	-1.6129

A 3.12 Optimized geometry for $[\text{CH}_3\text{CH}_2\text{NMo}(\text{NH}_2)_3]^+$, [2d-m]

N	1.828992	0.014545	2.192469
Mo	-0.024516	0.002681	1.649339
N	-0.975190	1.599082	2.175734
N	-0.000183	0.024315	-0.050127
C	0.018116	0.022853	-1.493189
N	-0.945444	-1.621518	2.144071
H	-1.143728	1.850535	3.153539
H	-1.372914	2.303171	1.554912
H	2.125367	0.004047	3.172005
H	2.641797	0.032342	1.575949
H	-1.111932	-1.893430	3.116751
H	-1.328375	-2.321985	1.510154
H	0.168822	1.065735	-1.816932

=== INFO:

The paramagnetic shielding results from currents induced by the external magnetic field, which re-enforce the external magnetic field.

--- REF: H. Fukui Mag. Res. Rev. 11 (1987) 205.

=====
 === PARAMAGNETIC NMR SHIELDING TENSORS (ppm)

===	paramagnetic b ⁽¹⁾ tensor	===	paramagnetic u ⁽¹⁾ tensor
-----	-----	-----	-----
	0.000 0.000 0.000		-1270.704 2.012 -0.185
	0.000 0.000 0.000		2.012 -1270.776 0.437
	0.000 0.000 0.000		-0.185 0.437 -240.799
-----	-----	-----	-----
	isotropic shielding = 0.000		isotropic shielding = -927.426
===	paramagnetic s ⁽¹⁾ tensor	===	paramagnetic gauge tensor
-----	-----	-----	-----
	45.776 0.047 -0.008		3.678 0.003 -0.001
	0.047 45.764 -0.007		0.003 3.677 -0.001
	-0.008 -0.007 -3.937		-0.001 -0.001 -0.084
-----	-----	-----	-----
	isotropic shielding = 29.201		isotropic shielding = 2.423

 CARTESIAN AXIS REPRESENTATION

==== total paramagnetic tensor

-----	-----	-----	-----
	-1221.250	2.062	-0.194
	2.062	-1221.335	0.428
	-0.194	0.428	-244.820
-----	-----	-----	-----

isotropic shielding = -895.802

 PRINCIPAL AXIS REPRESENTATION

==== Shieldings:

	-1223.356	-1219.230	-244.820
--	-----------	-----------	----------

==== Principal Axis System:

	0.700	0.714	0.000
	-0.714	0.700	0.000
	0.000	0.000	1.000
-----	-----	-----	-----

=== INFO:

When an external magnetic field interacts with electron density, it induces electronic currents to flow. The currents produce a magnetic field. This induced magnetic field may re-enforce the external magnetic field, or reduce it.

=== INFO:

The diamagnetic shielding results from currents induced by the external magnetic field, which reduce the external magnetic field.

--- REF: H. Fukui

Mag. Res. Rev. 11 (1987) 205.

=====
 === DIAMAGNETIC NMR SHIELDING TENSORS (ppm)

===	diamagnetic core tensor	===	diamagnetic valence tensor
-----	-----	-----	-----
	0.000 0.000 0.000		316.865 -0.012 -0.008

0.000	0.000	0.000	-0.012	316.870	0.013
0.000	0.000	0.000	-0.008	0.013	350.242

isotropic shielding = 0.000 isotropic shielding = 327.992

 CARTESIAN AXIS REPRESENTATION

==== total diamagnetic NMR tensor

316.865	-0.012	-0.008
-0.012	316.870	0.013
-0.008	0.013	350.242

isotropic shielding = 327.992

PRINCIPAL AXIS REPRESENTATION

==== Shieldings:

316.856 316.879 350.242

==== Principal Axis System:

0.787	0.616	0.000
0.616	-0.787	0.000
0.000	0.000	1.000

==== TOTAL NMR SHIELDING TENSOR (ppm)

 CARTESIAN AXIS REPRESENTATION

==== total shielding tensor

-904.386	2.051	-0.202
2.051	-904.465	0.441
-0.202	0.441	105.422

isotropic shielding = -567.809

PRINCIPAL AXIS REPRESENTATION

==== Shieldings:

-906.477 -902.374 105.423

==== Principal Axis System:

0.700	0.714	0.000
-0.714	0.700	0.000
0.000	0.000	1.000

*** MO ANALYSIS OF CONTRIBUTIONS TO U⁽¹⁾

==== INFO:

Calculations reveal that in general the paramagnetic shielding is very sensitive to electronic changes within the molecule. The magnitude of the paramagnetic shielding is largely dependent on the components of the u⁽¹⁾ matrix. These components are proportional to the coupling of occupied and virtual orbitals by the magnetic field, and inversely proportional to the energy difference between these orbitals.

Following, a simple orbital picture is presented, then a table.

The orbital picture includes the LUMO, HOMO and HOMO-LUMO GAP (HLG). In the table that follows, $k = 1, 2, 3$ is the magnetic field component, "vir" is the virtual orbital number, "occ" is the occupied orbital number, "sym" is the representation, "cmp" is the component of the representation, " $\langle M_k \rangle$ " is the coupling due to the k -th component of the magnetic field, " $e(\text{vir})-e(\text{occ})$ " is the energy difference, and "ulk~" is $\frac{1}{2} \langle M_k \rangle / [e(\text{vir})-e(\text{occ})]$, which is the main contribution to " $u^{\wedge}(1)$ ". Note that " $\langle M_k \rangle = \langle \text{vir} | [r_{\mu}] \times \text{grad}]_k | \text{occ} \rangle$ ". Only the five major components are listed.

--- REF: G. Schreckenbach
Relativity and Magnetic Properties. A Density Functional Study
Ph.D. Thesis 1996.

--- REF: Y. Ruiz-Morales
The Calculation and Interpretation of NMR Chemical Shifts
in Compounds of Transition Metals and Heavy Elements
Ph.D. Thesis 1997.

--- REF: J. Gerratt and I. M. Mills
J. Chem. Phys. 49 (1968) 1719.

MO	ENERGY (eV)
243 nmo	*****
39 LUMO	-1.904
	HLG ---> 3.847
38 HOMO	-5.751
1 1	-20282.190

k	R/I	vir (sym,cmp)	occ (sym,cmp)	ulk~	$\langle M_k \rangle$	$e(\text{vir})-e(\text{occ})$
1	real	39 (A , 39)	35 (A , 35)	-0.160151D+01	-0.587081D+00	4.988
1	real	42 (A , 42)	35 (A , 35)	0.119527D+01	0.554337D+00	6.310
1	real	44 (A , 44)	34 (A , 34)	0.115709D+01	0.623591D+00	7.332
1	real	42 (A , 42)	33 (A , 33)	-0.565803D+00	-0.282290D+00	6.788
1	real	43 (A , 43)	34 (A , 34)	0.565710D+00	0.282214D+00	6.787
2	real	40 (A , 40)	35 (A , 35)	-0.159751D+01	-0.586057D+00	4.991
2	real	43 (A , 43)	35 (A , 35)	0.119477D+01	0.554200D+00	6.311
2	real	44 (A , 44)	33 (A , 33)	-0.115721D+01	-0.623804D+00	7.334
2	real	42 (A , 42)	34 (A , 34)	0.564095D+00	0.281364D+00	6.786
2	real	43 (A , 43)	33 (A , 33)	0.562078D+00	0.280476D+00	6.789
3	real	39 (A , 39)	31 (A , 31)	-0.113197D+01	-0.655671D+00	7.881
3	real	40 (A , 40)	32 (A , 32)	-0.113023D+01	-0.654847D+00	7.883
3	real	39 (A , 39)	33 (A , 33)	-0.832438D+00	-0.334410D+00	5.466
3	real	40 (A , 40)	34 (A , 34)	-0.831574D+00	-0.334184D+00	5.468
3	real	42 (A , 42)	37 (A , 37)	0.626748D+00	0.280671D+00	6.093

A 3.14 Generation of spectra from calculated chemical shielding tensors

Generation of spectra from calculated values of the chemical shielding tensor was achieved using the Simpson program. A representative input file is included below. 'Shift 1' values are taken from the calculated shielding tensors; '448p' being the calculated isotropic shift (δ_{iso}); '-130p' the reduced anisotropy ($\delta_{33}-\delta_{\text{iso}}$) and '0.3553' being the asymmetry ($[\delta_{11}-\delta_{22}]/\delta_{33}$). 'Spin rate' and line broadening (faddlb) must be set according to those used in acquisition of the experimental spectrum to which the

calculated values are being compared. Two output files are created (calc.fid and calc.spe) upon successful simulation of the desired spectrum.

```
# MAS CSA spectrum
# Uses the gcompute method

spinsys {
  nuclei 15N
  channels 15N
  shift 1 448p -130p 0.3553 0 0 0 0
}

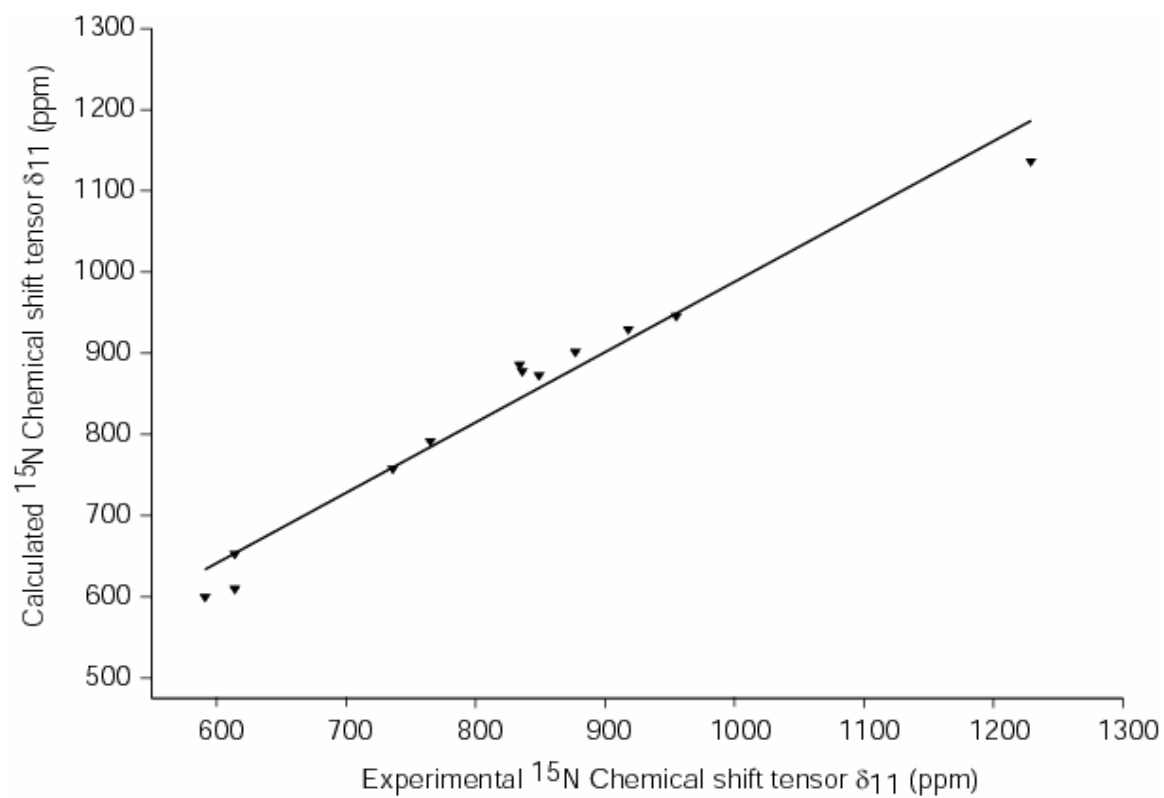
par {
  method          gcompute
  start_operator  Inx
  detect_operator Inp
  spin_rate       3500
  gamma_angles   40
  sw             gamma_angles*spin_rate
  crystal_file   rep168
  np             2048
  proton_frequency 501e6
}

proc pulseseq {} {
  maxdt 1
  delay 9999
}

proc main {} {
  global par

  set f [fsimpson]
  fsave $f calc.fid
  fzerofill $f 4096
  fadddb $f 100 0
  fft $f
  fsave $f calc.spe
}
```


A 3.15 Plot of the Experimental ^{15}N chemical shift tensor (δ_{11}) (ppm) versus calculated ^{15}N chemical shift tensor (δ_{11}) (ppm).



Appendix 4: GC-MS data

File : D:\DATA\CUMMINS\SES\269_2.D
Operator : emma
Acquired : 24 May 2004 15:29 using AcqMethod EMMA
Instrument : Instrumen
Sample Name: 269_2
Misc Info :
Vial Number: 1

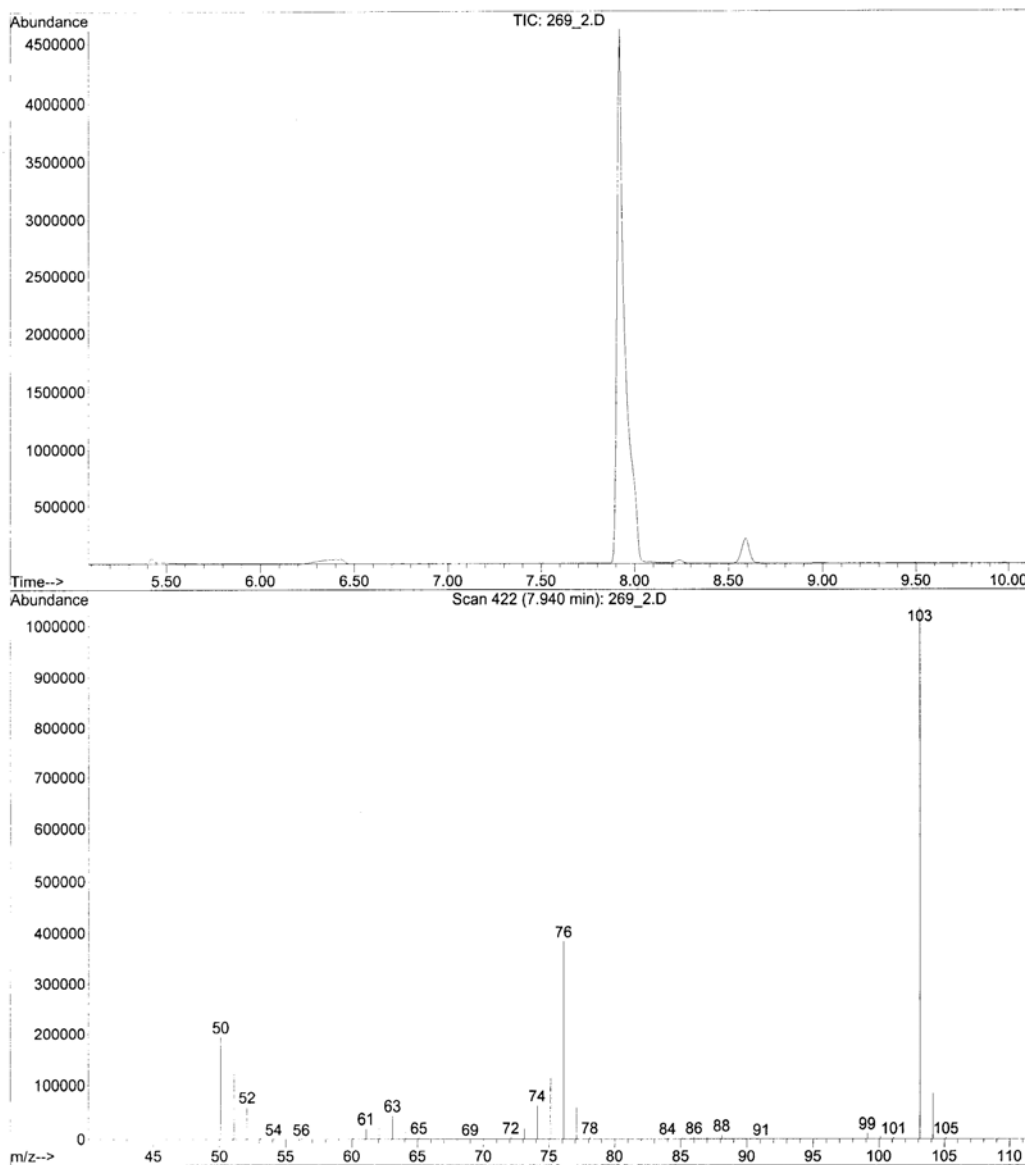


Figure 1. GC-MS chromatogram collected for a 0.017 mM solution of PhCN^{14} in C_6D_6 (top) and the ion fragment spectrum for the signal at retention time 7.940 min assigned to $[\text{PhCN}^{14}]^+$ (bottom).

File : D:\DATA\CUMMINS\SES\270.D
Operator : emma
Acquired : 24 May 2004 15:58 using AcqMethod EMMA
Instrument : Instrumen
Sample Name: 270
Misc Info : IIIexpt270 Mgketimide TFAA
Vial Number: 1

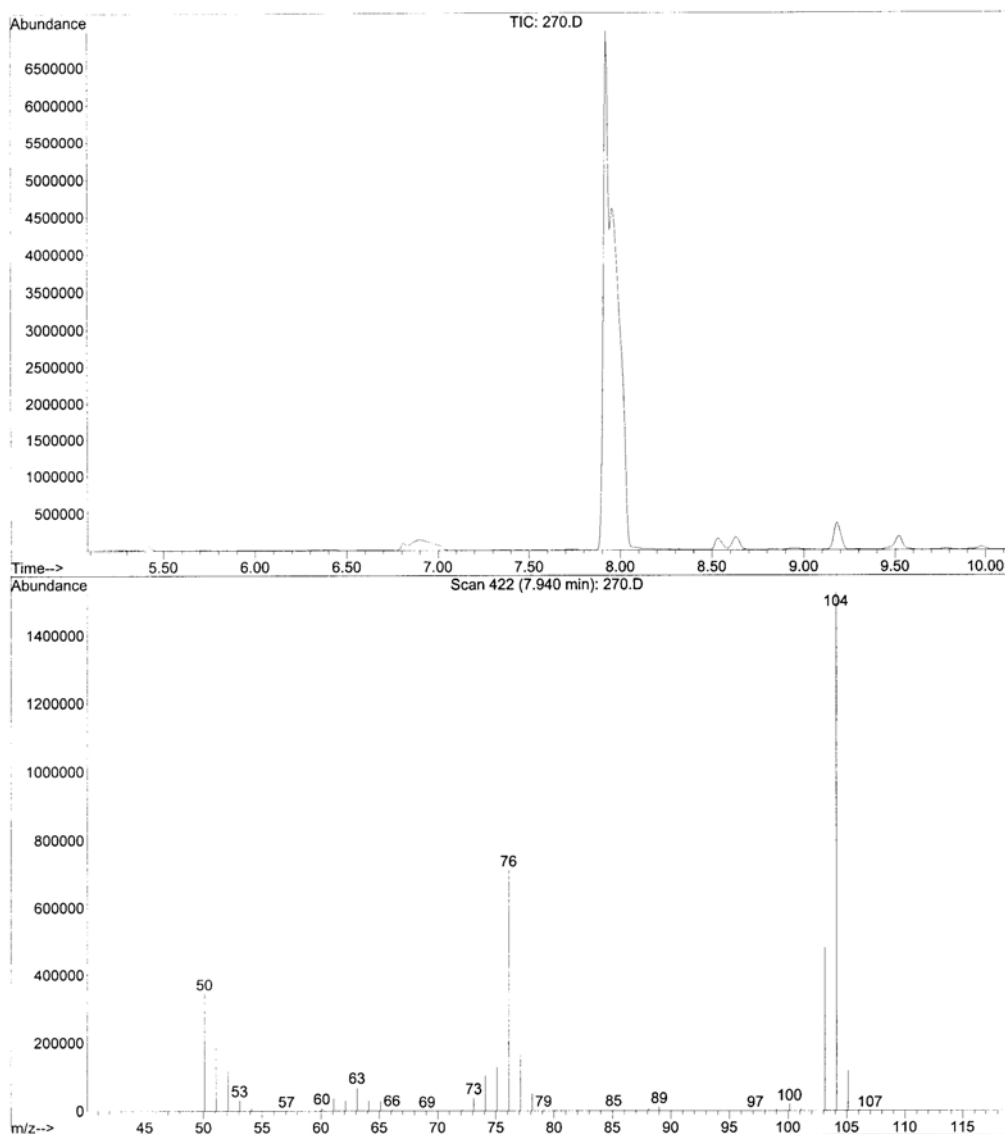


Figure 2. GC-MS chromatogram of the crude product mixture (diluted in 1.5 mL C_6D_6) isolated upon reaction of complex $[3]_2Mg(THF)_2$ with TFAA (top) and the ion fragment spectrum for the signal at retention time 7.940 min assigned to $[PhCN^{15}]^+$ (bottom).

Appendix 5: Synthesis of H₂TTP, (TTP)Li₂(OEt)₂ and (TTP)TiCl

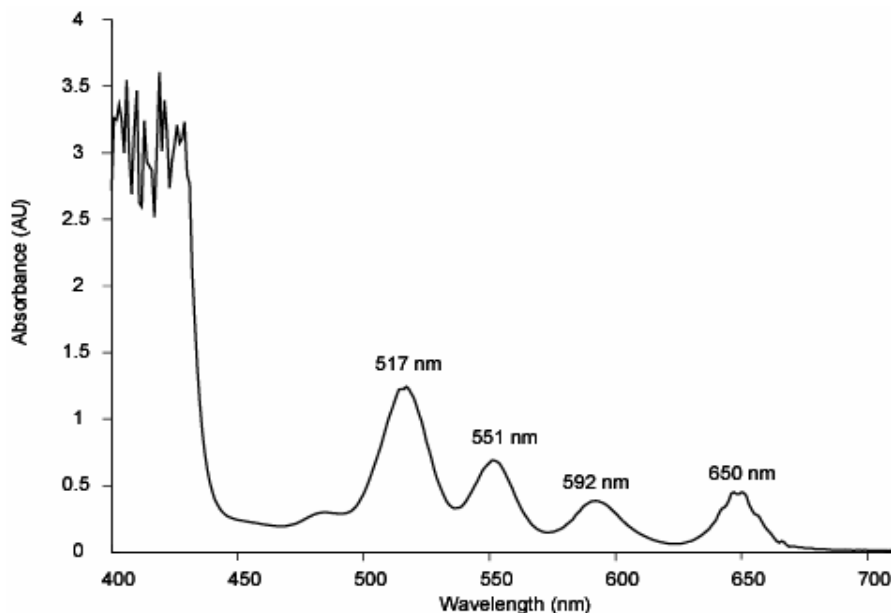
A 5.1: Synthesis, purification and characterization of H₂TTP

The procedure used in the preparation of tetratolylporphyrin (H₂TTP) was identical to that provided for the synthesis of tetraphenylporphyrin (H₂TPP) by Adler et al.¹ with the exception that tolualdehyde was used in place of benzaldehyde.

The purification of H₂TTP is necessary to effect the removal of small amounts of tetratolylchlorin (TTC) from the porphyrin product. Purification was carried out using the procedure developed by Rousseau and Dolphin for the purification of H₂TPP². In this procedure 1 g of H₂TPP is refluxed for 30 min in toluene (500 mL) in the presence of 0.5 g sodium dithionite. An aqueous work-up follows and isolation of the pure H₂TPP is achieved by recrystallization from CH₂Cl₂/methanol. Attempts to scale-up the purification (using *ca.* 3 g of H₂TTP in 1 L toluene) failed and the procedure was determined to be sensitive to the volume of solvent vs. porphyrin used in the reflux step.

H₂TTP ¹H NMR (300 MHz, C₆D₆, 20 °C) δ: 8.87 (s, 8 H, pyrrole), 8.11 (d, 8 H, ortho), 7.56 (d, 8 H, meta), 2.72 (s, 12 H, -CH₃), -2.76 (s, 2 H, NH).

UV-visible spectrum of purified H₂TTP (toluene):



¹ Adler, A. D.; Longo, F. R.; Finarelli, J. D.; Goldmacher, J.; Assour, J.; Korsakoff, L. *J. Org. Chem.* **1967**, *32*, 476.

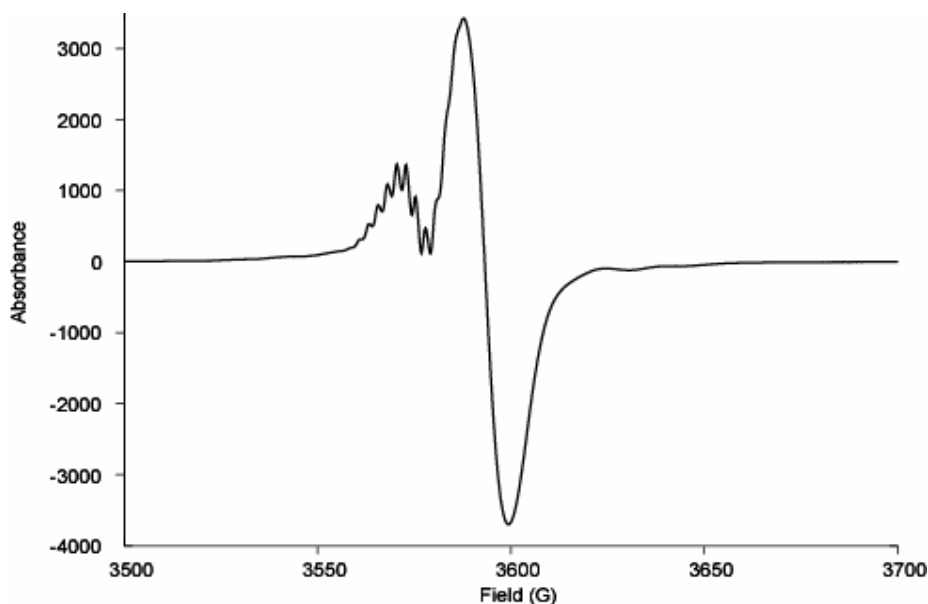
² Rousseau, K.; Dolphin, D. *Tetrahedron Lett.* **1974**, *48*, 4251.

^1H NMR data for a variety of para-substituted tetraphenylporphyrins are listed in an article by Falvo, Mink and Marsh³.

A 5.2: Synthesis of $(\text{TTP})\text{Li}_2(\text{OEt}_2)_2$ and $(\text{TTP})\text{TiCl}$

Synthesis of early transition metal porphyrin complexes is commonly achieved by the reaction of an alkali metal porphyrin complex with a suitable metal halide precursor. One of the first examples of a well-characterized alkali metal porphyrin complex was provided by Arnold in the synthesis of a dilithium salt of octaethylporphyrin $[\text{Li}(\text{THF})_4][\text{Li}(\text{oep})]$.⁴ The application of this procedure in the synthesis of a lithium-TTP complex has been reported⁵ however, the poor solubility of $(\text{THF})_2\text{Li}_2(\text{TTP})$ in common organic solvents forces the use of long reaction times and high temperatures in the preparation of most transition metal porphyrin complexes. Preparation of the etherate complex $(\text{TTP})\text{Li}_2(\text{OEt}_2)_2$ was reported in 1994 by Arnold et al.⁶ The authors point out that the “solubility properties of $(\text{TTP})\text{Li}_2(\text{OEt}_2)_2$ allows metalation reactions to be performed in Et_2O or hexanes at room temperature...” In agreement with this data we found the synthesis of $(\text{TTP})\text{TiCl}$ was readily achieved upon stirring a toluene (20 mL) solution of $(\text{TTP})\text{Li}_2(\text{OEt}_2)_2$ (0.91 g, 1.09 mmol) and $\text{TiCl}_3\cdot\text{THF}_3$ (0.416 g, 1.12 mmol) for 17 h at 25 °C. Filtration of the toluene solution through Celite followed by the removal of solvent *in vacuo* afforded $(\text{TTP})\text{TiCl}$ as a purple powder: 0.52 g (0.687 mmol, 63 %). ^1H NMR (300 MHz, C_6D_6 , 20 °C) δ : 2.36 (s, 12 H, tolyl CH_3)

EPR spectrum of $(\text{TTP})\text{TiCl}$ (toluene, 25 °C):



³ Falvo, R. E.; Mink, L. M.; Marsh, D. F. *J. Chem. Ed.* **1999**, 76, 237.

⁴ Arnold, J. *Chem. Commun.* **1990**, 976.

⁵ Berreau, L. M.; Hays, J. A.; Young, V. G.; Woo, L. K. *Inorg. Chem.* **1994**, 33, 105.

⁶ Brand, H.; Capriotti, J. A.; Arnold, J. *Inorg. Chem.* **1994**, 33, 4334. Full characterization of $(\text{TTP})\text{Li}_2(\text{OEt}_2)_2$ is provided in the experimental section of this paper.

Emma L. Sceats

Curriculum Vitae

EDUCATION

MASSACHUSETTS INSTITUTE of TECHNOLOGY, Cambridge, MA USA (Sept 2002-June 2004). Masters degree in Synthetic Inorganic Chemistry

Holder of the Robert T. Haslam Presidential Graduate Fellowship (2002-03). Teaching Assistant (Sept 2002-Feb 2003). Research under the guidance of Professor Christopher Cummins commenced December 2002. The primary focus of my research has been investigations of the reactivity of a dinitrogen-derived terminal nitride of molybdenum. The potential of this complex to serve as a platform in N-atom transfer reactions has been studied. Standard analytical techniques such as multinuclear NMR (^1H , ^{13}C , ^{31}P , ^{15}N , ^{11}B , ^{19}F , ^{51}V , ^{119}Sn , ^{27}Al), IR, EPR, X-ray crystallography and electrochemistry (mainly CV) have been used in the characterization of new complexes. Additionally, solid-state ^{15}N NMR spectroscopy has been carried out in collaboration with the research group of Professor R. Griffin. Information gained from the principle shielding tensors has been used in conjunction with DFT calculations to further our understanding of the electronic structure of these complexes. An oral presentation of this work was given at the ACS National Meeting in New York (Sept 2003).

BRISTOL UNIVERSITY, Bristol, UK (September 1998-July 2002)

MS Chemistry (with year in industry): First Class Honors. Achievements included: Commendation for academic achievement from University Dean of Science (1999-2000). Industrial Internship (awarded on merit) at DuPont Central Research & Development (2000-2001). My thesis research (supervisor: Prof S. Knox) involved the synthesis, isolation and chemical manipulation of novel diruthenium complexes.

Additional Information

Staff-Student Liaison Committee (2001-2002): Student representative.

Faculty Committee (2001-2002): Chemistry department student representative.

Royal Society of Chemistry Associate Member (2002-Date): Full member since 2000.

American Chemical Society: Member since 2001. Attended San Diego National Meeting (March 2001) and gave an oral presentation at the New York Meeting (Sept 2003).

WATFORD GRAMMAR SCHOOL FOR GIRLS, Watford, UK (1990-1997)

'A' levels: Chemistry (A), Math (A), Biology (B). GCSEs: 9 Passes (3 A*'s and 6 A's).

PRIZES & ACHIEVEMENTS

National Salters' Graduate Prize for Chemistry (January 2002) - For more information regarding this award visit www.salters.co.uk/institute/graduate_prizes.asp.

Robert T. Haslam Presidential Graduate Fellowship (March 2002) for study in Chemistry at Massachusetts Institute of Technology.

WORK EXPERIENCE

BRISTOL UNIVERSITY, *Bristol, UK (July 2002- September 2002)*

Research Chemist, Inorganic and Materials Section – 6-week summer internship studying Main Group chemistry within the research group of Dr Christopher Russell. I undertook two projects; one involving the development of new routes to multiply bonded phosphorus species and a second investigating the synthesis of novel antimony and bismuth compounds.

E.I. DUPONT DE NEMOURS & COMPANY, *Wilmington, DE, USA (2000-2001)*

Research Chemist, Central Research & Development – The main focus of my research involved the synthesis, characterization and catalytic studies of various carbene ligands and their transition metal complexes. Other research focused on the development of new routes to heterogeneous organic supports for use in catalysis. Procedures were carried out in an inert atmosphere dry box and using standard Schlenk techniques. Catalytic testing was run in a high-pressure autoclave. I frequently contributed data for company reports and had the opportunity to present my results at biweekly group meetings. I visited two of DuPont's nylon sites, one in Seaford, Delaware and a second, larger facility in Sabine, Texas, where I gave a formal presentation. I received an achievement award for co-organizing CR&D Safety Day.

ZENITH MEDIA, *London, UK (06/99-09/99)*

Media Assistant – Coordination of global advertising campaigns. Collaboration with clients, publishing houses and creative agencies. Report preparation and research presentation.

ACTIVITIES/INTERESTS

In my free time I enjoy participating in various sporting activities including running, working out and hiking. When at home in the UK I relax by walking my dog and riding my family's horses. Aside of my sporting endeavors, I enjoy cooking and holding dinner parties for my family and friends.

Acknowledgements

And so to the thank yous - as important a part of any thesis as the science contained within it because the achievements committed to paper reflect the dedication and commitment of a number of individuals – not only that of the author.

Naturally, my biggest thank you is dedicated to Kit. It has been wonderful to work for a supervisor whose love of chemistry and desire to stretch the limits of structure and bonding have made it exciting to go to work each day. The projects I have worked on have been many and varied. I certainly didn't think I would find myself studying solid state NMR spectroscopy(!) but it has been a particularly enjoyable part of my thesis work. Kit; I cannot thank you enough for giving me these opportunities.

I want to offer my thanks to the members of the Inorganic faculty (Professors Dan Nocera, Joseph Sadighi, Dick Schrock, Alan Davison and Steven Lippard) with whom I took classes and later had opportunity to discuss chemistry with in more informal gatherings.

A personal highlight of attending graduate school at such a tremendous place of learning as MIT is the peer group I have had opportunity to work with. This goes for every student I have interacted with during my stay at MIT but especially the members of the Cummins group with whom I have spent the better part of 6-7 days of the week for the past two years. Arjun Mendiratta was the first group member I shared a lab with. He tolerated Chris (Clough) and I moving into his lab and I want to thank him for his patience and help during this time. Arjun's research has also provided some cool new ideas for methods by which the activation of 'moly-nitride' could be achieved - so chapter 3 should probably be dedicated to him. Josh Figueroa was instrumental in me joining the group and for his encouragement to come and see what the Cummins lab had to offer, I thank him. He also carried out all of the X-ray crystallography included in this thesis and some of my structures have been a real bitch to solve, so thanks Josh! Fran Stephens and Chris Clough have been great friends and a wonderful source of information (chemical or otherwise) and entertainment. I want to wish them both the very best for the future - Fran in her new job at Los Alamos and Chris in the completion of his Ph.D and synthesis of the tungstaziridine hydride complex!

Other group members I spent some period of time with include James Blackwell, Paula Diaconescu, Erin Daida, Han Sen Soo and more recently Tetsuro Murahashi. At various points in time I was grateful for their friendship and advice. Linda Doerrer (who was on sabbatical in the Cummins group around the time I joined) has been a great friend and I am grateful to have had the opportunity to work with her – she is one of the kindest people I have ever met. I want to thank Allison Kelsey for all of the help and support she has given me and continues to provide the Cummins group.

I'd like to thank all of the people I had opportunity to work with at the Francis Bitter Magnet Laboratory. Thanks must go to Bob Griffin who kindly allowed me a significant amount of time on both solution and solid state instruments at this fabulous facility. Tony Bielecki has been a tremendous help in the acquisition of some important ^{15}N solution NMR spectra. Special thanks must go to Nikolaus Loening for providing me with a great introduction to solid state NMR spectroscopy and helping in the acquisition of so much of my data. Upon Niko's departure from the magnet lab, Patrick Van der Wel was handed this responsibility and it has been a real pleasure to work with him.

Without the support of some very good friends it would have been easy to lose perspective on my life and I am indebted to my Host family (John, Jeri and Nancy – thank you all – you are wonderful!) and Andrea Gabert (the best friend a person could hope for) for the love and friendship they have provided so generously over the past two years. I also want to thank Lisette Cummins and Amy Kelly for providing me with some much needed social stimulus during my stay here in Boston!

I cannot complete my acknowledgements without thanking the most important group of people in my life – my family. The encouragement and support they have always provided have enabled me to explore new opportunities and fulfill many personal ambitions. My Mum and Dad have always been such wonderful role models to me and for this I am forever grateful. Finally, I must say a big thank you to Mark for putting up with so much over the last few years but also for encouraging me to pursue this opportunity when we both knew it might not be the easiest path to follow.